Effect of Water Vapor on the Gas Sensing Properties for Pd-Loaded SnO_2 Gas Sensors

楠, 馬

https://doi.org/10.15017/1544014

出版情報：九州大学, 2015, 博士（工学）, 課程博士
バージョン：

Effect of Water Vapor on the Gas Sensing Properties for Pd-Loaded SnO_2 Gas Sensors

NAN MA

Department of Molecular and Material Sciences

Interdisciplinary Graduate School of Engineering Sciences

Kyushu University

July 2015

Contents

Abstract

Metal oxide semiconductor gas sensors are attractive to detect inflammable and toxic gases in variety of fields based on the electric resistance change of sensing layer in air and target gas. Tin dioxide (SnO_2) gas sensors are typically a wide bandgap n-type semiconductor sensor, with many obvious advantages such as low cost, long term stability, and high sensitivity to H_2 and CO. However, their gas sensing performance is seriously affected by the varying humidity in the ambient atmosphere, which greatly hinders their practical application. How to reduce the water vapor interfering effect on the gas sensing properties to keep high stability is the main goal in this research work. Loading noble metal Pd on the SnO_2 surface is one of the most effective methods to enhance the gas sensitivity and suppress the water poisoning effect. To further understand the mechanism of Pd on the sensing process in humid atmosphere is benefical to designing high performance gas sensors. Therefore, in this study, the role of Pd and its size effect on the gas sensing process was clarified in different humidity. Moreover, the sensitization effect of Pd was also investigated based on SnO_2 MEMS gas sensors and Sb-doped SnO_2 thick-film sensors under humid condition.

Pd-loaded SnO_2 nanoparticles were prepared by loading Pd on the calcined SnO_2 surface. The microstructure of SnO_2 and Pd-loaded SnO_2 nanoparticles was investigated. The oxygen adsorption behavior and sensor response to H_2 and CO for SnO_2 and Pd-loaded SnO_2 sensors were studied in different humidity. Pd-loaded SnO_2 with different Pd particle sizes were prepared, and the influence of the Pd size on the gas sensing properties of Pd-loaded SnO_2 under dry and humid conditions was discussed combining with the TPR measurement. In addition, the Pd sensitization effect in dry and humid atmospheres was examined based on SnO_2 MEMS gas sensors with low power consumption and Sb-doped SnO_2 thick-film sensors with high stability in humid atmosphere.

It was found that the mainly adsorbed oxygen species on the Pd-SnO_2 surface was changed to O^{2-} in humid atmosphere by loading Pd. This was very different from neat SnO_2 that it was O^- in the presence of water vapor. The O^{2-} adsorption on PdO expanded the depletion layer of the interface and prevented OH^- adsorption on the SnO_2 surface, leading to high sensor response and stability in humid atmosphere. Pd-loaded SnO_2 with different Pd particle sizes exhibited different sensing behavior to CO by changing from dry to humid atmosphere, due to the different catalytic activities of different nanosized Pd particles. The Pd loading also promoted the sensitivity of the SnO_2 MEMS gas sensors and the Sb-doped SnO_2 thick-film sensors under humid condition. Pd-loaded/Sb-doped SnO_2 sensors exhibited a great potential for practical application due to their high sensitivity and stability as well as low electric resistance in humid atmosphere.

List of Symbols and Abbreviations

L: Width of depletion layer

D: Grain size

q: Elementary charge of electrons

Vs: Height of the potential barrier

Ec: Energy of conduction band

Ev: Energy of valence band

E_F: Energy of Fermi level

k: Boltzmann constant

T: Temperature

N_D: Donor density

R_0: Electric resistance at the flat-band condition

P_{O2}: Oxygen partial pressure

P_{H2}: Hydrogen partial pressure

P_{CO}: Carbon monoxide partial pressure

Ra: Electrical resistance in air

Rg: Electrical resistance in target gas

D_K: Knudsen diffusion coefficient

PdNN: Pd derived from $Pd(NH_3)_2(NO_2)_2$

PdN: Pd derived from $Pd(NO_3)_2$

Chapter 1

Introduction

1.1 Background

Nowadays more and more gas sensors are employed in various fields, such as detecting inflammable and toxic gases in our living place and industries, monitoring air quality in environment, breath analysis in medical diagnosis, and quality control in the chemicals, food and cosmetics industries.[1-4] Therefore, sensitive gas sensors with small cross sensitivity have been extensively researched. Metal oxide semiconductor (MOS) gas sensors, one kind of chemoresistive sensors, are much more attractive due to high sensitivity, low cost, simplicity, and integratability.[5-8] The pioneering work of Seiyama et al.[9] and Taguchi[10] on MOS gas sensors in the early 1960s led to the production of the first SnO_2 gas sensing element. Since then, although various metal oxides such as WO_3, In_2O_3, CuO, TiO_2 have been reported as potential gas sensing materials, SnO_2 still plays predominate role in the field of MOS gas sensors for practical application.

SnO_2 is a typically wide bandgap n-type semiconductor, detecting gas based on the electric resistance change of sensing layer in air and target gas. Although SnO_2 gas sensors have many advantages, some disadvantages such as poor selectivity and stability extremely hinder their practical application.[11-13] Numerous kinds of gases from various sources are released into ambient atmosphere, therefore, it is a great challenge to detect a particular gas among various gases. Moreover, gas sensors are usually operated in ambient environment with varying humidity, so that their performance is inevitably affected by the surrounding water vapor.[14-17] How to reduce the water vapor interfering effect to keep long time stability by understanding the interaction of water vapor with the SnO_2 surface as well as with target gas in the gas sensing process is becoming

more and more of vital importance in this field.

Over the past few decades, much technological efforts have been made to improve the gas sensing performance to meet standards of practical use. Reducing the crystallite size and controlling the morphology of materials are effective methods to improve the gas sensitivity.[18, 19] There are several ways to modify the selectivity, such as controlling the operating temperature, adding catalyst and promoters, using selective filter, and using sensor arrays.[20, 21] One of the most commonly and effectively used methods to enhance the gas sensing performance is to add noble metals such as Pd, Pt, Au, Ag on metal oxides.[22-25] In particular, loading Pd on SnO_2 surface can effectively reduce the interference caused by water vapor, leading to a significant improvement in stability.[15] However, the role of Pd under humid condition is still far from fully understood. From the basic aspect, any factors that influence sensor performance in the gas interaction process, signal transduction process and gas diffusion process can be ascribed to receptor function, transducer function, and utility factor, respectively.[2, 26] In terms of this classification, loading Pd on the surface belongs to receptor function. It is very important to understand the basic sensing mechanism of MOS sensors, which could provide principles for designing high performance sensors.

Recently, MEMS techniques are popular in the field of gas sensors, especially for the purpose of minimizing the scale of devices and reducing power consumption. MEMS sensors are easier to integrate with other sensors to form sensor systems, providing selectivity to several gases.[1] The application of pulse heating mode can further reduce the power consumption and improve its feasibility as a portable gas senor. Particularly the heating and cooling characteristics of pulse heating mode are expected to provide gas sensors with new functions.[27]

In this chapter, a brief introduction on the gas sensing mechanism of MOS sensors is provided, and several factors for improving gas sensing performance

are summarized. Water vapor as commonly interfering gas in the practical application of sensors is reviewed in terms of its influence to the gas sensing properties. In addition, MEMS gas sensors are introduced due to their great advantages for practical use. Finally, the purpose and the organization of this thesis are proposed.

1.2 Theory of Semiconductor Gas Sensor

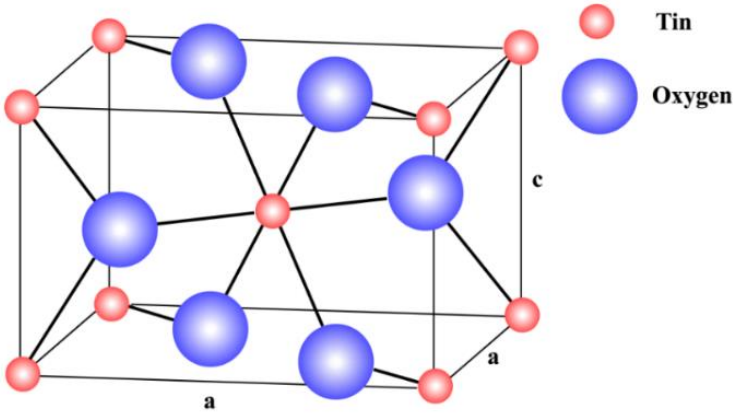

Figure 1-1 Rutile crystal structure of SnO_2.

The crystal structure of SnO_2 is shown in Fig. 1-1. It is the rutile structure with a tetragonal unit cell. The symmetry space group is P42/mnm and the lattice constants are $a = b = 4.7374$ Å and $c = 3.1864$ Å. In the bulk all Sn atoms are six-fold coordinated to three-fold coordinated oxygen atoms.[28] At the surface six-fold coordinated Sn^{4+} reduces to four-fold Sn^{2+} by removing oxygen anions from the stoichiometric surface.[29, 30] The variation of surface oxygen makes SnO_2 very useful to detect oxidizing and reducing gases.

The working principle of SnO_2 gas sensors is based on the variation of electric resistance in air and target gases due to the surface interaction between adsorbed oxygen species with target gases. SnO_2 gas sensors are usually operated in the temperature range of 200−500 ℃. Depending on temperature, oxygen molecules are chemisorbed on the SnO_2 surface as O_2^-, O^- and O^{2-}. Below 150 ℃

the oxygen species adsorb on the SnO_2 surface in the form of O_2^-, while above this temperature the atomic oxygen species O^- and O^{2-} are found on the surface.[31, 32] Once oxygen species adsorb on the SnO_2 surface, the electrons transfer from the bulk of SnO_2 to the adsorbed oxygen species. The electron density in the bulk decreases to form an electron depletion layer in the near surface region, leading to the band bending, as shown in Fig. 1-2. The electron transfer reaches equilibrium when the Fermi level of the adsorbed oxygen species is same as that of the semiconductor bulk.[33] In the presence of reducing gases (such as H_2 and CO), they react with the adsorbed oxygen species, releasing the surface-trapped electrons to the bulk. As a consequence, the electric resistance of the sensing layer is reduced. When introducing oxidizing gases (NO_2 and O_3), they occupy the additional surface states by trapping more electrons from the bulk, leading to an increase in the thickness of the depletion layer. Thus the electric resistance is increased by the adsorption of oxidizing gases.

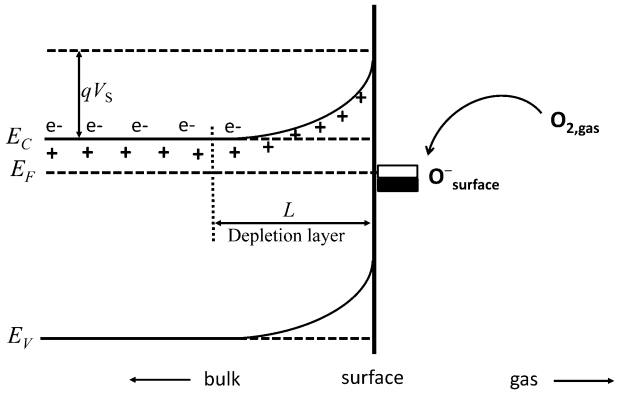

Figure 1-2 Band bending by chemisorption of oxygen species. E_C, E_V, and E_F is the energy of conduction band, valence band and the Fermi level, respectively. L is the thickness of the depletion layer, and V_S is potential barrier.[19]

1.3 Factors for Improving Gas Sensing Properties

For semiconductor gas sensors, high sensitivity, good selectivity, short response time, and long term stability are the pursuit goals in the research work. Three main factors are assumed to determine the gas sensing properties, namely, receptor function, transducer function, and utility factor, as shown in Fig. 1-3.[26] Receptor function is related to the reaction of target gas with adsorbed oxygen species on the surface combined with releasing electrons, which is greatly influenced by foreign receptor on the surface. Transducer function is corresponding to the transduction of charger transfer into electric resistance change, depending on the grain size and donor density. Utility factor concerns the penetration ability of the target gas into the gas sensing layer, relating to the chemical and physical properties of the target gas as well as the morphology of the sensing layer.[2]

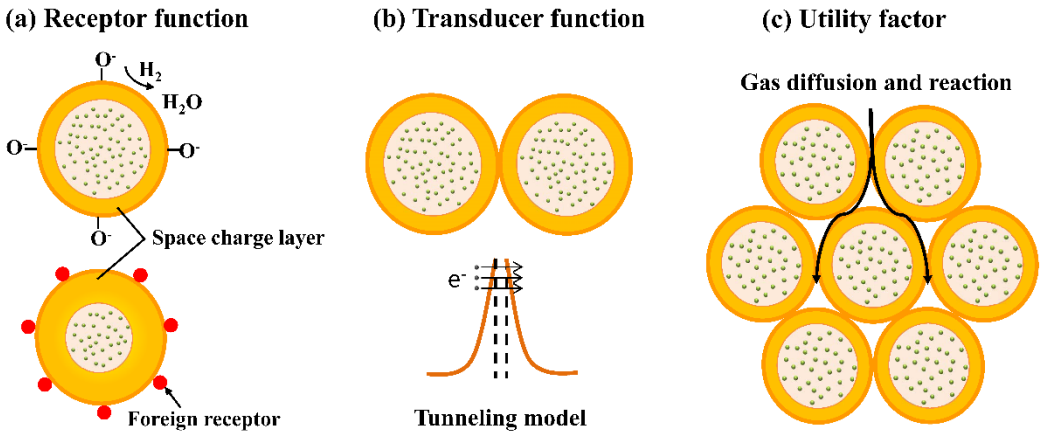

Figure 1-3 Three basic factors for controlling semiconductor gas sensor: (a) receptor function; (b) transducer function; (c) utility factor.

1.3.1 Effect of Pd loading

Among the various methods to improve gas sensing properties, loading noble metal Pd on the surface, which relates to the receptor function, is one of the most effective and extensively studied methods. A small amount of Pd on the surface

can not only enhance the gas sensing properties but also decrease the optimal operating temperature.[24, 34, 35] As an example, the effect of Pd on the H_2 response for SnO_2 gas sensors is illustrated in Fig. 1-4.[23] Obviously the sensitivity is significantly enhanced by loading Pd, moreover, the promoting effect of Pd is influenced by the Pd introduction method. The fixation method gave the highest response at low temperature due to the finest dispersion of Pd particles on the surface.

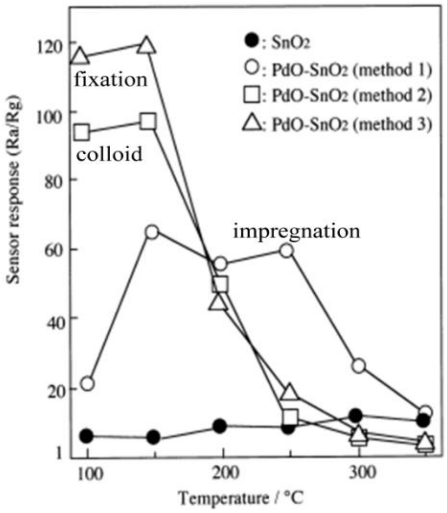

Figure 1-4 Sensor responses to 194 ppm H_2 in air at different temperatures for SnO_2 and Pd-loaded SnO_2 with different loading methods.

Generally speaking, the sensitization effect of Pd is greatly influenced by its distribution state that depended a lot on the noble metal precursors, material preparation procedures and deposition methods.[34, 36-40] Two methods are commonly used to introduce Pd on the SnO_2 nanoparticles: (1) Pd is impregnated on the calcined SnO_2 and then the mixture is heat-treated again; (2) Pd is introduced in the preparation process of SnO_2 particle, followed by heat treatment. In the former case, Pd disperses on the surface of SnO_2, and the particle size of Pd-SnO_2 is independent of Pd loading. In the latter case, Pd may diffuse into the SnO_2 lattice and modify the particle size of SnO_2.[36-38] This point has important consequences on the gas sensitivity, since the surface concentration of Pd depends on the SnO_2 surface area, which combines with particle size of SnO_2 to affect the sensitivity.

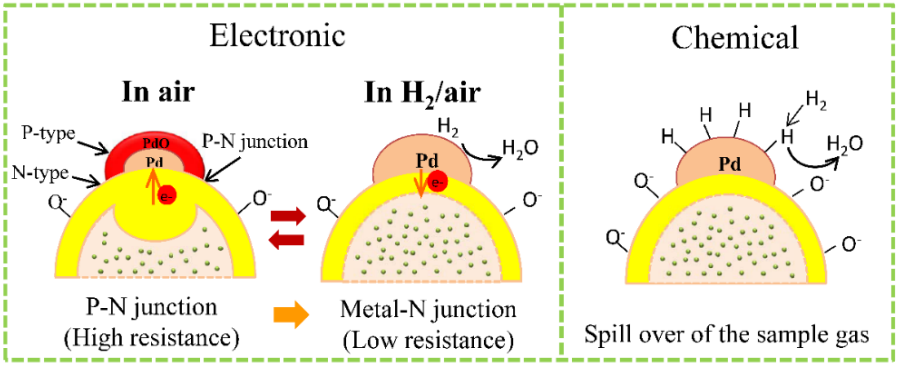

Figure 1-5 Mechanism of Pd in the gas sensing process.

Two types of sensitization mechanisms were proposed toward the role of Pd in the gas sensing process, that is, electronic sensitization (Fermi-level model) and chemical sensitization (spill-over model), as shown in Fig. 1-5.[22, 23, 26, 28] Electronic sensitization considers the electric resistance change due to the variation of contact potential of SnO_2 with Pd.[22] Pd exists as PdO in air at operating temperature, thus P-N junction is formed between the interface of P-type PdO and N-type SnO_2. The electrons are transferred from SnO_2 to PdO because of the larger work function of PdO, causing an electron depletion area on the SnO_2 near the contact area.[41] Thus the electric resistance is greatly increased in air. PdO reduces to metallic Pd when exposed to combustible gases. Consequently, electrons return back into the bulk of SnO_2 and the electric resistance dramatically reduces, leading to a high sensor response. The electronic sensitization for PdO has been confirmed by X-ray photoelectron spectroscopy, evidenced by the shift of XPS binding energies of Sn3$d_{3/2}$ and O1$s_{1/2}$.[22] Chemical sensitization occurs via a spill-over effect, in which Pd activates the target gas to facilitate its oxidation on the SnO_2 surface. Pd enhances the sensitivity by increasing the rate of oxidation process due to the catalytic action of Pd.

The above “Fermi-level” and “spill-over” models explain the role of Pd in the gas sensing process in terms of oxidized or metallic Pd. However, the Pd state is dependent on the surrounding atmosphere and the Pd amount. Koziej et al.

studied the role of Pd by investigating the structure of Pd constituent and the sensor response during sensor operation process.[42] They found that in the case of 0.2 wt.% Pd-SnO_2, a small concentration of Pd loaded on the surface, Pd was still in the oxidized state when low concentration CO and H_2 were introduced, which situation was very different from the previously reported "Fermi-level" or "spill-over" model. They proposed that Pd is dispersed at an atomic level on the SnO_2 surface by binding to the surface lattice oxygen, as shown in Fig. 1-6. Pd atoms could provide initial adsorption sites for atmospheric gases by lowering the energy barrier of adsorption/dissociation.

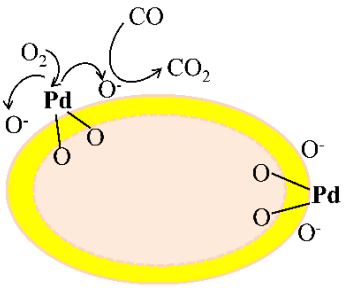

Figure 1-6 Effect of Pd as local sites at the surface of SnO_2.

In addition, Pd is also one of the effective receptors to suppress the water vapor poisoning effect on the gas sensing properties. However, the role of Pd in humid atmosphere is more complicated. Sakai et al.[43] developed Pd-loaded SnO_2 gas sensor to detect T-VOC gases, which showed high stability in humid atmosphere. They considered electronic sensitization of Pd playing an important role for high stability in humidity. Koziej et al.[44] proposed that Pd may create new adsorption sites, and increase the reactant for CO sensing reaction and decrease the activation energy of CO to make it more favorable than the adsorption of water. Additionally, OH^- reacts with CO for Pd-loaded SnO_2 sensor, contributing to the increase of sensor signal.[45] Therefore, the promotion effect of Pd in humid atmosphere needs to be further clarified for designing gas sensors with lower water interference.

1.3.2 Effect of grain size

The grain size controls the transducer function. Metal oxide semiconductor gas sensors with smaller particle sizes are expected to exhibit improved gas sensing properties due to larger surface/bulk ratio. The grain size effect on the gas sensitivity was systematically studied by Xu et al. in the early 1990s.[18, 46] SnO_2-based samples with various crystallite sizes in the range of 5−32 nm were prepared by doping proper additives. It was found the gas sensitivity to H_2 and CO was nearly independent on the crystallite size *D* in the range of $D > 20$ nm, and gradually increased with *D* reducing to 10 nm, but it steeply increased when the crystallite size *D* was below 10 nm, as shown in Fig. 1-7.

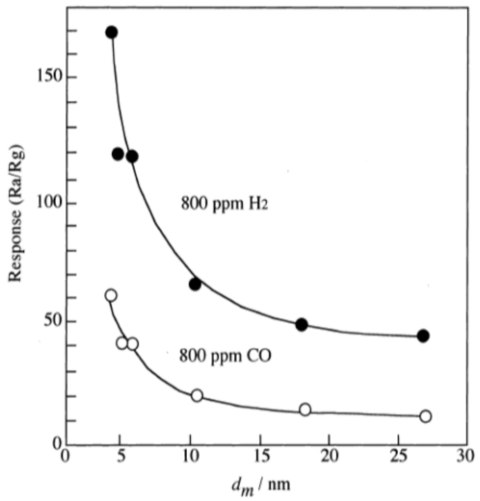

Figure 1-7 Influence of SnO_2 grain size on sensor response to H_2 and CO in air at 300 ℃.[18]

Xu et al. proposed a semiquantitative model to explain the grain size effect on the gas sensitivity based on the relationship between crystallite size *D* and width of the depletion layer *L*, as shown in Fig. 1-8.[18] When *D* is far larger than 2*L*, the electrons overcome the grain boundary barriers to transport from one grain to another. Grain boundary controls the electric resistance as well as sensitivity. As *D* becomes comparable to 2*L*, the electrons move through the conduction channel which is formed by the depletion region in the neck. In this case necks govern the gas sensitivity. As the crystallite size further reduces, when $D < 2L$, the

whole grain is almost fully depleted of electrons and the energy bands become flat in the whole structure. Therefore, the sensitivity of gas sensor is controlled by the grains.

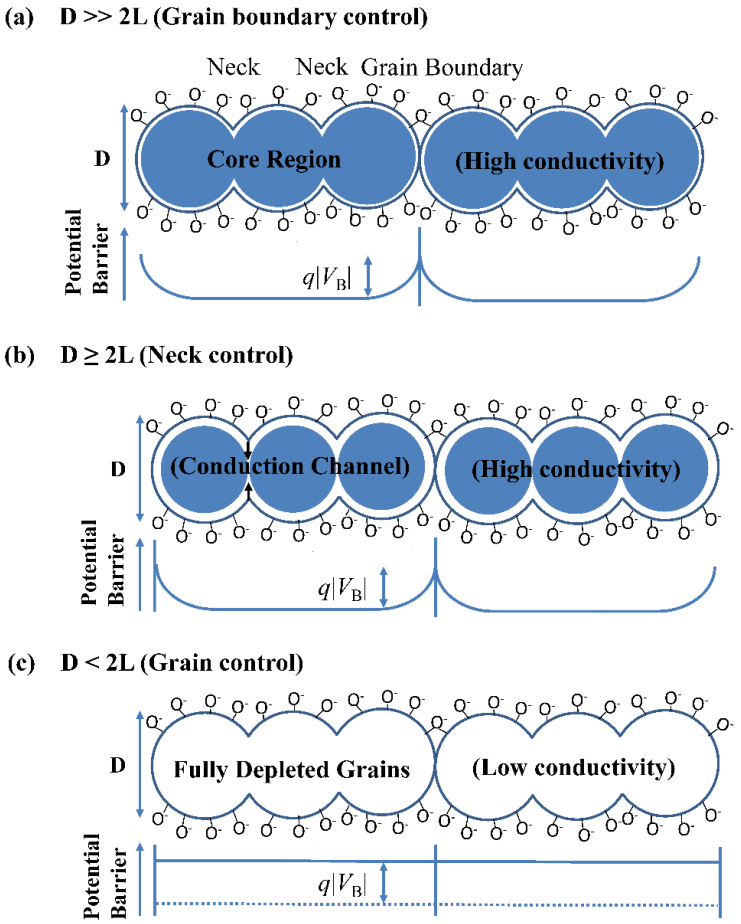

Figure 1-8 Schematic models for grain-size effects on the sensitivity of metal-oxide gas sensors: (a) $D >> 2L$ (grain boundary control); (b) $D \geq 2L$ (neck control); (c) $D < 2L$ (grain control).[47]

Rothschild and Komem[47] simulated the effect of grain size on the sensitivity of SnO_2 gas sensor by calculating the effective carrier concentration as a function of the surface state density for SnO_2 with grain size of 5−80 nm. It was demonstrated that the carriers concentration steeply increase as the surface density reaches a critical values corresponding to the fully depleted grains. The simulation results indicated that the sensitivity is proportional to $1/D$ (D: average grain size),

and this was well verified by the experimental result.

For sensing materials with larger grains, the width of depletion layer L is much smaller than the grain size D, and the electrons transfer between adjacent grains is controlled by the Schottky barriers qVs, whose height is determined by the amount and type of adsorbed oxygen.[19] In this case, the electric resistance can be written as follow:

$$\frac{R}{R_0} = \exp(\frac{qV_S}{kT}) \qquad [1\text{-}1]$$

Where R_0 is the electric resistance at the flat-band condition, V_S is the potential barrier, q is elementary charge of electron, k is the Boltzmann constant, T is temperature.

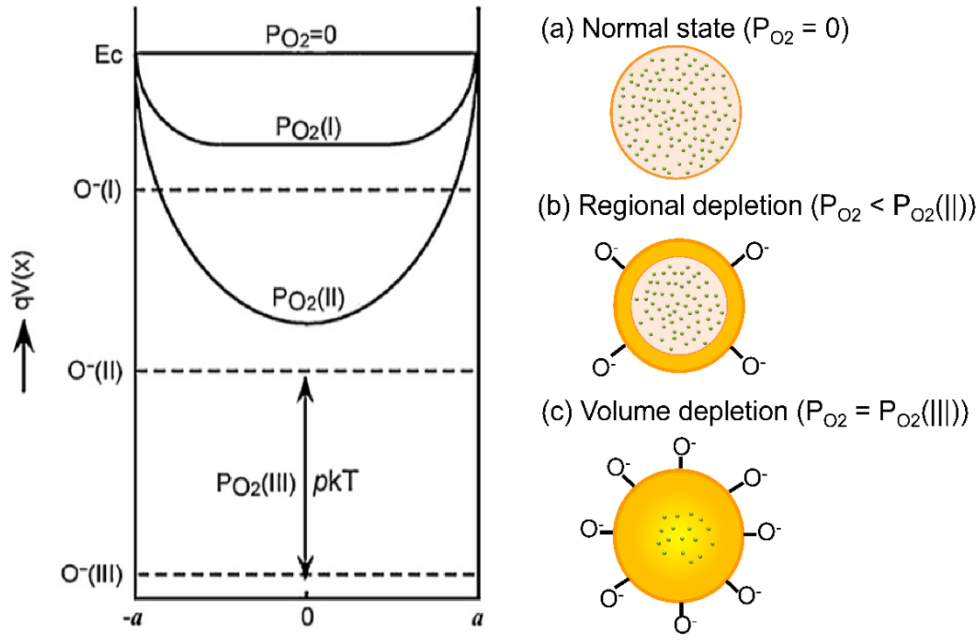

Figure 1-9 Band energy diagram and depletion state for a small semiconductor crystal under exposure to different oxygen partial pressure.

However, the electron conduction for sensing material with smaller grains is very different from that with larger ones. Figure 1-9 shows the band energy diagram and depletion state change with increasing oxygen partial pressure for small grains.[33, 48] When the oxygen partial pressure P_{O2} is small, less amount of

oxygen species adsorb on the surface, leading to a thin depletion layer. With increasing P_{O2} (< P_{O2}(Ⅰ)), more electrons are extracted from the semiconductor, leading to the increase of depletion layer ($L < D$). In this case, the depletion state is same as that in larger grains, which is named regional depletion. After the depletion layer extends to the whole grain ($L = D$), by further increasing P_{O2} (P_{O2} = P_{O2}(Ⅲ), the electron transfer from bulk to the surface continues by shifting down Fermi level to a designated amount *pkT*, while the band bending profile is unchanged. In this case, the electron density in the bulk decreases gradually as the Fermi level shift increases, which is called volume depletion.

In the stage of volume depletion, theoretical formulas for the electric resistance of gas sensors were proposed based on the power laws in the case of spherical SnO_2. The electric resistance was expressed as the function of oxygen partial pressure by combining the volume depletion model as well as oxygen adsorption and reaction.[48, 49] Oxygen species adsorb on the SnO_2 surface in the forms of O_2^-, O^- and O^{2-}:

$$O_2 + e^- = O_2^- \qquad [R1]$$

$$O_2 + 2e^- = 2O^- \qquad [R2]$$

$$O_2 + 4e^- = 2O^{2-} \qquad [R3]$$

The corresponding electric resistance can be expressed as following equations respectively:

$$\frac{R}{R_0} = \frac{3}{a} K_1 P_{O2} + c \qquad (O_2^-) \qquad [1\text{-}2]$$

$$\frac{R}{R_0} = \frac{3}{a} (K_2 P_{O2})^{\frac{1}{2}} + c \qquad (O^-) \qquad [1\text{-}3]$$

$$\frac{R}{R_0} = \{\frac{1}{4}\big(c(n)\big)^2 + \frac{6N_D}{a} (K_3 P_{O2})^{\frac{1}{2}}\}^{\frac{1}{2}} + c \qquad (O^{2-}) \qquad [1\text{-}4]$$

Here R_0 is the electric resistance at the flat-band condition, a is the grain radius, c is a constant, N_D is the donor density, K_1, K_2 and K_3 are equilibrium constants of adsorption.

The sensor response to hydrogen was also theoretically investigated, which was defined as following equations:[50, 51]

$$H_2 + O^- = H_2O + e^- \quad [R4]$$

$$H_2 + O^{2-} = H_2O + 2e^- \quad [R5]$$

$$\frac{Ra}{Rg} = \left(\frac{3c}{aN_D}\right)^{1/2} \cdot {P_{H2}}^{1/2} + const \quad \text{(Reaction with } O^-\text{)} \quad [1\text{-}5]$$

$$\frac{Ra}{Rg} = f\left(\frac{3(k_2/k_{-1})}{aN_D}\right)^{1/2} \cdot {P_{H2}}^{1/2} \quad \text{(Reaction with } O^{2-}\text{)} \quad [1\text{-}6]$$

Here *Ra* and *Rg* are the electrical resistances in air and hydrogen gas, respectively, k_2 and k_{-1} are the rate constants of forward and reverse reactions of R3, P_{H2} is the hydrogen partial pressure, and *f* is an amplifying factor. As described above, the gas sensing properties of semiconductor gas sensors are depend on grain size and donor density, which is well explained by theoretical equations. Figure 1-10 shows the depletion state change with grain size and donor density. Theoretical investigation on semiconductor gas sensors is not only useful for better understanding the gas sensing mechanism but also beneficial to the material design and sensor fabrication.

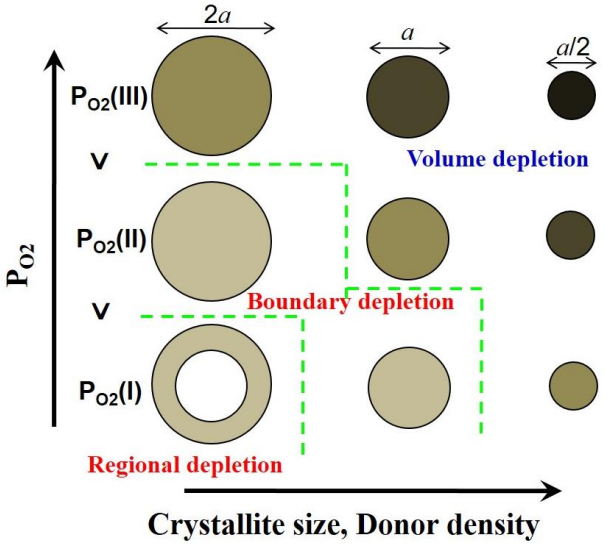

Figure 1-10 Schematic diagram for three depletion stages in particles with various diameters under different oxygen partial pressures.[27]

1.3.3 Influence of film thickness

The thickness of sensing film and its porosity are closely related to the utility factor, which greatly affect the response time and the sensitivity, because target gas reacts with adsorbed oxygen species on the surface accompanying with diffusing into deep region of the film. A fast response time depends on the diffusion rate of the target gas as well as the pore size of the film. A high sensitivity is related to the equilibrium of surface reaction and gas diffusion rate. If the interaction is too strong the gas molecules cannot reach the deep inside. Therefore, a thinner film with high porosity contributes to a faster response time and higher sensitivity.[19]

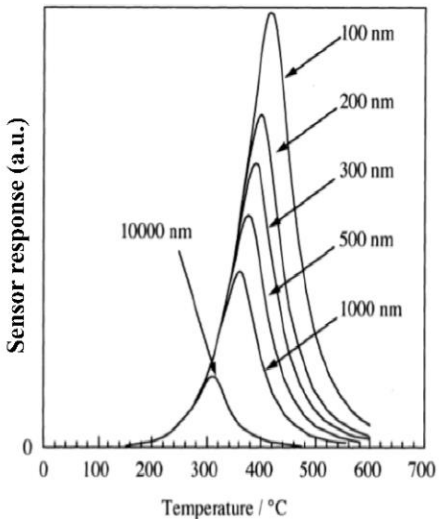

Figure 1-11 Dependence of sensor response on temperature at various film thicknesses.[26]

The dependence of H_2S and H_2 on the film thickness was well investigated based on SnO_2 by combining the experimental results and gas diffusion-reaction theory.[52-54] It was found that the sensor response to H_2S and H_2 was dramatically reduced with increasing the film thickness. The sensor response to H_2 is always larger than that to CO for SnO_2 gas sensor, due to the smaller H_2 molecule with higher Knudsen diffusion coefficient D_K.[53] Figure 1-11 showed the simulation results of how temperature and thickness affect the sensor response.[26] The sensor

response exhibited a volcano shape with increasing temperature, while the maximum value of sensor response as well as its temperature were reduced with increasing thickness. At the optimal temperature, the gas molecule sufficiently reacted with the surface and effectively diffused into the sensing layer.

1.4 Water Vapor Effect on the Gas Sensing Properties

Water vapor exists in the ambient environment with varying concentration, which is one of unavoidable species on any surface exposed in ambient conditions. Water adsorption on the surface is one of the most important considerations in the practical application of SnO_2 gas sensors. SnO_2 sensors are not only just sensitive to inflammable gases but also exhibits sensitivity to water vapor, as being reflected by the reduced electric resistance in the presence of reducing gas and water. The study about the role of water vapor in the gas sensing process was performed as early as in 1977, 9 years later after the first Taguchi sensor was produced in Japan.[15] Although the research about water vapor effect has been continued for nearly 40 years, even gas sensors with lower water interference have been developed and considerable results were obtained by using various methods, the role of water vapor in the gas sensing process is still far from fully understood. The water vapor effect on the gas sensing properties of SnO_2-based gas sensors was reviewed in this section.

1.4.1 Resistance change in the presence of water vapor

The sensor response is usually defined as the ratio of electric resistance in air and target gas. Therefore, the electric resistance change induced by water vapor is first considered for better understanding the water vapor effect. Yamazoe et al. investigated the water adsorption on the SnO_2 surface by temperature programmed desorption (TPD) in He carrier gas.[31, 55, 56] The TPD chromatograms showed two desorption peaks of water at around 100 and 400 ℃, corresponding

to desorption of molecular water and surface hydroxyl groups, respectively.[31] A large decrease in electric conductivity was observed at the high temperature desorption peak in TPD, concluding that hydroxyl groups increase the electric conductivity of SnO_2 but molecular water showed little influence on it. Many other researchers came to the similar conclusions,[57-59] that is the reduced electric resistance in the presence of water vapor was attributed to the hydroxyl group adsorption on the surface.

Ihokura and Watson measured the electric resistance of SnO_2 in dry air and humid air (60% RH) between 200−620 ℃, pointing out that the electric resistance in humid air was about 3−7 times lower than that in dry air.[57] However, loading noble metals such as Pd to some extent reduces the interfering effect of water vapor to the electric resistance. Sakai et al.[43] reported a high electric resistance stability in a wide range of humidity for 0.5% Pd-loaded SnO_2 operated at 300 ℃, considering that the electronic sensitization of Pd was contributed to the sensor stability in humidity. It was also reported that the variation of electric resistance with humidity was negligible for 1.27 wt.% NiO-doped SnO_2. On the basis of diffuse reflectance infrared Fourier transform spectroscopy (DRIFTS) analysis, they proposed that NiO played a role as a humidity adsorber and protected SnO_2 from being affected by water vapor.[60] Besides Pd and NiO, CuO, Co and Ce were also effective to reduce the dependence of electric resistance on humidity for SnO_2 gas sensor.[61, 62]

1.4.1 Sensor response change in the presence of water vapor

H_2 and CO are the most widely used gases to study the water vapor effect on SnO_2 sensors. Because only simple products (H_2O and CO_2, respectively) are produced during the sensing process, it simplifies the interpretation of the obtained results. Therefore, the water vapor effect on the gas sensing performance of SnO_2 sensors was discussed based on the sensing behavior to H_2 and CO.

The interfering effect of water vapor on H_2 detection for SnO_2-based sensors has been reported in many papers.[50, 63-65] Yamazoe et al.[50] explained the decrease of sensor response to H_2 in humid atmosphere from the view point of adsorbed oxygen species on the surface. Namely, O^{2-} adsorbed on the SnO_2 surface only in dry atmosphere and showed an amplifying effect to H_2 sensor response; while this amplifying effect disappeared in the absence of O^{2-} in humid atmosphere. Pavello et al.[64] investigated the effect of humidity on H_2 detection in a wide range of humidity and operating temperature. It was found that in high humidity the sensor response not only reduces but also its maximum value shifts to higher temperature.

However, the gas sensing properties to CO in the presence of water vapor is more complicated for SnO_2-based gas sensors. Not like sensing to the H_2, which sensor response is always reduced by water vapor, for CO either decreased or increased sensor signal in humid atmosphere were reported for both neat SnO_2 and noble metal loaded SnO_2. Smatt et al.[66] compared the sensor response to CO in humid atmosphere based on two kinds of mesoporous SnO_2 with different morphology. With increasing humidity, SnO_2 in spherical particle shape showed a decreasing CO response, while the non-spherical SnO_2 exhibited an opposite tendency. However, for SnO_2 gas sensors, even made by the same SnO_2 particles, a completely different sensing behavior to CO was observed in humid air depending on the materials and geometry of electrodes.[67] In the case of Au electrodes with 200 and 400 μm gaps, as well as Pt electrodes with 200 μm gap, the CO response was also enhanced by water vapor. However, for Pt electrodes with 400 μm gap a seriously interfering effect of humidity was observed. Harbeck et al.[68] studied the DRIFT spectra of SnO_2 and 0.2%Pd-doped SnO_2 in various CO concentration in dry and humid atmospheres. They found that the sensor signals of SnO_2 were not influenced by the humidity, while the Pd-doped SnO_2 showed higher sensor signals in humid atmosphere. It was proposed that the

hydroxyl groups do not seem to react with CO in the absence of water vapor in the case of Pd-doped SnO_2. Besides material morphology, electrodes and dopants, it was also reported that the decrease or increase of sensor response to CO was related to temperature and the history of material.[15] Although many literatures reported the phenomena of humidity-induced CO response change, it is still unclear what changes are caused by water vapor in the CO sensing process. Therefore, much more research works are needed to further understand the CO sensing mechanism in the presence of water vapor.

1.4.3 Gas sensing mechanism in the presence of water vapor

The effect of water vapor on the gas sensing properties has been studied for several decades,[14, 16, 50, 69-71] and several controversial mechanisms were proposed based on SnO_2 gas sensors. Yamazoe et al.[16, 50] proposed that the adsorption of water molecules on the SnO_2 surface inhibited O^{2-} adsorption, leaving O^- as the mainly adsorbed oxygen species in humid atmosphere. This was experimentally evidenced by the relationship between the electric resistance and oxygen partial pressure in dry and humid atmospheres. The electric resistance was linearly proportional to $P_{O2}^{1/4}$ in dry atmosphere, and it showed a linear relationship to $P_{O2}^{1/2}$ in humid atmosphere. According to the theoretical formulas 1-3 and 1-4 as well as experimental results, they suggested that the adsorbed oxygen species changed from O^{2-} in dry atmosphere to O^- in humid atmosphere, resulting in the decrease of sensor response in humid atmosphere.

Some researchers proposed that water vapor adsorbs on the SnO_2 surface with releasing electrons, leading to a decreased electric resistance in a similar way as reducing gases.[14, 45, 63, 72] H_2O molecule is dissociated to hydroxyl group OH^- and proton H^+. The former one bounds with surface Sn atom to form terminal OH^-, and the latter one easily reacts with lattice oxygen or ionsorbed oxygen to form rooted OH^-. Three surface interaction mechanisms between SnO_2 and water

vapor have been proposed to explain the resistance reduction.[14, 63] In the first mechanism, H_2O reacts with surface lattice oxygen to form terminal OH^- and rooted OH^- groups, with releasing an electron:

$$H_2O + Sn_{lat} + O_{lat} \leftrightarrow (OH - Sn_{lat}) + (O_{lat}H)^+ + e^- \quad [1]$$

N. Barsan *et al.* investigated CO-water interaction in the case of Pd-doped SnO_2 by measuring work function and electric resistance in the background of humid air, and explained the water adsorption by this mechanism. The terminal OH^- groups are believed to be surface dipoles with a strong influence on electronic affinity.[14]

In the second mechanism, two terminal OH^- groups are formed from the dissociation of water and the binding of proton H^+ with lattice oxygen. At the same time the resulting oxygen vacancy produces two electrons:

$$H_2O + 2Sn_{lat} + O_{lat} \leftrightarrow 2(OH - Sn_{lat}) + V_o^{\cdot\cdot} + 2e^- \quad [2]$$

In the case of Pt-doped SnO_2, they considered the second mechanism as the explanation for the increased CO response in the presence of humidity, that is, the new created oxygen vacancies by water vapor adsorption could provide additional adsorption site to oxygen species.[63]

In the third mechanism, H_2O reacts with ionosorbed oxygen to form two terminal OH^- groups, bounding with surface Sn atoms and releasing a free electron:

$$H_2O + 2Sn_{lat} + O_{ad}^- \leftrightarrow 2(OH - Sn_{lat}) + e^- \quad [3]$$

S. Capone *et al.* reported that the interfering effect of water vapor in the case of SnO_2 with narrow Pt electrodes due to the competition between oxygen and water vapor adsorption on the SnO_2 surface.[67] It seems that the mechanism of water vapor adsorption is more complicated, and it changes depending on the target gases, dopants, electrodes, and the history of gas sensors.[67, 73-75] Therefore, it is important to further clarify the role of water vapor in the gas sensing process. In

the present study, the main purpose is to investigate the water vapor effect on the gas sensing properties of Pd-loaded SnO_2.

1.5 MEMS Gas Sensor

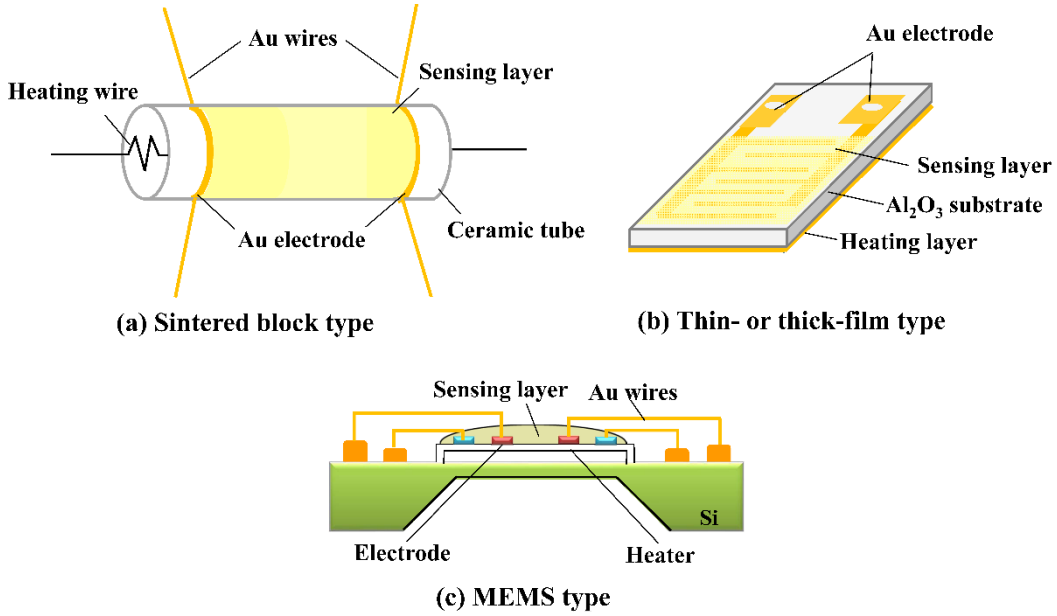

Figure 1-12 Three types gas sensor device: (a) sintered block type;[81] (b) thin- or thick-film type; (c) MEMS type.

Gas sensing devices generally consist of three parts, i.e., sensing film, electrodes and heaters. Gas sensors are heated by the heater to reach an optimum operating temperature. Most of SnO_2 gas sensors are fabricated based on the sintered block type with heating wire placed inside of ceramic tube, and the film type with heating paste on the backside of substrate, as shown in Fig. 1-12a, b. However, such kinds of gas sensors need high power consumption since they are usually operated at high temperature (200−500 ℃) to achieve good performance, which is unfavorable for power saving and device integration.[76] It was reported that the power consumption of screen-printed film type device is typically in the range of 200 mW to about 1W.[77] In recent years, SnO_2 gas sensing films have been incorpoarated into Micro-Electro-Mechanical-Systems (MEMS) devices for

reducing the power consumption and improving the gas sensing properties.[76, 78-80] MEMS device is equipped with micro hearers and electrodes on a micromachined silicon substrate, and the heaters can heat a small area of membrane with minimal heat conduction, as shown in Fig. 1-12c.

With micro heaters, the power consumption of MEMS gas sensors can be reduced to tens of mW.[77] Elmi et al. developed MEMS type SnO_2 gas sensors with extremely low power consumption of 8.9 mW at 400 ℃, showing good sensitivity to VOC.[82] Dai et al. have constructed a kind of MEMS-based IDEs-microheater chip not only with low power consumption (32 mW at 350 ℃) but also contributing high sensor performance to 100 ppb ethanol.[76] By reducing power consumption, MEMS sensor devices can be driven by a battery, which is benefical to miniaturize the device. This feature makes the sensor devices more portable and easier to install in a small space to integrate sensor systems. Moreover, the application of pulse heating in MEMS gas senors can further reduce the power consumption and improve its feasibility as a portable gas senor.[83] The heating and cooling characteristics of pulse heating are expected to provide sensor with different properties. In addition, MEMS gas sensors with small scale can be easily integrated on-chip to form array-based gas sensors. By composing of different MEMS sensors with different selectivity, the arrays show the improved selectivity.[21, 84, 85]

1.6 Motivation and Organization of the Dissertation

As the most promising gas sensing material for practical application, SnO_2 has undergone extensively research and development. Although various SnO_2 gas sensors with excellent gas sensing properties have been reported, the problem of sensor stability in the presence of humidity is still not satisfactorily resolved. How to reduce the water vapor interfering effect on the gas sensing properties becomes a challenging task in the research work. Among the various methods, loading Pd

on the surface is one of the most effective methods to reduce the water vapor poisoning. Unfortunately, many papers only reported the phenomena of Pd-induced stability in humid atmosphere, but the detailed reason is not clarified deeply. It is well-known that Pd is one of the catalysts, and its particle sizes greatly affect the oxidation of reducing gases. However, the Pd size effect on the gas sensing performance in humid atmosphere was not clearly clarified. In addition, MEMS type gas sensors as one of most promising sensor for practically application, their gas performance based on Pd-SnO_2 in humid atmosphere is less reported. Moreover, due to the low sensitivity and high stability of Sb-doped SnO_2 in humid atmosphere, the sensitization effect of Pd on Sb-doped SnO_2 sensors is meaningful to be studied. The aim of present study is to further understanding the role of Pd and its particle sizes effect on the gas sensing process in humid atmosphere, as well as the application of Pd sensitizer on MEMS sensors and Sb-doped SnO_2 thick-film sensors, which may be beneficial for designing high performance gas sensors.

The objective of the present study is to focus on: (1) the reason of the Pd enhancing effect in humid atmosphere; (2) the effect of Pd particle size on the gas sensing properties in the presence of water vapor; (3) the gas sensing performance for Pd-loaded SnO_2 MEMS type gas sensors; (4) the application of Pd sensitizer on Sb-doped SnO_2 thick-film sensors. Based on the above aims, the organization of the dissertation is as follows.

Chapter 1 introduces the background of SnO_2 gas sensors, including the basic mechanism of semiconductor gas sensors, the methods for improving gas sensing properties, as well as the interfering effect of water vapor on the gas sensing properties. Finally, MEMS gas sensors are introduced.

Chapter 2 describes the preparation process of Pd-loaded SnO_2 nanoparticles as well as the sensor devices. The role of Pd in the gas sensing process under humid condition is analyzed by investigating the oxygen adsorption behavior and

sensing properties to H_2 and CO in the presence of water vapor. The suppression effect of Pd on water vapor poisoning is further clarified.

Chapter 3 focuses on the influence of Pd particle sizes on the gas sensing properties in humid atmosphere. Two kinds of Pd-loaded SnO_2 nanoparticles are prepared, with smaller and larger Pd particle sizes, respectively. The oxygen adsorption behavior and gas sensing properties to H_2 and CO are investigated in dry and humid atmospheres in terms of Pd-loaded SnO_2 with different Pd particle size.

Chapter 4 investigated the gas sensing performance of MEMS gas sensors. The MEMS sensors are fabricated by injection method using SnO_2 and Pd-loaded SnO_2 nanoparticles. The gas sensing properties to H_2 and CO are investigated under dry and humid conditions by operating the MEMS sensors in constant heating and pulse heating modes. The H_2 response of MEMS gas sensors and conventionally thick-film sensors were compared based on the constant heating mode.

Chapter 5 reports the gas sensing properties of Pd-loaded/Sb-doped SnO_2. The role of Pd and its size effect on the Sb-doped SnO_2 sensors is examined by investigating the gas sensing properties to H_2 and CO in dry and humid atmosphere.

Chapter 6 summarizes the experimental results with regard to chapter 2, 3, 4 and 5. The role of Pd as well as its size effect on the gas sensing process in humid atmosphere is proposed. The improved gas sensing performance by applying Pd sensitizer is reported based on the SnO_2 MEMS sensors and the Sb-doped SnO_2 thick-film sensors. Finally, some suggestions for the future work are provided.

References

[1] Kim ID, Rothschild A, Tuller HL. Advances and new directions in gas-sensing devices. Acta Materialia. 2013;61:974–1000.

[2] Yamazoe N. Toward innovations of gas sensor technology. Sensors and Actuators B: Chemical. 2005;108:2–14.

[3] Miller DR, Akbar SA, Morris PA. Nanoscale metal oxide-based heterojunctions for gas sensing: A review. Sensors and Actuators B: Chemical. 2014;204:250–272.

[4] Kohl D. Function and applications of gas sensors. Journal of Physics D: Applied Physics. 2001;34:125–149.

[5] Comini E. Metal oxide nano-crystals for gas sensing. Analytica Chimica Acta. 2006;568:28–40.

[6] Korotcenkov G. Metal oxides for solid-state gas sensors: What determines our choice? Materials Science and Engineering: B. 2007;139:1–23.

[7] Barsan N, Koziej D, Weimar U. Metal oxide-based gas sensor research: How to? Sensors and Actuators B: Chemical. 2007;121:18–35.

[8] Wang C, Yin L, Zhang L, Xiang D, Gao R. Metal oxide gas sensors: sensitivity and influencing factors. Sensors. 2010;10:2088–2106.

[9] Seiyama T, Kato A, Fujiishi K, Nagatani M. A new detector for gaseous components using semiconductive thin films. Analytical Chemistry. 1962;34:1502–1503.

[10] Williams DE. Semiconducting oxides as gas-sensitive resistors. Sensors and Actuators B: Chemical. 1999;57:1–16.

[11] Pijolat C, Pupier C, Sauvan M, Tournier G, Lalauze R. Gas detection for automotive pollution control. Sensors and Actuators B: Chemical. 1999;59:195–202.

[12] Pijolat C, Rivière B, Kamionka M, Viricelle J, Breuil P. Tin dioxide gas sensor as a tool for atmospheric pollution monitoring: problems and possibilities for improvements. Journal of Materials Science. 2003;38:4333–4346.

[13] Barsan N, Schweizer-Berberich M, Göpel W. Fundamental and practical aspects in the design of nanoscaled SnO_2 gas sensors: a status report. Fresenius' Journal of Analytical Chemistry. 1999;365:287–304.

[14] Barsan N, Weimar U. Understanding the fundamental principles of metal oxide based gas sensors; the example of CO sensing with SnO_2 sensors in the presence of humidity. Journal of Physics: Condensed Matter. 2003;15:813–839.

[15] Pavelko R. The influence of water vapor on the gas-sensing phenomenon of tin dioxide-based gas sensors. Chemical Sensors: Simulation and Modeling. 2012;2:297–338.

[16] Yamazoe N, Suematsu K, Shimanoe K. Two types of moisture effects on the receptor function of neat tin oxide gas sensor to oxygen. Sensors and Actuators B: Chemical. 2013;176:443–452.

[17] Santarossa G, Hahn K, Baiker A. Free energy and electronic properties of water adsorption on the SnO_2 (110) surface. Langmuir. 2013;29:5487–5499.

[18] Xu CN, Miura N, Yamazoe N. Grain size effects on gas sensitivity of porous SnO_2-based elements. Sensors and Actuators B: Chemical. 1991;3:147–155.

[19] Franke ME, Koplin TJ, Simon U. Metal and metal oxide nanoparticles in chemiresistors: does the nanoscale matter? Small. 2006;2:36–50.

[20] Morrison SR. Selectivity in semiconductor gas sensors. Sensors and actuators. 1987;12:425–440.

[21] Prades J, Hernández-Ramírez F, Fischer T, Hoffmann M, Müller R, López N, et al. Quantitative analysis of CO-humidity gas mixtures with self-heated nanowires operated in pulsed mode. Applied Physics Letters. 2010;97:243105.

[22] Matsushima S, Teraoka Y, Miura N, Yamazoe N. Electronic interaction between metal additives and tin dioxide in tin dioxide-based gas sensors. Japanese Journal of Applied Physics. 1988;27:1798–1802.

[23] Yamazoe N. New approaches for improving semiconductor gas sensors. Sensors and Actuators B: Chemical. 1991;5:7–19.

[24] Schweizer-Berberich M, Zheng J, Weimar U, Göpel W, Barsan N, Pentia E, et al. The effect of Pt and Pd surface doping on the response of nanocrystalline tin dioxide gas sensors to CO. Sensors and Actuators B: Chemical. 1996;31:71–75.

[25] Hübner M, Koziej D, Grunwaldt J-D, Weimar U, Barsan N. An Au clusters related spill-over sensitization mechanism in SnO_2-based gas sensors identified by operando HERFD-XAS, work function changes, DC resistance and catalytic conversion studies. Physical Chemistry Chemical Physics. 2012;14:13249–13254.

[26] Yamazoe N, Sakai G, Shimanoe K. Oxide semiconductor gas sensors. Catalysis Surveys from Asia. 2003;7:63–75.

[27] Yamazoe N, Shimanoe K. New perspectives of gas sensor technology. Sensors and Actuators B: Chemical. 2009;138:100–107.

[28] Batzill M, Diebold U. The surface and materials science of tin oxide. Progress in Surface Science. 2005;79:47–154.

[29] Gercher VA, Cox DF, Themlin JM. Oxygen-vacancy-controlled chemistry on a metal oxide surface: methanol dissociation and oxidation on SnO_2 (110). Surface Science. 1994;306:279–293.

[30] Yamaguchi Y, Nagasawa Y, Shimomura S, Tabata K, Suzuki E. A density functional theory study of the interaction of oxygen with a reduced SnO_2 (110) surface. Chemical Physics Letters. 2000;316:477–482.

[31] Yamazoe N, Fuchigami J, Kishikawa M, Seiyama T. Interactions of tin oxide surface with O_2, H_2O and H_2. Surface Science. 1979;86:335–344.

[32] Barsan N, Weimar U. Conduction model of metal oxide gas sensors. Journal of Electroceramics. 2001;7:143–167.

[33] Yamazoe N, Shimanoe K. Receptor function and response of semiconductor gas sensor. Journal of Sensors. 2009;2009.

[34] Matsushima S, Maekawa T, Tamaki J, Miura N, Yamazoe N. New methods for supporting palladium on a tin oxide gas sensor. Sensors and Actuators B: Chemical. 1992;9:71–78.

[35] Liewhiran C, Tamaekong N, Wisitsoraat A, Tuantranont A, Phanichphant S. Ultra-sensitive H_2 sensors based on flame-spray-made Pd-loaded SnO_2 sensing films. Sensors and Actuators B: Chemical. 2013;176:893–905.

[36] Cabot A, Dieguez A, Romano-Rodrıguez A, Morante J, Barsan N. Influence of the catalytic introduction procedure on the nano-SnO_2 gas sensor performances: Where and how stay the catalytic atoms? Sensors and Actuators B: Chemical. 2001;79:98–106.

[37] Dieguez A, Vila A, Cabot A, Romano-Rodrıguez A, Morante J, Kappler J, et al. Influence on the gas sensor performances of the metal chemical states introduced by impregnation of calcinated SnO_2 sol–gel nanocrystals. Sensors and Actuators B: Chemical. 2000;68:94–99.

[38] Cabot A, Arbiol J, Morante JR, Weimar U, Barsan N, Göpel W. Analysis of the noble metal catalytic additives introduced by impregnation of as obtained SnO_2 sol–gel nanocrystals for gas sensors. Sensors and Actuators B: Chemical. 2000;70:87–100.

[39] Cabot A, Vila A, Morante J. Analysis of the catalytic activity and electrical characteristics of different modified SnO_2 layers for gas sensors. Sensors and Actuators B: Chemical. 2002;84:12–20.

[40] Lim CB, Oh S. Microstructure evolution and gas sensitivities of Pd-doped SnO_2-based sensor prepared by three different catalyst-addition processes. Sensors and Actuators B: Chemical. 1996;30:223–231.

[41] Xu CN, Tamaki J, Miura N, Yamazoe N. Nature of sensitivity promotion in Pd-loaded SnO_2 gas sensor. Journal of the Electrochemical Society. 1996;143:148–150.

[42] Koziej D, Hübner M, Barsan N, Weimar U, Sikora M, Grunwaldt J-D. Operando X-ray absorption spectroscopy studies on Pd-SnO_2 based sensors. Physical Chemistry Chemical Physics. 2009;11:8620–8625.

[43] Sakai Y, Kadosaki M, Matsubara I, Itoh T. Preparation of total VOC sensor with sensor-response stability for humidity by noble metal addition to SnO_2. Journal of the Ceramic Society of Japan. 2009;117:1297–1301.

[44] Koziej D, Barsan N, Shimanoe K, Yamazoe N, Szuber J, Weimar U. Spectroscopic insights into CO sensing of undoped and palladium doped tin dioxide sensors derived from hydrothermally treated tin oxide sol. Sensors and Actuators B: Chemical. 2006;118:98–104.

[45] Schmid W, Barsan N, Weimar U. Sensing of hydrocarbons and CO in low oxygen conditions with tin dioxide sensors: possible conversion paths. Sensors and Actuators B: Chemical. 2004;103:362–368.

[46] Xu CN, Tamaki J, Miura N, Yamazoe N. Correlation between gas sensitivity and crystallite size in porous SnO_2-based sensors. Chemistry Letters. 1990:441–444.

[47] Rothschild A, Komem Y. The effect of grain size on the sensitivity of nanocrystalline metal-oxide gas sensors. Journal of Applied Physics. 2004;95:6374–6780.

[48] Yamazoe N, Suematsu K, Shimanoe K. Gas reception and signal transduction of neat tin oxide semiconductor sensor for response to oxygen. Thin Solid Films. 2013;548:695–702.

[49] Yamazoe N, Shimanoe K. Theory of power laws for semiconductor gas sensors. Sensors and Actuators B: Chemical. 2008;128:566–573.

[50] Yamazoe N, Suematsu K, Shimanoe K. Extension of receptor function theory to include two types of adsorbed oxygen for oxide semiconductor gas sensors. Sensors and Actuators B: Chemical. 2012;163:128–135.

[51] Yamazoe N, Shimanoe K. Roles of shape and size of component crystals in semiconductor gas sensors II. Response to NO_2 and H_2. Journal of the Electrochemical Society. 2008;155:93–98.

[52] Vuong DD, Sakai G, Shimanoe K, Yamazoe N. Hydrogen sulfide gas sensing properties of thin films derived from SnO_2 sols different in grain size. Sensors and Actuators B: Chemical. 2005;105:437–442.

[53] Sakai G, Baik NS, Miura N, Yamazoe N. Gas sensing properties of tin oxide thin films fabricated from hydrothermally treated nanoparticles: dependence of CO and H_2 response on film thickness. Sensors and Actuators B: Chemical. 2001;77:116–121.

[54] Sakai G, Matsunaga N, Shimanoe K, Yamazoe N. Theory of gas-diffusion controlled sensitivity for thin film semiconductor gas sensor. Sensors and Actuators B: Chemical. 2001;80:125–131.

[55] Tamaki J, Nagaishi M, Teraoka Y, Miura N, Yamazoe N, Moriya K, et al. Adsorption behavior of CO and interfering gases on SnO_2. Surface Science. 1989;221:183–196.

[56] Egashira M, Nakashima M, Kawasumi S, Selyama T. Temperature programmed desorption study of water adsorbed on metal oxides. 2. Tin oxide surfaces. The Journal of Physical Chemistry. 1981;85:4125–4130.

[57] Watson J. The stannic oxide gas sensor. Sensor Review. 1994;14:20–23.

[58] Ghiotti G, Chiorino A, Martinelli G, Carotta M. Moisture effects on pure and Pd-doped SnO_2 thick films analysed by FTIR spectroscopy and conductance measurements. Sensors and Actuators B: Chemical. 1995;25:520–524.

[59] Martinelli G, Carotta M, Passari L, Tracchi L. A study of the moisture effects on SnO_2 thick films by sensitivity and permittivity measurements. Sensors and Actuators B: Chemical. 1995;26:53–55.

[60] Kim HR, Haensch A, Kim ID, Barsan N, Weimar U, Lee JH. The role of NiO doping in reducing the impact of humidity on the performance of SnO_2-based gas sensors: synthesis strategies, and phenomenological and spectroscopic studies. Advanced Functional Materials. 2011;21:4456–4463.

[61] Malyshev V, Pislyakov A. SnO_2-based thick-film-resistive sensor for H_2S detection in the concentration range of 1–10 mgm^{-3}. Sensors and Actuators B: Chemical. 1998;47:181–188.

[62] Fukui K KA. Improvement of humidity dependence in gas sensor based on SnO_2. Sensors and Actuators B: Chemical. 2000;65:316–318.

[63] Großmann K, Wicker S, Weimar U, Barsan N. Impact of Pt additives on the surface reactions between SnO_2, water vapour, CO and H_2; an operando investigation. Physical Chemistry Chemical Physics. 2013;15:19151–19158.

[64] Pavelko R, Vasiliev A, Llobet E, Vilanova X, Correig X, Sevastyanov V. The influence of wide range humidity on hydrogen detection with sensors based on nano-SnO_2 materials. Proceedings of the 13th International Symposium on Olfaction and Electronic Nose: AIP Publishing; 2009. 29–33.

[65] Pavelko R, Vasiliev A, Llobet E, Sevastyanov V, Kuznetsov N. Selectivity problem of SnO_2 based materials in the presence of water vapors. Sensors and Actuators B: Chemical. 2012;170:51–59.

[66] Smått JH, Linden M, Wagner T, Kohl CD, Tiemann M. Micrometer-sized nanoporous tin dioxide spheres for gas sensing. Sensors and Actuators B: Chemical. 2011;155:483–488.

[67] Capone S, Siciliano P, Quaranta F, Rella R, Epifani M, Vasanelli L. Moisture influence and geometry effect of Au and Pt electrodes on CO sensing response of SnO_2 microsensors based on sol–gel thin film. Sensors and Actuators B: Chemical. 2001;77:503–511.

[68] Harbeck S, Szatvanyi A, Barsan N, Weimar U, Hoffmann V. DRIFT studies of thick film un-doped and Pd-doped SnO_2 sensors: temperature changes effect and CO detection mechanism in the presence of water vapour. Thin Solid Films. 2003;436:76–83.

[69] Barsan N, Ionescu R. The mechanism of the interaction between CO and an SnO_2 surface: the role of water vapour. Sensors and Actuators: B Chemical. 1993;12:71–75.

[70] Hahn S, Barsan N, Weimar U, Ejakov S, Visser J, Soltis R. CO sensing with SnO_2 thick film sensors: role of oxygen and water vapour. Thin Solid Films. 2003;436:17–24.

[71] Pavelko RG, Daly H, Hardacre C, Vasiliev AA, Llobet E. Interaction of water, hydrogen and their mixtures with SnO_2 based materials: the role of surface hydroxyl groups in detection mechanisms. Physical Chemistry Chemical Physics. 2010;12:2639–2647.

[72] Emiroglu S, Barsan N, Weimar U, Hoffmann V. In situ diffuse reflectance infrared spectroscopy study of CO adsorption on SnO_2. Thin Solid Films. 2001;391:176–185.

[73] Ionescu R, Vancu A, Moise C, Tomescu A. Role of water vapour in the interaction of SnO_2 gas sensors with CO and CH_4. Sensors and Actuators B: Chemical. 1999;61:39–42.

[74] Ménini P, Parret F, Guerrero M, Soulantica K, Erades L, Maisonnat A, et al. CO response of a nanostructured SnO_2 gas sensor doped with palladium and platinum. Sensors and Actuators B: Chemical. 2004;103:111–114.

[75] Căldăraru M, Sprinceana D, Popa V, Ionescu N. Surface dynamics in tin dioxide-containing catalysts II. Competition between water and oxygen adsorption on polycrystalline tin dioxide. Sensors and Actuators B: Chemical. 1996;30:35–41.

[76] Dai Z, Xu L, Duan G, Li T, Zhang H, Li Y, et al. Fast-response, sensitivitive and low-powered chemosensors by fusing nanostructured porous thin film and IDEs-microheater chip. Scientific Reports. 2013;3.

[77] Simon I, Barsan N, Bauer M, Weimar U. Micromachined metal oxide gas sensors: opportunities to improve sensor performance. Sensors and Actuators B: Chemical. 2001;73:1–26.

[78] Gong J, Chen Q, Fei W, Seal S. Micromachined nanocrystalline SnO_2 chemical gas sensors for electronic nose. Sensors and Actuators B: Chemical. 2004;102:117–125.

[79] Han CH, Han SD, Singh I, Toupance T. Micro-bead of nano-crystalline F-doped SnO_2 as a sensitive hydrogen gas sensor. Sensors and Actuators B: Chemical. 2005;109:264–269.

[80] Moon S, Lee H, Choi N, Lee J, Choi C, Yang W, et al. Low power consumption micro C_2H_5OH gas sensor based on micro-heater and screen printing technique. Sensors and Actuators B: Chemical. 2012;187:814–817.

[81] Sun YF, Liu SB, Meng FL, Liu JY, Jin Z, Kong LT, et al. Metal oxide nanostructures and their gas sensing properties: a review. Sensors. 2012;12:2610–2631.

[82] Elmi I, Zampolli S, Cozzani E, Mancarella F, Cardinali G. Development of ultra-low-power consumption MOX sensors with ppb-level VOC detection capabilities for emerging applications. Sensors and Actuators B: Chemical. 2008;135:342–351.

[83] Jaegle M, Wöllenstein J, Meisinger T, Böttner H, Müller G, Becker T, et al. Micromachined thin film SnO_2 gas sensors in temperature-pulsed operation mode. Sensors and Actuators B: Chemical. 1999;57:130–134.

[84] Guo B, Bermak A, Chan PC, Yan GZ. A monolithic integrated 4 × 4 tin oxide gas sensor array with on-chip multiplexing and differential readout circuits. Solid-State Electronics. 2007;51:69–76.

[85] Mitzner KD, Sternhagen J, Galipeau DW. Development of a micromachined hazardous gas sensor array. Sensors and Actuators B: Chemical. 2003;93:92–99.

Chapter 2

Effect of Water Vapor on Pd-Loaded SnO_2 Nanoparticles Gas Sensor

In this chapter, Pd-loaded SnO_2 were synthesized by impregnating method using $Pd(NH_3)_2(NO_2)_2$ precursor solution and hydrothermally prepared SnO_2 nanoparticles. The effect of water vapor on Pd-loaded SnO_2 sensor was studied by investigating the oxygen adsorption behavior and gas sensing properties toward hydrogen and carbon monoxide under humid condition. The suppression effect of Pd on water vapor poisoning in Pd-loaded SnO_2 gas sensors was further clarified.

2.1 Introduction

Humidity is one of the most important considerations in the practical use of sensors, which deteriorates the sensitivity of sensors seriously.[1-5] Even though many corresponding researches have been performed to explain this phenomenon to further reduce the water vapor poisoning effect on the sensor performance,[2, 4-7] the reaction mechanisms of how the water vapor interferes with the detection of the target gas are still not yet clarified in detail.

It is well-known that Pd is one of the most effective receptors not only for enhancing the sensitivity but also for suppressing the water vapor poisoning.[2, 6, 8] Generally, it is explained by the chemical and sensitization effects toward the role of Pd in the gas sensing process.[9, 10] However, the effect of Pd in wet atmosphere is still not clarified enough. Yamazoe et al.[4, 5, 7] proposed that the adsorbed oxygen species was influenced by water vapor in the case of neat SnO_2, from O^{2-} in dry atmosphere changed to O^- in humid atmosphere, resulting in the decrease of sensor response in wet atmosphere. Such findings motivated us to study the oxygen adsorption behavior and gas sensing properties of Pd-loaded SnO_2 under humid condition. Therefore, the oxygen adsorption behavior of SnO_2 and Pd-loaded SnO_2 was investigated in different humid atmospheres, and the

adsorbed oxygen species on the surface was confirmed by power laws. Additionally the gas sensing properties to H_2 and CO were studied in dry and wet atmospheres. The role of Pd in the gas sensing process in humid atmosphere was further clarified.

2.2 Experimental

2.2.1 Synthesis of Pd-loaded SnO_2 nanoparticles

A list of chemicals used in the experiment is shown in Table 2-1. The preparation process of SnO_2 nano-particles can be described as follow: $SnCl_4 \cdot 5H_2O$ aqueous solution (1 mol/L, 100 ml) was slowly dropped into NH_4HCO_3 solution (1 mol/L, 500 ml) with stirring. The resulting precipitate was centrifuged (6000 rpm, 10 min, 25 ℃) and washed with NH_4NO_3 solution (1 mol/L) several times to remove Cl^- ions. After checking by $AgNO_3$ solution and confirming no Cl^- ions residual, the precipitate was centrifuged in high speed (10000 rpm, 10 min, 25 ℃) and washed by deionized water 2 times to eliminate the NH_4NO_3. Then the gel was hydrothermally treated in an ammonia solution (pH = 10.5) under the pressure of 10 MPa at 200 ℃ for 3 h. The obtained SnO_2 sol was dried at 120 ℃ until the water was completely evaporated, and then heat-treated at 600 ℃ in oxygen atmosphere.

Table 2-1 A full List of Chemicals Used in the Experiment

chemicals	chemical formula	purity / %	chemical company
Tin chloride penta-hydrate	$SnCl_4 \cdot 5H_2O$	98	Sigma-Aldrich Co., Ltd., USA
Ammonium bicarbonate	NH_4HCO_3	99	Wako Co., Ltd., Japan
Ammonium nitrate	NH_4NO_3	99	Kishida Chemical Co., Ltd., Japan
Ammonia	NH_3	28	Kishida Chemical Co., Ltd., Japan
α-terpineol	$C_{10}H_{18}O$	98	Wako Co., Ltd., Japan
Hydrogen peroxide	H_2O_2	30	Kishida Chemical Co., Ltd., Japan
Palladium diammine nitrite	$Pd(NH_3)_2(NO_2)_2$	5	Strem Chemicals Co., Ltd., USA

To load Pd particles on the SnO_2 surface, the SnO_2 powder was dispersed in deionized water and then impregnated with $Pd(NH_3)_2(NO_2)_2$ aqueous solution under ultrasonic vibration for 1 h, followed by ammonia solution treatment (pH =

9.5), filtration, drying at 120 ℃ and heat-treatment at 500 ℃ in air. The material preparation process was shown in Fig. 2-1.

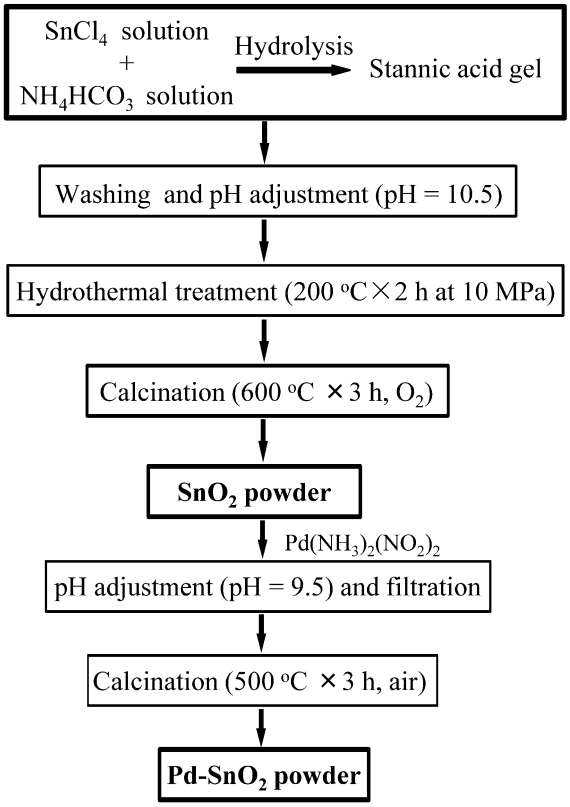

Figure 2-1 Flowchart for the preparation of Pd-loaded SnO_2 powder.

2.2.2 Characterization of materials

The loading amount of Pd was determined by energy-dispersive X-ray fluorescence spectrometer (XRF, EDX-800, Shimadzu, Japan). The crystal structure of powders was analyzed by X-ray diffraction with copper Kα radiation (λ = 1.5418 Å) filtered through a Ni foil (XRD, RINT 2100, Rigaku, Japan). The crystallite sizes of powders were calculated from XRD peaks by the Scherrer equation,

$$D = k \cdot \lambda / \beta \cos\theta \qquad [2\text{-}1]$$

Where D is the mean crystallite size, k is a constant (0.9), λ is the wavelength of the X-ray (1.5418 Å), β is the full width at half maximum of the peak, and the θ is the center angle of the peak.

Specific surface area and peak pore radius were measured by surface area analyzer (BET, Belsorp, BEL, Japan). The microstructure was observed by transmission electron microscopy (TEM) and high resolution TEM (HRTEM) (Tecnai-F20, FEI, US).

CO pulse adsorption method was used to decide the Pd particle size, dispersion state, and Pd surface area on SnO_2 in this study (BEL-CAT, BEL, Japan), which is one of the effective methods to investigate the distribution state of catalyst on supporting materials.[11-13] It was conducted on the quartz tube reactor, and the effluent gas was monitored by online quadrupole mass spectroscopy. Powders (25 mg) were pretreated at 400 ℃ for 5 min in a flow of air to remove the impurities on the surface, and then cooled to 40 ℃. After exposing to He for 5 min, the sample was heated to 80 ℃ in a flow of 5% H_2/N_2 to reduce the PdO to Pd, followed by flushing with He for 10 min. Then 1% CO/N_2 was pulse-injected into the reactor system after the temperature was reduced to 40 ℃. The pretreatment and measurement process of CO pulse adsorption was shown in Fig. 2-2. The stoichiometry of one CO molecule per one Pd atom on the surface of Pd particle was used for the calculation of Pd dispersion. The Pd particle size was calculated by using the equation $d = 6V/S$, where V and S indicate the volume and surface area of Pd, respectively. In this experiment, CO pulse adsorption measurement was also conducted on neat SnO_2. It was found that no CO adsorbed on the surface of neat SnO_2.

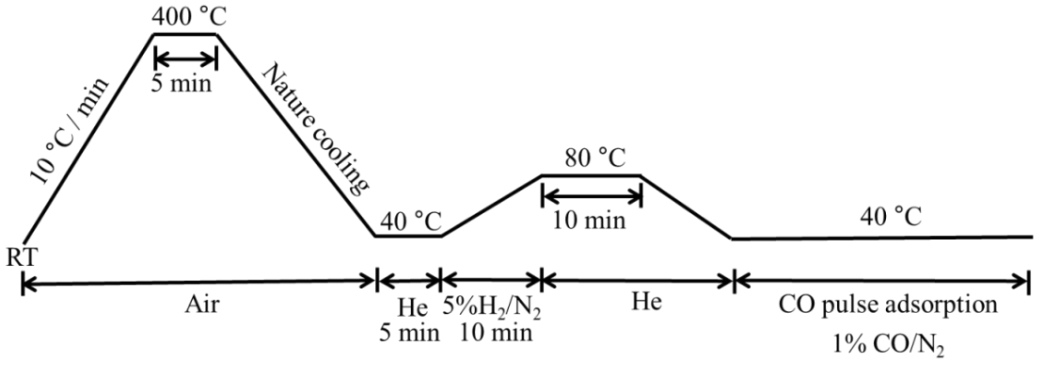

Figure 2-2 Procedures for pretreatment and measurement of CO pulse adsorption.

The temperature programmed reduction (TPR) measurement was carried out with 1000 ppm H_2/N_2 and CO/N_2. Prior to the experiment, 50 mg of powder was calcined at 400 ℃ for 30 min with a heating rate of 10 ℃/min in air, then cooled to 50 ℃. After the powder was He-purged for 10 min, the TPR experiment was performed with H_2/N_2 and CO/N_2 respectively, the temperature being increased from 50 to 500 ℃ with a ramp of 10 ℃/min. Figure 2-3 shows the procedure of pretreatment and measurement for TPD. Thermal conductivity detector (TCD) and mass spectrometer (MS) were employed to monitor the H_2 consumption, H_2O, and CO_2 emission.

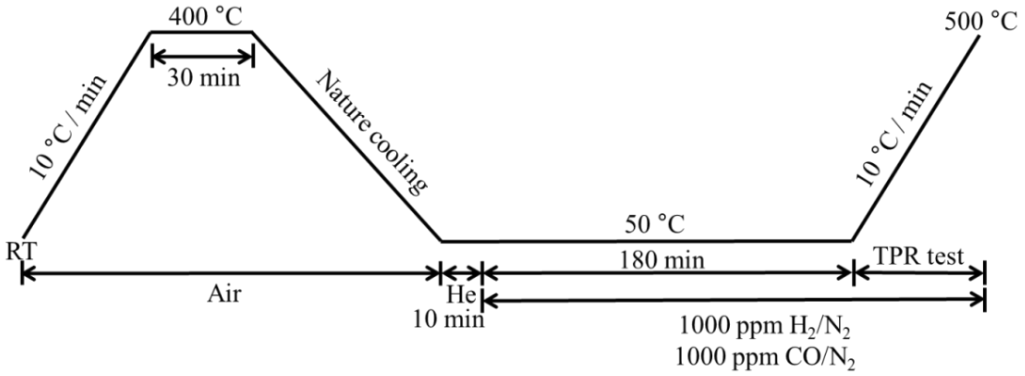

Figure 2-3 Procedure for pretreatment and TPR measurement.

2.2.3 Fabrication of gas sensor devices

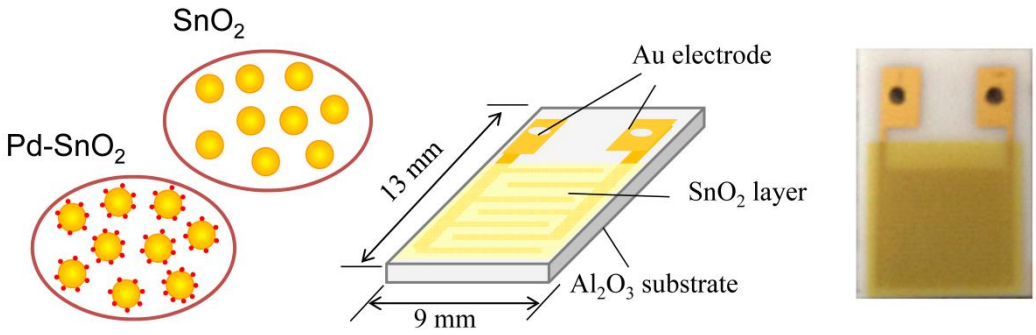

Figure 2-4 Schematic diagram and photograph for sensor device.

Sensing films were prepared by screen printing on an alumina substrate (9 × 13 × 0.38 mm^3) attached with Au electrodes (line width: 180 μm, distance between lines: 90 μm, sensing area: 64 mm^2). The Au electrodes were

screen-printed on the alumina substrate using Au paste, and then heat-treated at 850 ℃ in air for 3 h. Aqueous solution mixed with 100 ml deionized water, 10 ml H_2O_2 and 2 ml NH_3 was used to wash the substrate with Au electrodes at 80 ℃ for 30 min. The obtained powders were mixed with an appropriate amount of α-terpineol to form uniform paste, and then screen-printed on the alumina substrate with Au electrodes. Schematic diagram and photograph of sensor device are shown in Fig. 2-4. The resulting devices were heat-treated at 580 ℃ for 3 h in air to remove the organic binder and stabilize the sensing layer.

2.2.4 Measurement of gas sensing properties

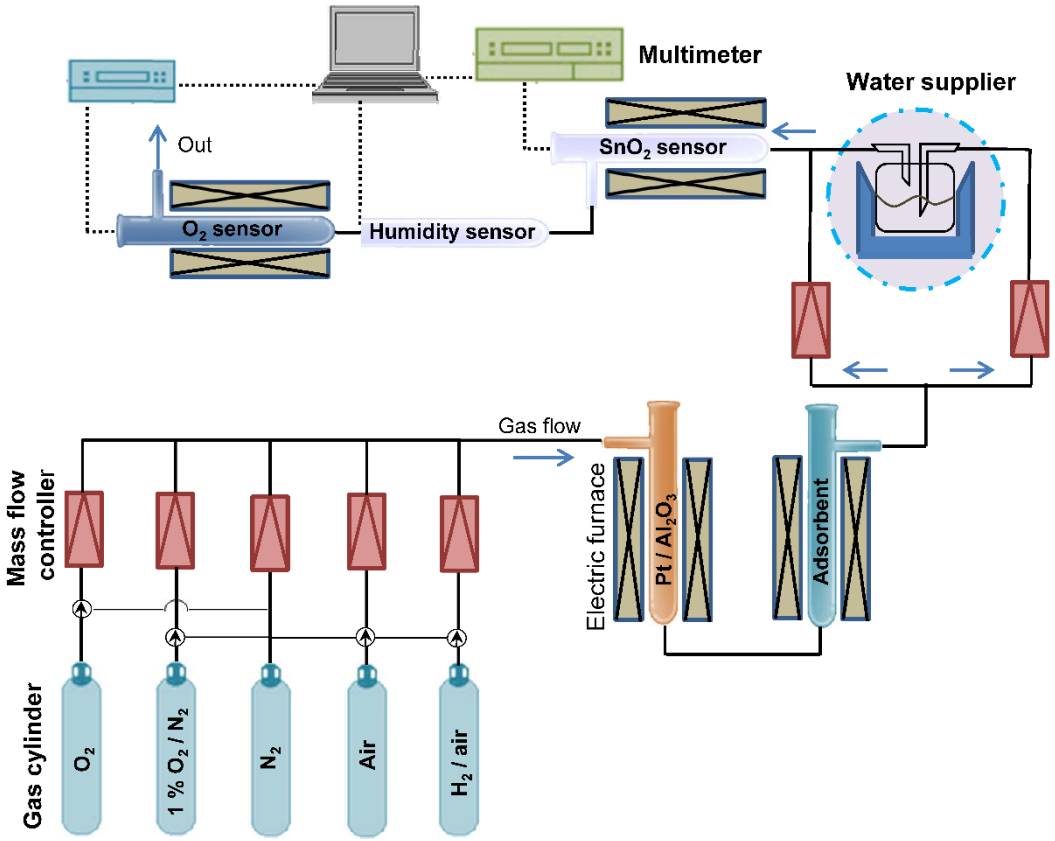

Figure 2-5 Schematic diagram of gas sensing measurement system.

The measurements were carried out in a conventional gas flow apparatus equipped with an electric furnace, as shown in Fig. 2-5. The total gas flow rate was precisely controlled to 80 cm^3/min by mass flow controllers (MFC). Before the sensing test, gases (air, O_2 and N_2) were pretreated by catalyst Pt/Al_2O_3 (5

wt%, Wako Co., Ltd., Japan) and zeolite (5A 1/16, Wako Co., Ltd., Japan) to remove impurity gases (such as CO and hydrocarbon) and water, respectively. The water vapor was controlled strictly by using a set of humidity supplier and humidity sensor system (TR-77Ui, T&D Corporation, Japan). The oxygen partial pressure was measured by an oxygen sensor (zirconia oxygen cell) operated at 750 ℃. A multimeter (Model 2701, Keithley Instruments Inc.) was connected to the sensor to monitor the electric resistance. The DC voltage of 4 V was applied to the series circuit of a standard resistor and the sensor device, and the voltage across the standard resistor was measured by multimeter to evaluate the electric resistance of the sensor devices.

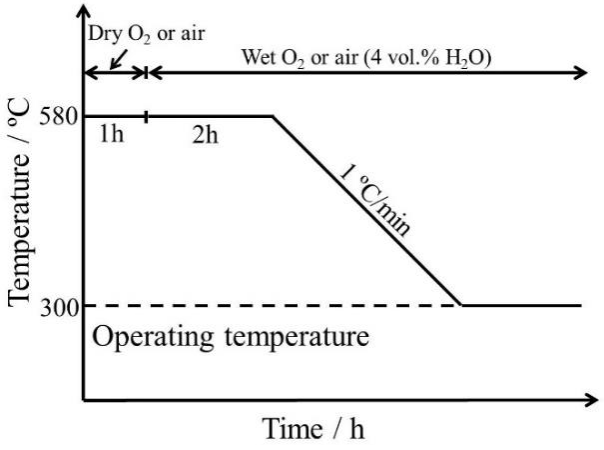

Figure 2-6 Pretreatment process before sensing properties measurement.

Prior to measurements, sensors were pretreated at 580 ℃ for 1 h in dry atmosphere to eliminate the impurities that adsorbed at low temperature. To reach to an equilibrium of water vapor adsorption, the sensors were treated at 580 ℃ for 2 h after introducing water vapor (4 vol.% H_2O), and then the temperature was reduced gradually to 350 or 300 ℃ with keeping the same humidity. After the electric resistance became stable, the humidity changed to the designated amount. The detailed pretreatment process was shown in Fig. 2-6. The oxygen adsorption behavior and gas sensing properties to H_2 and CO were measured in humidity of 0−4 vol.% H_2O. The sensor response (S) was defined as the ratio of the electric resistance in synthetic air (Ra) and in hydrogen gas (Rg).

2.3 Results and Discussion

2.3.1 Materials characterization

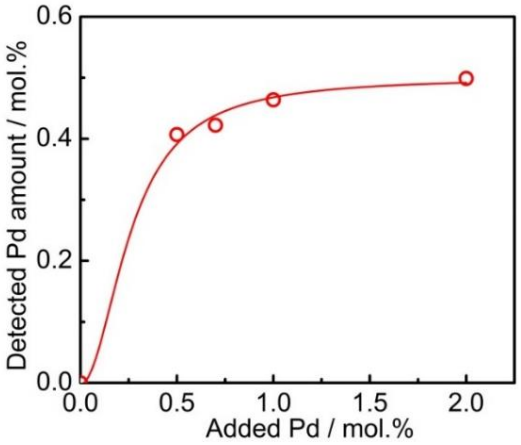

Figure 2-7 Pd loading amount as a function of the precursor concentration.

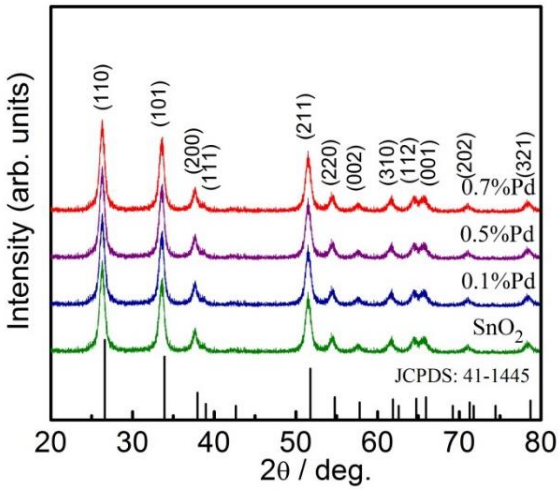

Figure 2-8 X-ray diffraction patterns of SnO_2 and Pd-loaded SnO_2.

Figure 2-7 shows the Pd loading amount as a function of the precursor concentration. The Pd loading amount reached a saturation level when the precursor concentration increased to 0.7 mol.%. This precursor solution gives a very small Pd particle, as mentioned later, but the Pd particles seem to easily disperse in solution because the adhesion to SnO_2 surface is weak. Therefore, most of the Pd species was dispersed in solution when the Pd precursor concentration was above 0.7 mol.%, and it was removed by filtration process.

Figure 2-8 shows the XRD patterns of SnO_2 and Pd-loaded SnO_2 (0.1, 0.5, 0.7 mol.%). It was demonstrated that all the samples exhibited the same tetragonal phase (JCPDS: 41−1445). No phase corresponding to Pd or PdO was detected in the Pd-loaded SnO_2 powders due to extremely low Pd amount.

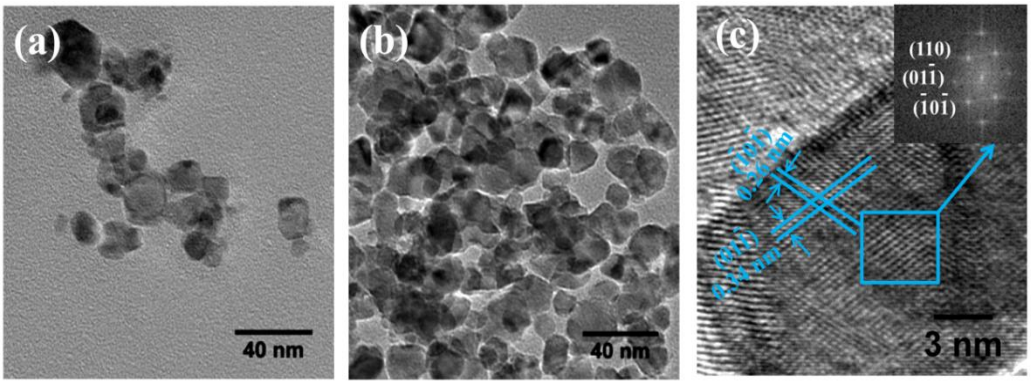

Figure 2-9 TEM images of SnO_2 (a) and 0.7% Pd-SnO_2 (b); HRTEM image of 0.7%Pd-SnO_2 (c); the fast Fourier transform (inset).

Table 2-2 Specific Surface Area of SnO_2 and 0.7% Pd-SnO_2, as well as Pd Amount, Particle Size, Dispersion and Surface Area of Pd on SnO_2 for 0.7% Pd-SnO_2

sample	specific surface area (m^2/g)	Pd amount (mol.%)	particle size of Pd (nm)	dispersion of Pd (%)[a]	surface area of Pd (m^2/g)
SnO_2	27.1	—	—	—	—
0.7%Pd	27.1	0.42	2.6	43	0.65

[a] Dispersion of Pd was defined as the ratio of Pd atoms available for CO chemisorption to the total Pd atoms.

Figure 2-9 is the TEM images of SnO_2 and 0.7% Pd-SnO_2. Clearly, Pd-loaded SnO_2 maintained the same morphology as neat SnO_2 particles. The particle size of SnO_2 and 0.7% Pd-SnO_2 was almost the same, ca. 15 nm. The interplanar spacing of 0.34 and 0.26 nm corresponded to $(01\bar{1})$ and $(\bar{1}0\bar{1})$ planes in a tetragonal SnO_2 structure, respectively. The fast Fourier transform pattern indicated a good single crystalline quality. However, no Pd or PdO clusters were directly observed by HRTEM even when the Pd loading amount reached 0.7 mol.%. Because the Pd loading amount was extremely low, it is presumed that no large Pd or PdO cluster was formed on the SnO_2 surface. It has

been reported that Pd tends to form clusters of PdO on the SnO_2 surface if Pd-loaded SnO_2 powder was prepared by the wet impregnating method.[14] On the other hand, the atomic numbers of Pd and Sn are very close (46 and 50, respectively), which leads to a difficulty in distinguishing the Pd phase on the SnO_2 background.[15] To overcome such difficulty, Pd characteristics on the SnO_2 surface were investigated by CO pulse chemisorption method. Table 2-2 shows particle size, distribution, and surface area of Pd on SnO_2 for 0.7% Pd-loaded SnO_2. It was found that calculated particle size of Pd was 2.6 nm, and the particles were finely dispersed on the surface of SnO_2.

Table 2-3 Average Crystallite Size, Specific Surface Area and Peak Pore Radius for Neat SnO_2 and Pd-Loaded SnO_2

Sample	Average crystallite size (nm)	Specific surface area (m^2/g)	Peak pore radius (nm)
SnO_2	11.7	27.1	9
0.1%Pd-SnO_2	11.9	28.3	8
0.5%Pd-SnO_2	11.6	27.8	9
0.7%Pd-SnO_2	11.8	27.1	8

The crystallite size, specific surface area and peak pore radius of SnO_2 and Pd-loaded SnO_2 powders are summarized in Table 2-3. It was found that Pd had no significant effect on the SnO_2 crystallite size. The crystallite sizes calculated from the (110) peak by the Scherrer equation were almost the same for SnO_2 and Pd-SnO_2 powders, about 12 nm. Furthermore, the specific surface area and peak pore radius of all the powders had not much difference. It is well-known that the morphology of powders, especially the crystallite size, influences the sensor response more greatly.[16] On the basis of above results, it was found that Pd loading did not change the morphology of SnO_2. Thus, we can eliminate the influence of morphology to the sensor response and only focus on the effect of Pd on the sensing properties.

2.3.2 Oxygen adsorption behavior in different humidity

Figure 2-10 shows the electric resistance change with water vapor concentration in air at 300 and 350 ℃. The electric resistance of all the sensors was reduced drastically in the presence of small amount of water vapor. However, the change tended to become small at 350 ℃. As for it, it is thought that the surface hydroxyl group is desorbed at 350 ℃ as shown in the report of Yamazoe.[17] Interestingly the electric resistances of 0.7% Pd-SnO_2 were about 40 and 6 times higher than those of neat SnO_2 at 300 and 350 ℃, respectively, in wet atmosphere. Obviously, the reduction of electric resistance in wet atmosphere was effectively suppressed by loading Pd. Additionally the electric resistance was increased with raising Pd loading amount in wet atmosphere. So far, it is well-known that Pd loading to SnO_2 gives high electric resistance and sensor response because of electronic sensitization by junction of P-type PdO and N-type SnO_2.[18] However, the effect in wet atmosphere is not clarified enough. Therefore, on the basis of results, neat SnO_2 and 0.7% Pd-SnO_2 sensors were used to investigate the oxygen adsorption behavior and sensor response to H_2 and CO in different humidity.

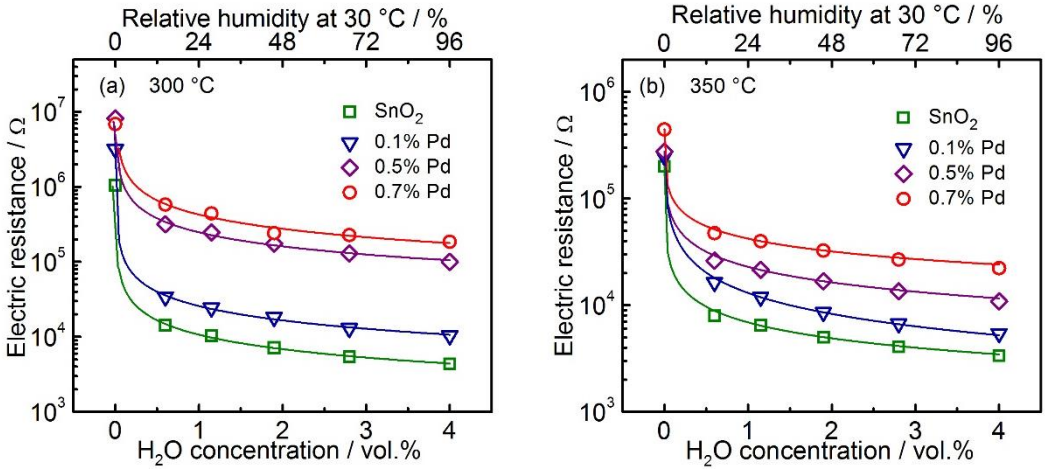

Figure 2-10 Electric resistance in different humidity air for neat SnO_2 and Pd-loaded SnO_2 at 300 ℃ (a) and 350 ℃ (b).

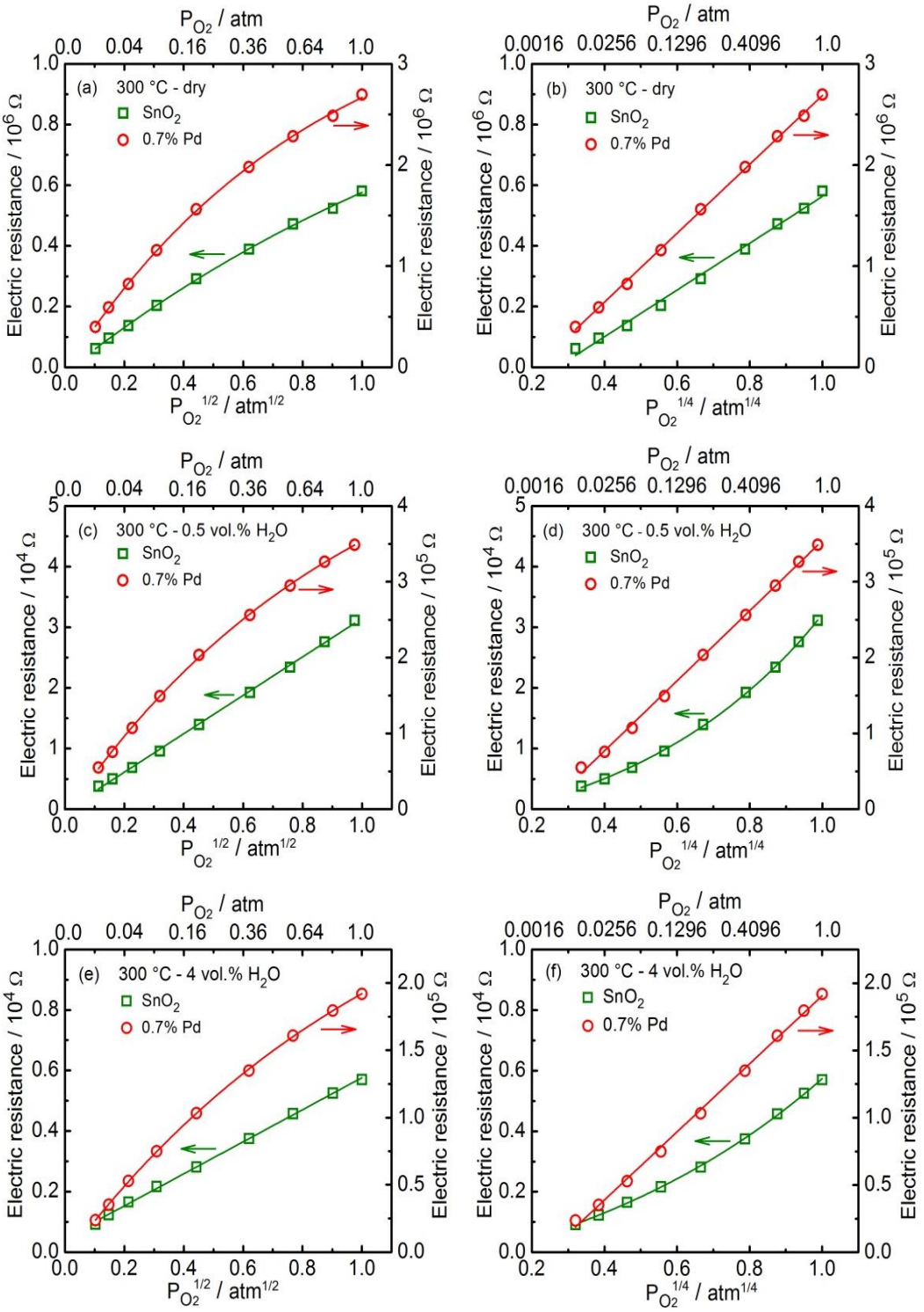

Figure 2-11 Dependence of the resistance on the $P_{O2}^{1/4}$ and $P_{O2}^{1/2}$ at 300 ℃: (a, b) dry; (c, d) 0.5 vol.% H_2O; (e, f) 4 vol.% H_2O.

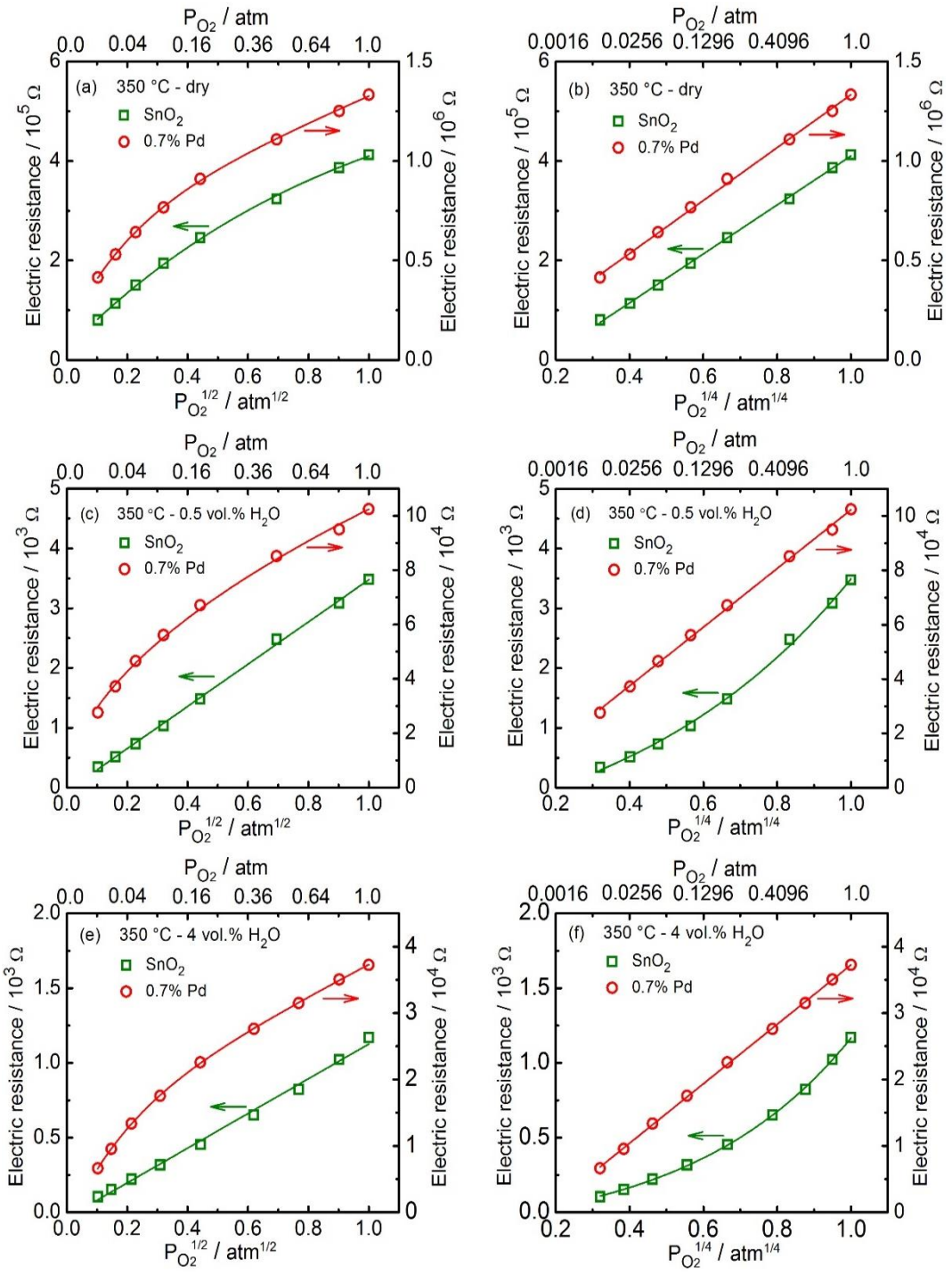

Figure 2-12 Dependence of the resistance on the $P_{O2}^{1/4}$ and $P_{O2}^{1/2}$ at 350 ℃: (a, b) dry; (c, d) 0.5 vol.% H_2O; (e, f) 4 vol.% H_2O

Figure 2-11 shows the dependence of electric resistance on oxygen partial pressure at 300 ℃ in dry and wet atmospheres. In dry atmosphere, the electric resistances of both neat SnO_2 and 0.7% Pd-SnO_2 were linearly proportional to

$P_{O2}^{1/4}$ in the measured range (Fig. 2-12b). Such a linear relationship agreed with the theoretical Equation 1-4, indicating the adsorbed oxygen species was O^{2-}. However, with increasing humidity to 0.5 vol.% H_2O (Fig. 2-12c, d), the dependence of electric resistance on oxygen partial pressure was changed for neat SnO_2. And the electric resistance was linearly proportional to $P_{O2}^{1/2}$, meaning that the oxygen adsorption species was changed from O^{2-} to O^- in wet atmosphere. The results were in agreement with the previous report for neat SnO_2.[5] O^{2-} was only formed in dry atmosphere, and it was strongly suppressed by adsorbed OH^- group even in low humidity atmosphere, thus leaving O^- as the mainly adsorbed oxygen species. On the other hand, oxygen adsorption behavior for 0.7% Pd-SnO_2 sensor in humidity of 0.5 vol.% H_2O was completely different from those for neat SnO_2; that is, a linear proportion of electric resistance to $P_{O2}^{1/4}$ was observed. It seems the mainly adsorbed oxygen species had no change from dry to wet atmosphere, adsorbing as O^{2-}. In high humidity of 4 vol.% H_2O (Fig. 2-12e, f), SnO_2 and 0.7% Pd-SnO_2 showed the same oxygen adsorption behavior as that in humidity of 0.5 vol.% H_2O. In addition, such a behavior of electrical resistance to oxygen partial pressure was observed even at 350 ℃ as shown in Fig. 2-12. From these results, it seems the sensing model at 350 ℃ is almost the same as that at 300 ℃ although the degree of change in electric resistance under humid condition is different.

2.3.3 Sensor response to H_2 and CO in different humidity

The sensor response to 600 ppm H_2 and CO in different humidity at 300 and 350 ℃ is shown in Fig. 2-13. In dry atmosphere, neat SnO_2 showed maximum sensor response to H_2 and CO at both 300 and 350 ℃ because such inflammable gases directly combusted on the surface of thick film by catalyzing of Pd at high temperature and did not diffuse into the vicinity of the electrode.[17-19] With increase in operating temperature to 350 ℃, such oxidation becomes active, and the sensor response to H_2 was even deteriorated for neat SnO_2 and 0.7% Pd-SnO_2. However, the sensor response to CO for neat SnO_2 and 0.7% Pd-SnO_2 was increased with increase in operating temperature because of the CO reaction activity different from H_2. The most interesting characteristic is sensor response

under humid condition. The sensor response of both SnO_2 and 0.7 % Pd-SnO_2 was reduced in the presence of small amount of water vapor, but the reduction level of sensor response for 0.7% Pd-SnO_2 in wet atmosphere was significantly different from that of neat SnO_2. The sensor response to H_2 and CO decreased seriously for neat SnO_2 in wet atmosphere, whereas H_2 response decreased only 3 times, and CO response decreased even lower by loading Pd. In addition, the change of sensor response in the range of 0.5 to 4 vol.% H_2O were very small for 0.7% Pd-SnO_2, especially in the case operated at 350 ℃. Obviously Pd loading inhibited the decrease of sensor response in wet atmosphere, resulting in a much higher sensor response for 0.7% Pd-SnO_2.

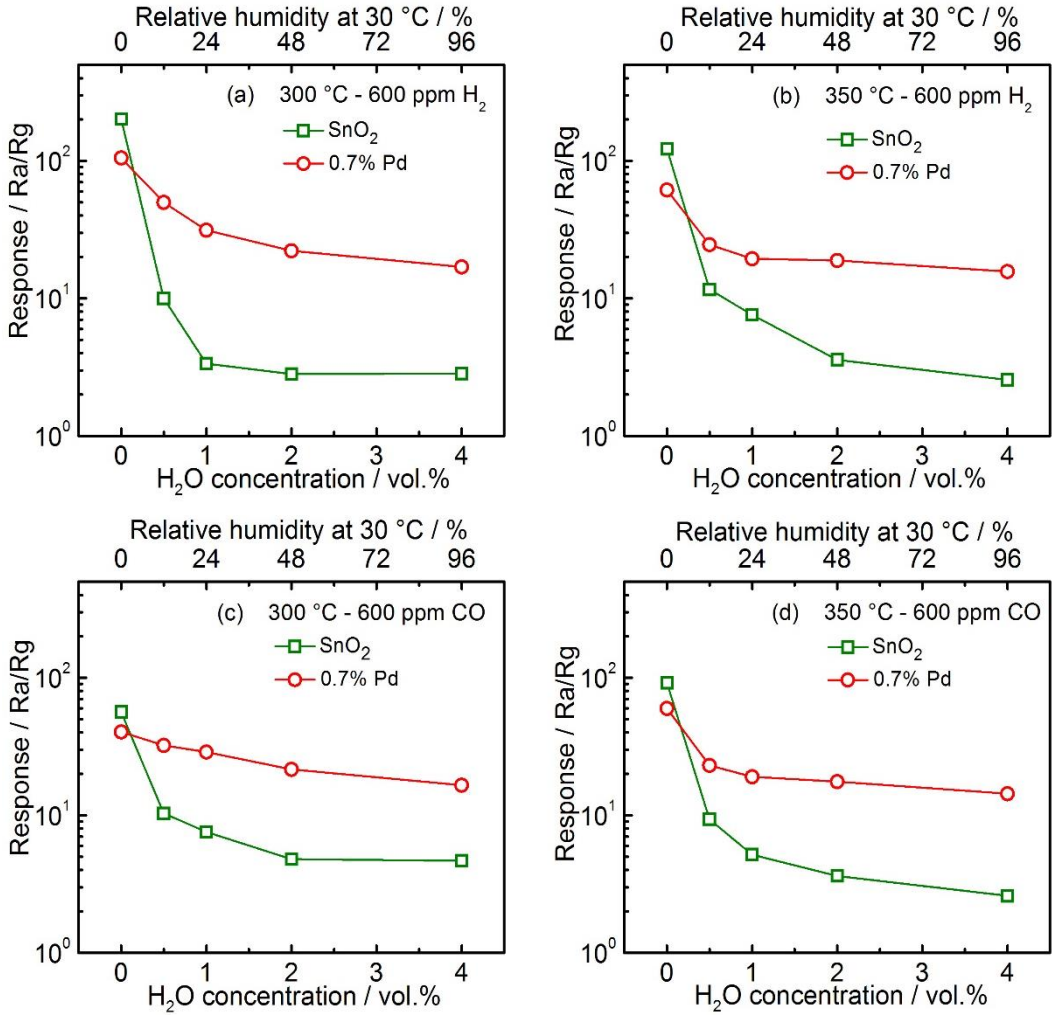

Figure 2-13 Sensor response to 600 ppm H_2 (a, b) and 600ppm CO (c, d) for SnO_2 and 0.7% Pd-SnO_2 in different humidity at 300 and 350 ℃.

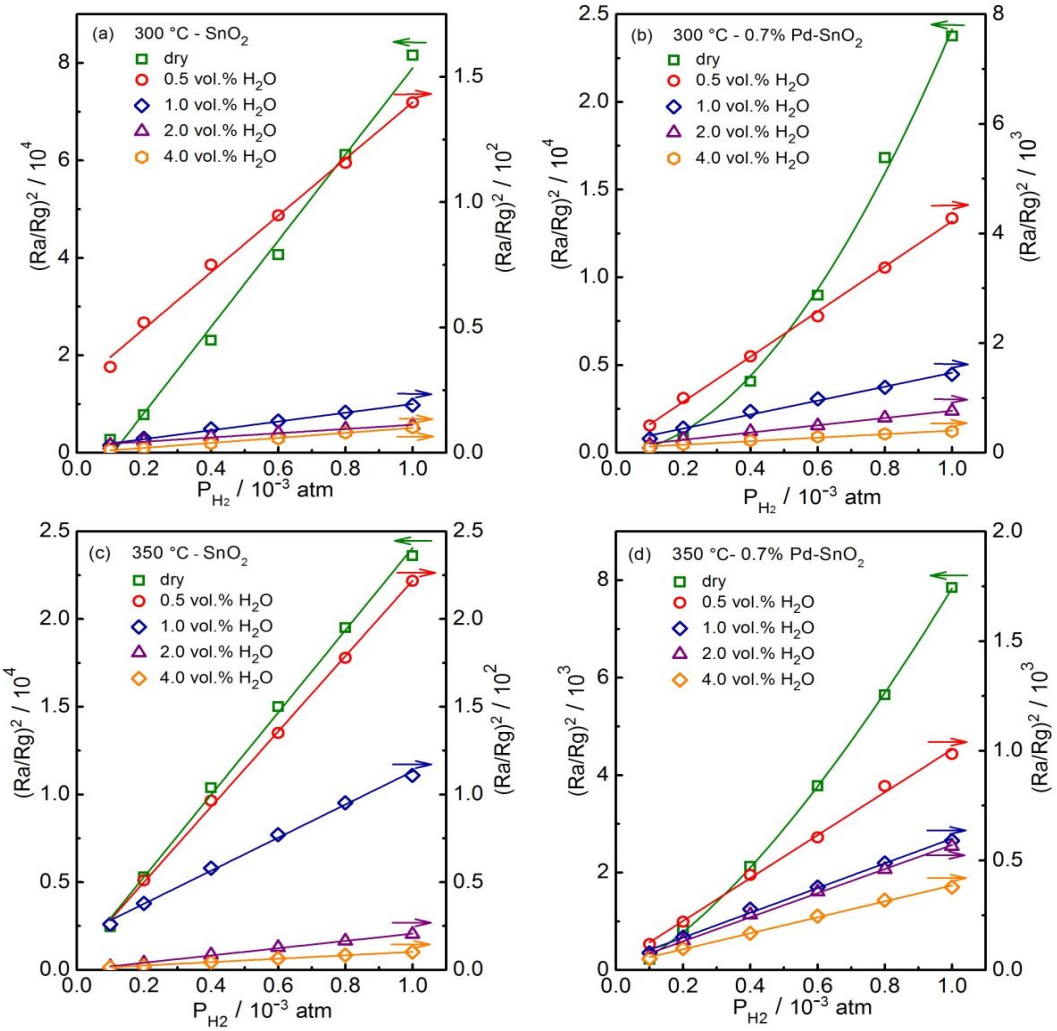

Figure 2-14 Relationship between the sensor response and the H_2 partial pressure for neat SnO_2 and 0.7% Pd-SnO_2 at 300 ℃ (a, b) and 350 ℃ (c, d) in different humidity.

Figures 2-14 and 2-15 show the square of the sensor response as a function of the H_2 and CO partial pressure for neat SnO_2 and 0.7% Pd-SnO_2 in different humidity. According to the theoretical Equations 1-5 and 1-6, the square of sensor response to H_2 and CO should have the linear relationship with the gas partial pressure for neat SnO_2 and 0.7% Pd-SnO_2 in both dry and wet atmosphere. In Figure 2-14a, c, a good linearity of $(Ra/Rg)^2$ to the P_{H2} was observed for neat SnO_2 in both dry and wet atmosphere, which was in agreement with Equation 1-5 and 1-6. H_2 reacted with adsorbed oxygen species O^{2-} and O^- as reported previously.[5] On the other hand, 0.7% Pd-SnO_2 sensor showed a nonlinear fit of

$(Ra/Rg)^2$ with P_{H2} in dry atmosphere although it showed a good linearity of $(Ra/Rg)^2$ to the P_{H2} in wet atmosphere. Such behavior was observed for not only H_2 but also CO, as shown in Fig. 2-15. Currently the reason why a nonlinear fit of $(Ra/Rg)^2$ with P_{H2} in dry atmosphere occurs is not clear well, but it is supposed that reactivity of PdO related to such a behavior. The details should be investigated more. For 0.7% Pd-SnO_2, the important point is that an adsorption species such as O^{2-} exists under humid condition.

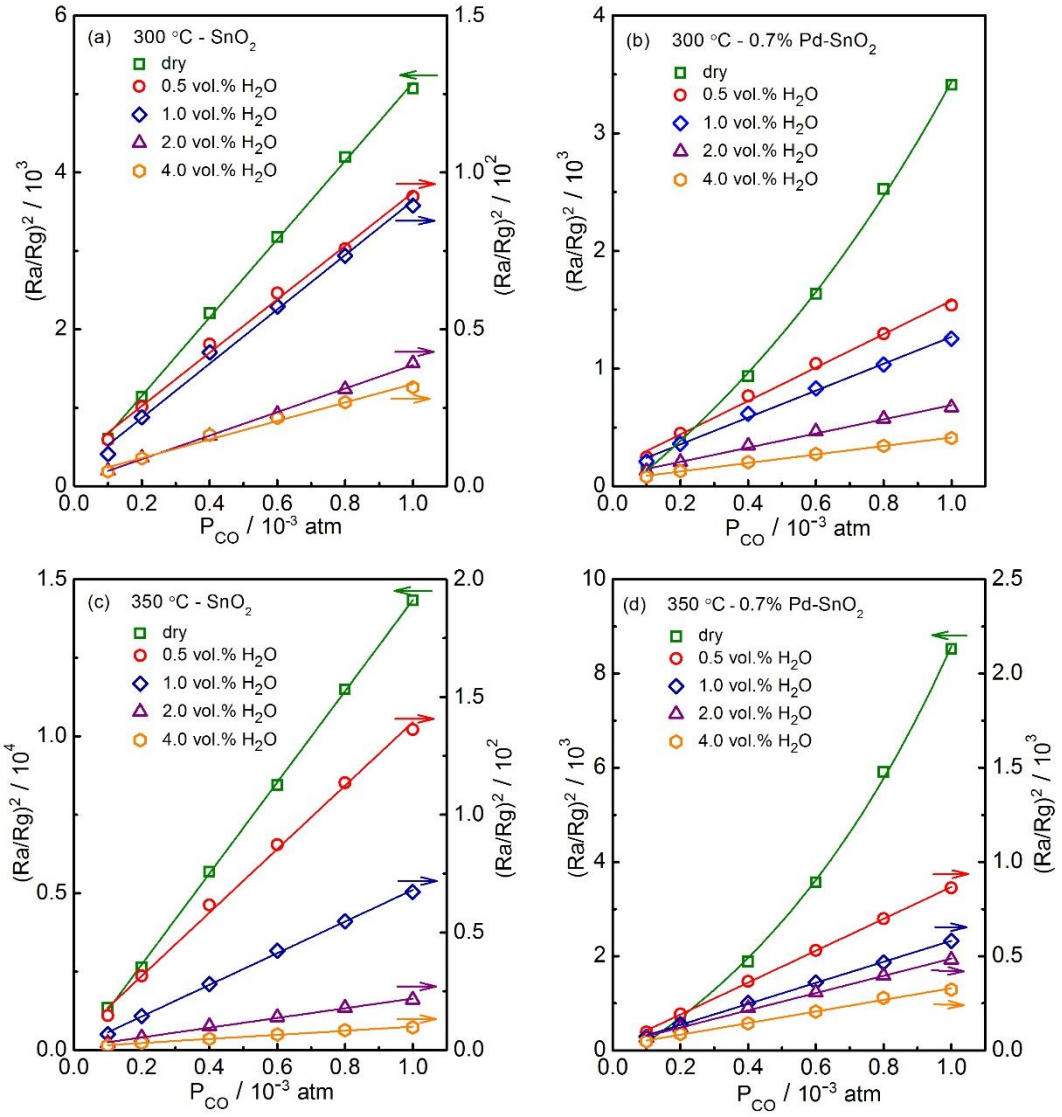

Figure 2-15 Relationship between the sensor response and the CO partial pressure for neat SnO_2 and 0.7% Pd-SnO_2 at 300 ℃ (a, b) and 350 ℃ (c, d) in different humidity.

2.3.4 TPR measurements of neat SnO_2 and Pd-loaded SnO_2

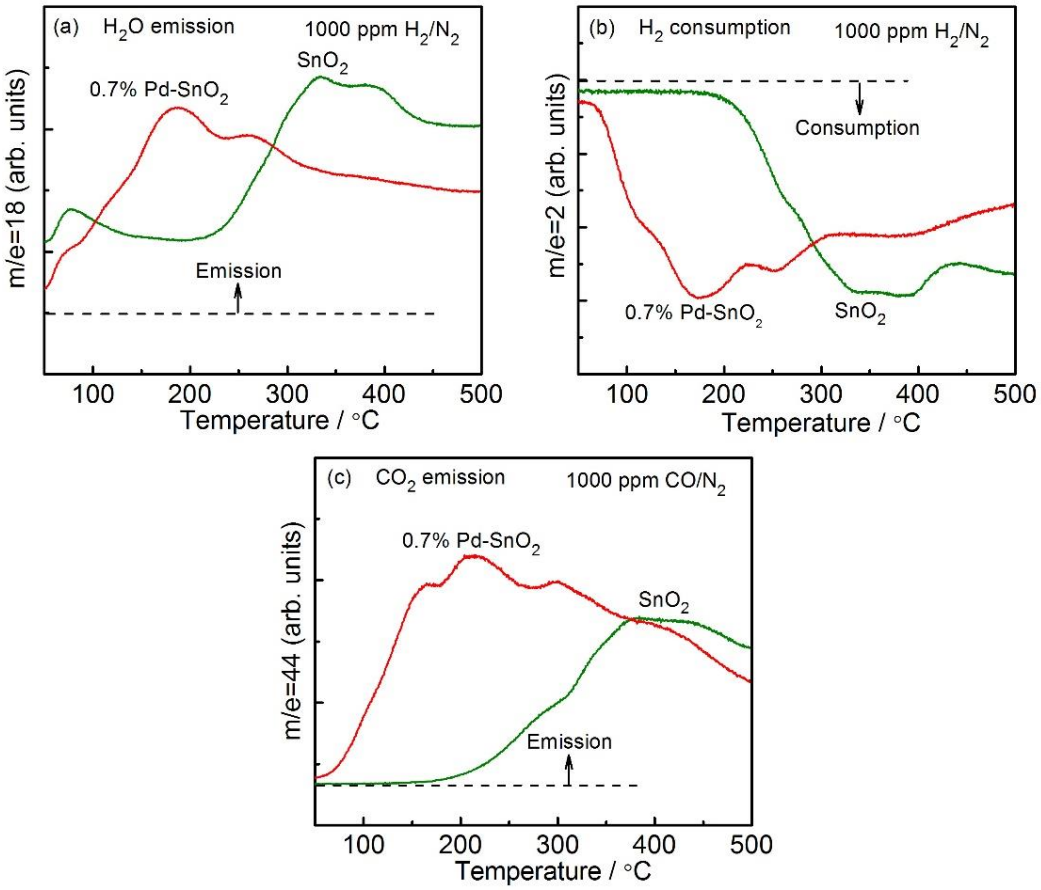

Figure 2-16 (a) H_2O desorption spectra and (b) H_2 consumption spectra of H_2-TPR and (c) CO_2 emission spectra of CO-TPR for neat SnO_2 and Pd-loaded SnO_2.

To investigate any difference in reactivity between neat SnO_2 and 0.7% Pd-SnO_2, TPR was carried out. Figure 2-16 shows H_2O desorption and H_2 consumption spectra of H_2-TPR and CO_2 emission spectra of CO-TPR for neat SnO_2 and 0.7% Pd-SnO_2. H_2O desorption and H_2 consumption spectra for 0.7% Pd-SnO_2 are different from those for neat SnO_2. In the case of neat SnO_2, large peak was observed in the range of 300−400 ℃. This peak seems to be due to O^{2-} and O^- adsorbed on SnO_2 surface as reported previously.[17] However, 0.7% Pd-SnO_2 showed two large peaks at 180 and 250 ℃. Additionally a slight and gentle peak was also observed above 300 ℃. In the emission spectra of CO-TPR, the point different from H_2-TPR was to show a peak at 400 ℃ although other

peaks shifted a little to lower temperature. The peak in high temperature may be considered by partially reduction of SnO_2 surface because SnO_2 surface is reduced catalytically by Pd under CO existence.[19] From these results, it is thought that two kinds of oxygen species are related to Pd. One is O^{2-} adsorbed on PdO and another is PdO itself. Furthermore it seems that small amount of oxygen adsorbs on the SnO_2 surface.

2.3.5 Model of oxygen adsorption on Pd-loaded SnO_2 under humid condition

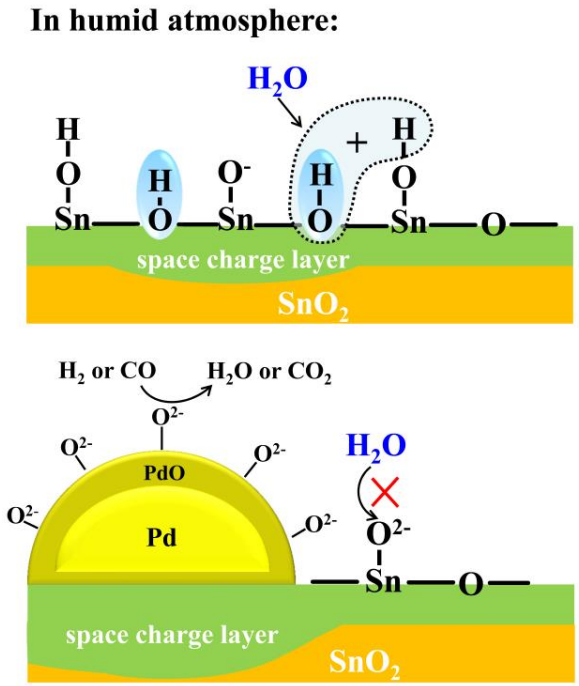

Figure 2-17 Schematic drawing of gas sensing model for neat SnO_2 and Pd-loaded SnO_2 in humid atmosphere.

Schematic drawing of gas sensing model for Pd-loaded SnO_2 in humid atmosphere is shown in Fig. 2-17, as compared with that for neat SnO_2. In the case of neat SnO_2, under humid condition, the OH^- groups competitively adsorb on the SnO_2 surface, and O^{2-} adsorption is disturbed by OH^-. From the results of the dependence of electric resistance on oxygen partial pressure, mainly oxygen species adsorbed in humid atmosphere may be estimated as O^- for neat SnO_2.

However, such disturbance by water vapor was also inhibited by loading Pd. Pd existing as PdO is dispersed finely on the SnO_2 surface as shown in Table 2-2. The ratio between the surface area of Pd and SnO_2 was just about 2.4%. Interestingly, such small Pd/PdO particles lead the electric resistance of SnO_2 increase about 40 times at 300 ℃ in humid atmosphere. Therefore, it was thought that PdO greatly expand the depletion layer of SnO_2, which prevent the adsorption of OH^- groups. On the basis of results of the dependence of electric resistance on oxygen partial pressure and the TPR, the assumption of O^{2-} adsorption on Pd-SnO_2 surface is brought out. In addition, as one possibility, it is considered PdO may provide initial adsorption sites for O^{2-} adsorption, which is hard to be affected by water vapor. Such O^{2-} adsorption on PdO seems to let the depletion layer of the interface expand more and may prevent OH^- adsorption on SnO_2 surface.

2.4 Conclusions

The suppression effect of Pd on water vapor poisoning in Pd-loaded SnO_2 gas sensor was clarified with regard to oxygen adsorption behavior and gas sensing properties toward reducing gas (H_2 and CO) in humid atmosphere. The following conclusions are drawn from the present study.

1. The adsorbed oxygen species on Pd-loaded SnO_2 surface was O^{2-} both in dry and humid atmospheres, and the oxygen adsorption was not influenced by water vapor. However, for neat SnO_2, it was adsorbed as O^{2-} in dry atmosphere but changed to O^- in humid atmosphere.
2. The water vapor poisoning effect on electric resistance and sensor response was significantly reduced by loading Pd in humid atmosphere.
3. On the basis of the dependence of electric resistance on oxygen partial pressure and the TPR results, we propose that O^{2-} adsorption on PdO enlarged the depletion layer of the interface and prevented OH^- adsorption on the SnO_2 surface.

References

[1] Barsan N, Weimar U. Understanding the fundamental principles of metal oxide based gas sensors; the example of CO sensing with SnO_2 sensors in the presence of humidity. Journal of Physics: Condensed Matter. 2003;15: 813–839.

[2] Pavelko RG, Daly H, Hardacre C, Vasiliev AA, Llobet E. Interaction of water, hydrogen and their mixtures with SnO_2 based materials: the role of surface hydroxyl groups in detection mechanisms. Physical Chemistry Chemical Physics. 2010;12:2639–2647.

[3] Choi KI, Hübner M, Haensch A, Kim HJ, Weimar U, Barsan N, et al. Ambivalent effect of Ni loading on gas sensing performance in SnO_2 based gas sensor. Sensors and Actuators B: Chemical. 2013;183:401–410.

[4] Yamazoe N, Suematsu K, Shimanoe K. Two types of moisture effects on the receptor function of neat tin oxide gas sensor to oxygen. Sensors and Actuators B: Chemical. 2013;176:443–452.

[5] Yamazoe N, Suematsu K, Shimanoe K. Gas reception and signal transduction of neat tin oxide semiconductor sensor for response to oxygen. Thin Solid Films. 2013;548:695–702.

[6] Harbeck S, Szatvanyi A, Barsan N, Weimar U, Hoffmann V. DRIFT studies of thick film un-doped and Pd-doped SnO_2 sensors: temperature changes effect and CO detection mechanism in the presence of water vapour. Thin Solid Films. 2003;436:76–83.

[7] Yamazoe N, Suematsu K, Shimanoe K. Extension of receptor function theory to include two types of adsorbed oxygen for oxide semiconductor gas sensors. Sensors and Actuators B: Chemical. 2012;163:128–135.

[8] Koziej D, Barsan N, Shimanoe K, Yamazoe N, Szuber J, Weimar U. Spectroscopic insights into CO sensing of undoped and palladium doped tin dioxide sensors derived from hydrothermally treated tin oxide sol. Sensors and Actuators B: Chemical. 2006;118:98–104.

[9] Yamazoe N. New approaches for improving semiconductor gas sensors. Sensors and

Actuators B: Chemical. 1991;5:7–19.

[10] Safonova OV, Neisius T, Ryzhikov A, Chenevier B, Gaskov AM, Labeau M. Characterization of the H_2 sensing mechanism of Pd-promoted SnO_2 by XAS in operando conditions. Chemical communications. 2005:5202–5204.

[11] Kimura K, Einaga H, Teraoka Y. Preparation of highly dispersed platinum catalysts on various oxides by using polymer-protected nanoparticles. Catalysis Today. 2011;164:88–91.

[12] Einaga H, Kawarada J, Kimura K, Teraoka Y. Preparation of platinum nanoparticles on TiO_2 from DNA-protected particles. Colloids and Surfaces A: Physicochemical and Engineering Aspects. 2014;455:179–184.

[13] Einaga H, Urahama N, Tou A, Teraoka Y. CO Oxidation Over TiO_2-Supported Pt–Fe Catalysts Prepared by Coimpregnation Methods. Catalysis Letters. 2014;144:1653–1660.

[14] Belmonte JC, Manzano J, Arbiol J, Cirera A, Puigcorbe J, Vila A, et al. Micromachined twin gas sensor for CO and O_2 quantification based on catalytically modified nano-SnO_2. Sensors and Actuators B: Chemical. 2006;114:881–892.

[15] Marikutsa AV, Rumyantseva MN, Yashina LV, Gaskov AM. Role of surface hydroxyl groups in promoting room temperature CO sensing by Pd-modified nanocrystalline SnO_2. Journal of Solid State Chemistry. 2010;183:2389–2399.

[16] Xu CN , Miura N, Yamazoe N. Grain size effects on gas sensitivity of porous SnO_2-based elements. Sensors and Actuators B: Chemical. 1991;3:147–155.

[17] Yamazoe N, Fuchigami J, Kishikawa M, Seiyama T. Interactions of tin oxide surface with O_2, H_2O and H_2. Surface Science. 1979;86:335–44.

[18] Matsushima S, Teraoka Y, Miura N, Yamazoe N. Electronic interaction between metal additives and tin dioxide in tin dioxide-based gas sensors. Japanese Journal of Applied Physics. 1988;27:1798–1802.

[19] Shimanoe K, Arisuda S, Oto K, Yamazoe N. Influence of reduction treatment on CO sensing properties of SnO_2-based gas sensor. Electrochemistry. 2006;74:183–185.

Chapter 3

Pd Size Effect on the Gas Sensing Properties of Pd-Loaded SnO_2 in Humid Atmosphere

It is well-known that the sensing properties of SnO_2 gas sensor can be improved by sensitization with Pd even in humid atmosphere. However, the sensitization effect was greatly influenced by the distribution state of Pd on the SnO_2 surface. In this chapter, Pd particles of different nano-sizes were loaded on the SnO_2 surface by using different Pd precursors for the purpose of investigating the Pd size effect on gas sensing properties in humid atmosphere.

3.1 Introduction

The sensing properties of SnO_2 gas sensor can be effectively improved by Pd even in the presence of water vapor.[1] However, the sensitization effect of Pd was greatly influenced by the distribution state that depended a lot on the noble metal precursors, material preparation procedures, and deposition methods.[2-7] Pd may disperse on SnO_2 surface by impregnating Pd on the calcined SnO_2, and it also may diffuse into the SnO_2 lattice and modify the particle size of SnO_2 by introducing it in the SnO_2 preparation process.[4-6] This point has important consequences on the gas sensitivity, since the surface concentration of Pd depends on the SnO_2 surface area, which combines with particle size of SnO_2 to affect the sensitivity. It was recognized that the large dispersion of small Pd particles gives a high sensor response in dry atmosphere.[2, 6] However, the gas sensing mechanism is more complicated for Pd loaded SnO_2 in humid atmosphere. It was reported that Pd on the SnO_2 surface and Pd in the bulk of SnO_2 showed a completely different CO sensing mechanism in humid atmosphere.[8] In addition, OH^- can react with CO for the Pd-loaded SnO_2 sensor, contributing to the increase of sensor signal.[9] The catalytic doping also can activate the surrounding lattice oxygen and change the reaction route in humid atmosphere, which was reported in the Pt-doped SnO_2 sensor.[10] These results suggest that it is important to further clarify the effect of

Pd distribution state to the sensor performance in humid atmosphere. Therefore, in this chapter, Pd-loaded SnO_2 nanoparticles with different Pd particle size were prepared, and the influence of Pd size and its distribution state on the gas sensing performance was investigated in humid atmosphere.

3.2 Experimental

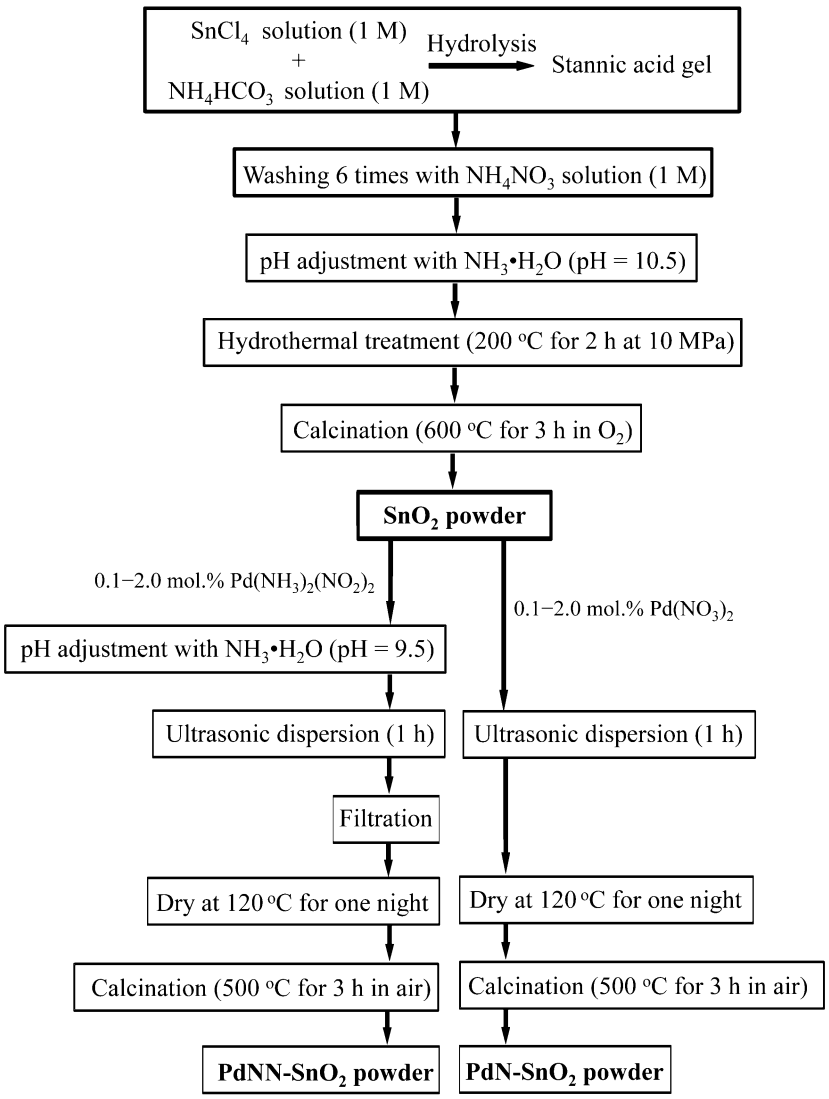

Figure 3-1 Flowchart for the preparation of Pd-loaded SnO_2 powder.

SnO_2 nano-particles were synthesized by hydrothermal method as described in Chapter 2. Pd nanosized particles were loaded on the SnO_2 surface by impregnation method using $Pd(NH_3)_2(NO_2)_2$ and $Pd(NO_3)_2$ aqueous solution

(abbreviated them to PdNN-SnO_2 and PdN-SnO_2, respectively). SnO_2 powder was dispersed in deionized water and then impregnated with $Pd(NH_3)_2(NO_2)_2$ or $Pd(NO_3)_2$ aqueous solution under ultrasonic vibration for 1 h. The former one followed by ammonia solution treatment (pH = 9.5) and filtration process. Finally the obtained two kinds of Pd-loaded SnO_2 powders were dried at 120 ℃ and heat-treated at 500 ℃ for 3 h in air. The material preparation process was shown in Fig. 3-1. Gas sensors were fabricated by depositing powders on alumina substrate and then heat-treated at 580 ℃. Before measurement, the sensors were pretreated in humid atmosphere (4 vol.% H_2O) at 580 ℃, as described in Chapter 2.

The obtained Pd loading amount on SnO_2 surface was determined by energy dispersive X-ray fluorescence spectrometer (XRF, EDX-800, Shimadzu, Japan). The crystal structure of powder was analyzed by X-ray diffraction with copper Kα radiation (λ = 1.5418 Å) filtered through a Ni foil (XRD, RINT 2100, Rigaku, Japan). The crystallite size of powder was calculated from XRD (110) peak by the Scherrer equation. The microstructure was observed by transmission electron microscopy (TEM) (Tecnai-F20, FEI, US). Specific surface area was measured by surface area analyzer (BET, BELSOR, BEL, Japan). CO pulse adsorption method (BEL-CAT, BEL, Japan) was used to detect the particle size, dispersion state and surface area of Pd on SnO_2. Temperature programmed reduction by hydrogen (H_2-TPR) and CO (CO-TPR) was carried out in a flow of 1000 ppm H_2/N_2 and CO/N_2, respectively (BEL-CAT, BEL, Japan). The pretreatment and measurement process for CO pulse adsorption and TPR were same as described in Chapter 2.

3.3 Results and Discussion

3.3.1 Materials characterization

Figure 3-2 is the TEM images of SnO_2 and two typical Pd-loaded SnO_2 surface. Obviously Pd-loaded SnO_2 maintained the same morphology as neat SnO_2 particles. The average particle sizes of neat SnO_2 and two kinds of Pd-loaded SnO_2 were almost the same, about 15 nm. X-ray diffraction

demonstrated that all the samples exhibited the same tetragonal phase (JCPDS: 41-1445). No phase corresponding to Pd or PdO was detected in the Pd-loaded SnO_2 powders due to the extremely low Pd amount. It was not shown here for simplicity. Pd-loaded SnO_2 and neat SnO_2 have no obvious difference in the particle size, crystallite size, and specific surface area, meaning that they were independent of Pd and loading method, as shown in Table 3-1. This is in agreement with a previous report that Pd has no influence to the morphology of SnO_2 by introducing it on the calcined SnO_2 surface.[5] Thus, we can eliminate the influence of morphology on the sensor response, and only focus on the effect of Pd size and its distribution state on the gas sensing properties.

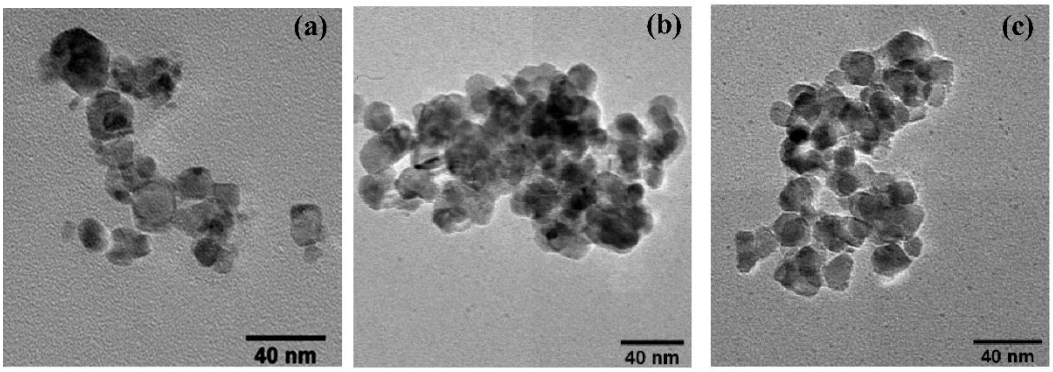

Figure 3-2 TEM images of SnO_2 (a), 0.7% PdNN-SnO_2 (b), and 0.5% PdN-SnO_2 (c).

Table 3-1. Crystallite Size and Specific Surface Area for SnO_2 and Pd-loaded SnO_2, as well as Pd Amount, Particle Size, Dispersion and Surface Area of Pd for Pd-loaded SnO_2

sample	crystallite size of SnO_2 (nm) [a]	specific surface area (m^2/g) [b]	Pd amount (mol.%) [c]	particle size of Pd (nm) [d]	dispersion of Pd (%) [d]	surface area of Pd(m^2/g) [d]
SnO_2	11.7	27.1	/	/	/	/
0.1% PdN	11.9	28.4	0.09	3.5	32	0.10
0.3% PdN	11.5	27.9	0.27	4.6	24	0.23
0.5% PdN	11.6	29.9	0.47	5.3	21	0.31
0.7% PdN	12.0	28.7	0.68	10.3	11	0.24
0.7% PdNN	11.8	27.1	0.42	2.6	43	0.65

[a] Crystallite size of SnO_2 was calculated from XRD (110) peak by Scherrer equation.

[b] Specific surface area was measured by BET method.

[c] Pd amount was measured from XRF analysis.

[d] Particle size, dispersion and surface area of Pd were measured by CO pulse adsorption method. Dispersion of Pd was defined as the ratio of Pd atoms available for CO chemisorption to the total Pd atoms.

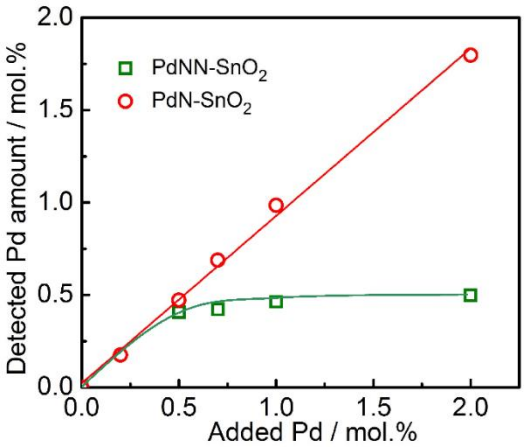

Figure 3-3 Pd loading amount as a function of precursor concentration.

Figure 3-3 shows Pd loading amount as a function of the precursor concentration for two kinds of Pd-loading methods. In the case of PdNN-SnO_2, the Pd loading amount reached a saturation level when the precursor concentration increased to 0.7 mol.%. It seems that the week adhesion of Pd to the SnO_2 surface lead to Pd dispersion in solution. Thus, most of Pd was dispersed in solution when the Pd precursor concentration was above 0.7 mol.%, and it was removed by the filtration process. On the other hand, in the case of PdN-SnO_2, Pd loading amount increased with increasing Pd added amount, because $Pd(NO_3)_2$ solution directly mixed with SnO_2 and almost no Pd was lost in the preparation process. The actual Pd loading amount, particle size, dispersion and surface area of Pd on SnO_2 for Pd-loaded SnO_2 were compared in Table 3-1. The obtained total Pd amount on the SnO_2 surface have no too much difference for 0.7% PdNN-SnO_2 and 0.5% PdN-SnO_2, although a different Pd amount was introduced in the material preparation process. Interestingly, it is found that Pd was loaded on the SnO_2 surface in different distribution state for two kinds of Pd introduction methods. In the case of PdN-SnO_2, Pd particle size increased from 3.5 nm to 10.3 nm with increasing Pd added amount. However, PdNN-SnO_2 gave smaller nano-sized Pd (2.6 nm) even the Pd added amount increased to 0.7 mol.% Pd. With almost the same Pd loading amount, 0.7% PdNN-SnO_2 and 0.5% PdN-SnO_2 are characterized by smaller Pd particles size with larger dispersion and larger Pd particles size with smaller dispersion, respectively. The effect of the Pd

distribution state on SnO_2 surface to the gas sensing properties was investigated in humid atmosphere in the following section.

3.3.2 Oxygen adsorption behavior in different humidity

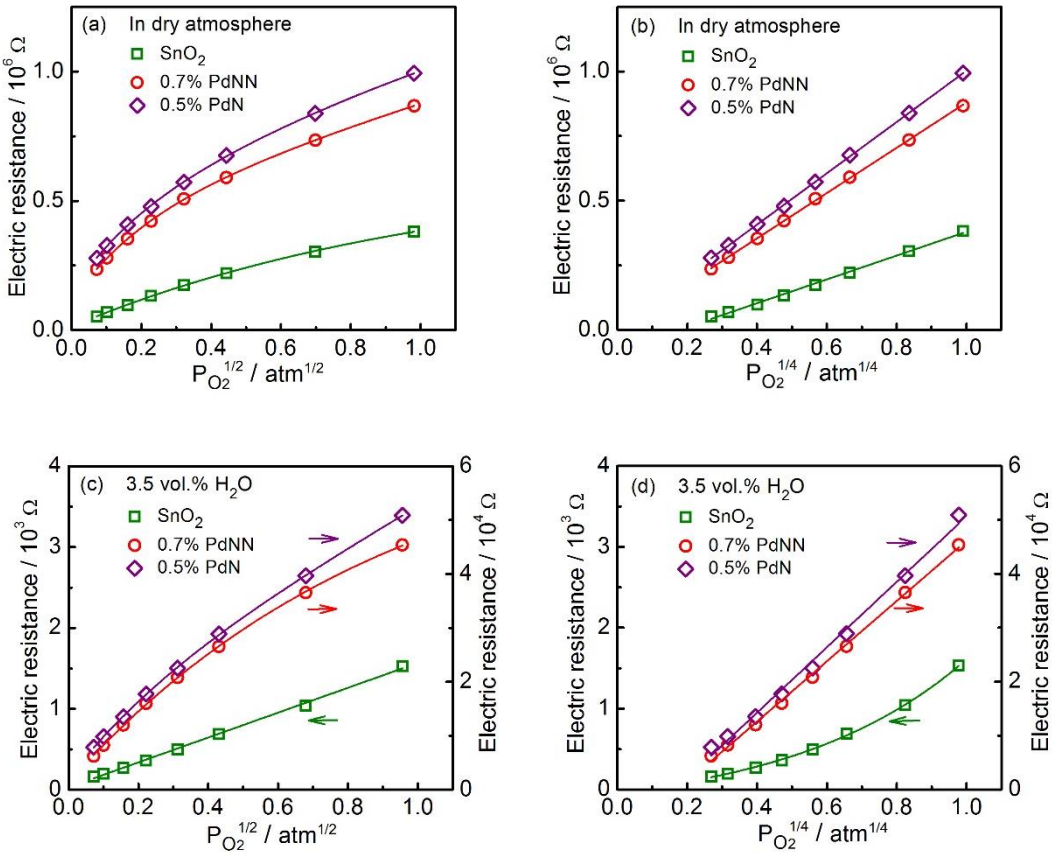

Figure 3-4 Dependence of the resistance on the $P_{O2}^{1/2}$ and $P_{O2}^{1/4}$ in dry and humid atmosphere at 350 ℃: (a, b) dry; (c, d) 3.5 vol.% H_2O.

Oxygen adsorption on the SnO_2 surface is a vital step for gas sensing. It is necessary to clarify the oxygen adsorption behavior in order to further understand the gas sensing mechanism. Therefore, the dependence of electric resistance on oxygen partial pressure in dry and humid atmosphere at 350 ℃ was studied in Fig. 3-4. In dry atmosphere, the electric resistances of neat SnO_2 and Pd-loaded SnO_2 were linearly proportional to $P_{O2}^{1/4}$ in the measured range (Fig. 3-4b). Such a linear relationship agreed with the previous reports.[11-13] Yamazoe et al. proposed theoretical model and formulas about the relationship between electric resistance and oxygen partial pressure in volume depletion state of spherical SnO_2.

According to the mainly adsorbed oxygen species O^- and O^{2-} on the SnO_2 surface, the following two equations are proposed:

$$\frac{R}{R_0} = \frac{3}{a}(K_1 P_{O2})^{\frac{1}{2}} + c \quad (O^- \text{ formation}) \qquad [3\text{-}1]$$

$$\frac{R}{R_0} = \{\frac{1}{4}c^2 + \frac{6N_D}{a}(K_2 P_{O2})^{\frac{1}{2}}\}^{\frac{1}{2}} + c \quad (O^{2-} \text{ formation}) \qquad [3\text{-}2]$$

Here R_0 is the electric resistance at flat-band condition, a grain radius, c a constant, N_D donor density, and K_1 and K_2 equilibrium constants of adsorption. On the basis of the above equations, we can judge the oxygen species by measuring the electric resistance change with oxygen partial pressure. Therefore, it can be concluded the mainly adsorbed oxygen species was O^{2-} on the SnO_2 and Pd-SnO_2 surface in dry atmosphere according to Equation 3-2 due to the linear relationship of the electric resistance with $P_{O2}^{1/4}$. In humidity of 3.5 vol.% H_2O (Fig. 3-4c, d), the electric resistance was linearly proportional to $P_{O2}^{1/2}$ for neat SnO_2, meaning that the oxygen adsorption species was changed to O^- in wet atmosphere according to Equation 3-1. The results were in agreement with the previously report for neat SnO_2.[12] Two kinds of Pd-loaded SnO_2 showed totally different oxygen adsorption behavior from neat SnO_2 in humid atmosphere, and a linear proportion of electric resistance to $P_{O2}^{1/4}$ was observed in humid atmosphere. This means that the mainly adsorbed oxygen species have no change from dry to humid atmosphere, adsorbing as O^{2-} on the surface. The different distribution state of Pd has no influence in oxygen adsorption behavior at 350 ℃. In addition, the electric resistance was greatly enhanced by loading Pd.

Figure 3-5 is the dependence of electric resistance on $P_{O2}^{1/4}$ in different humidity at 350 ℃ for SnO_2 and Pd-loaded SnO_2. For neat SnO_2, a linear relationship of electric resistance with $P_{O2}^{1/4}$ was observed in dry and low humidity (0.05 vol.% H_2O), but this gradually disappeared with increasing humidity. It seems the amount of O^{2-} was reduced with increasing humidity, leaving O^- as the mainly adsorbed oxygen species on the SnO_2 surface. However, for 0.7% PdNN-SnO_2 and 0.5% PdN-SnO_2, the linearity of electric resistance with $P_{O2}^{1/4}$ had no change from dry to humid atmosphere although the resistance reduced with increasing water vapor concentration. The mainly adsorbed oxygen species O^{2-} on the Pd-SnO_2 surface was not influenced by water vapor except that

the numbers of oxygen adsorption sites decreased. Because OH^- groups compete with oxygen species to adsorb on the SnO_2 surface, they disturb the O^{2-} adsorption. However such disturbance of water vapor to O^{2-} was suppressed by loading Pd. Pd may provide new adsorption sites for O^{2-} to make it more favorable than the adsorption of water vapor. It turned out that the oxygen adsorption behavior was changed by loading Pd.[14]

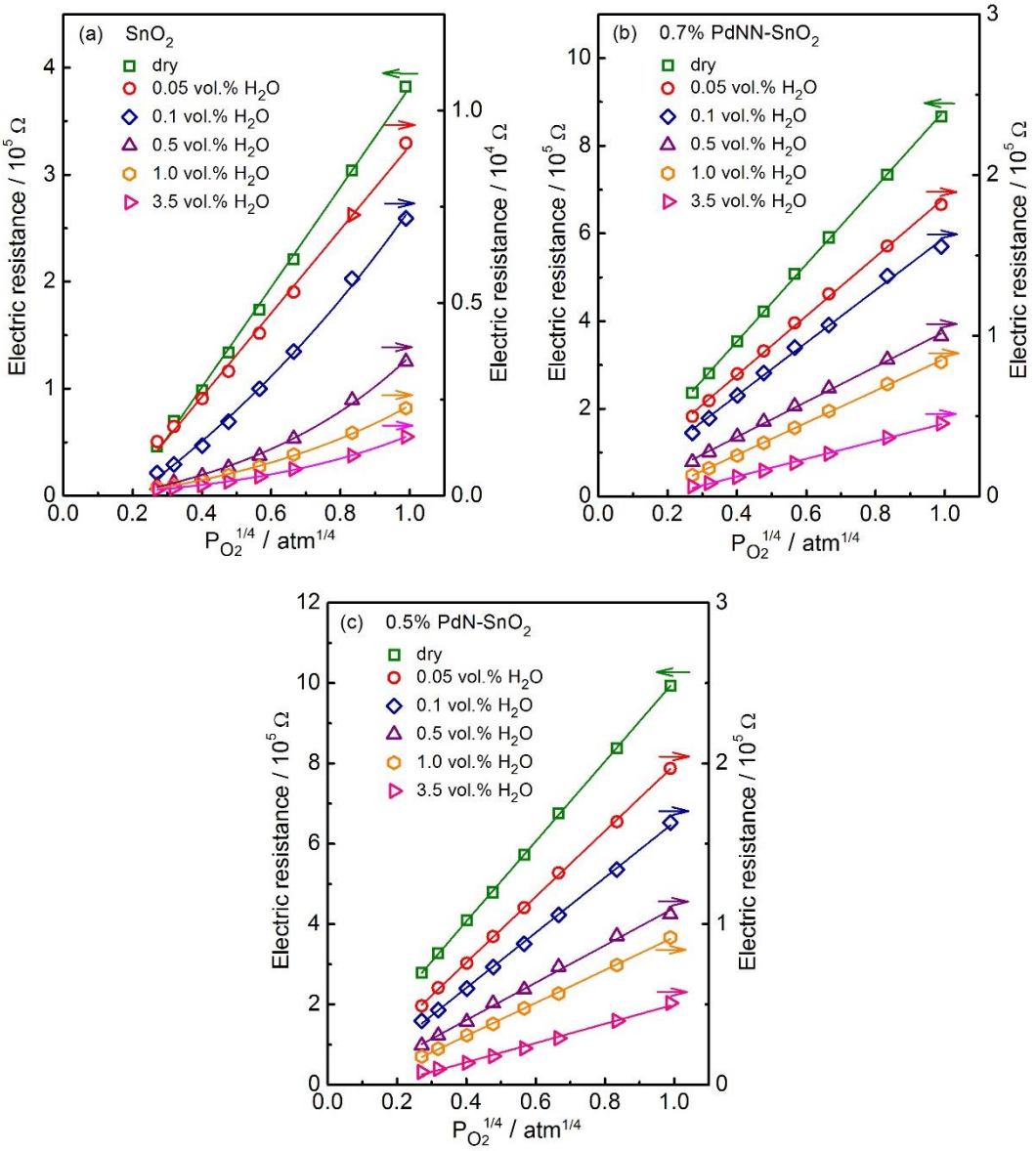

Figure 3-5 Dependence of the electric resistance on $P_{O2}^{1/4}$ in different humidity at 350 ℃: (a) SnO_2, (b) 0.7% PdNN-SnO_2, (c) 0.5% PdN-SnO_2.

3.3.3 Sensor response to H_2 and CO in different humidity

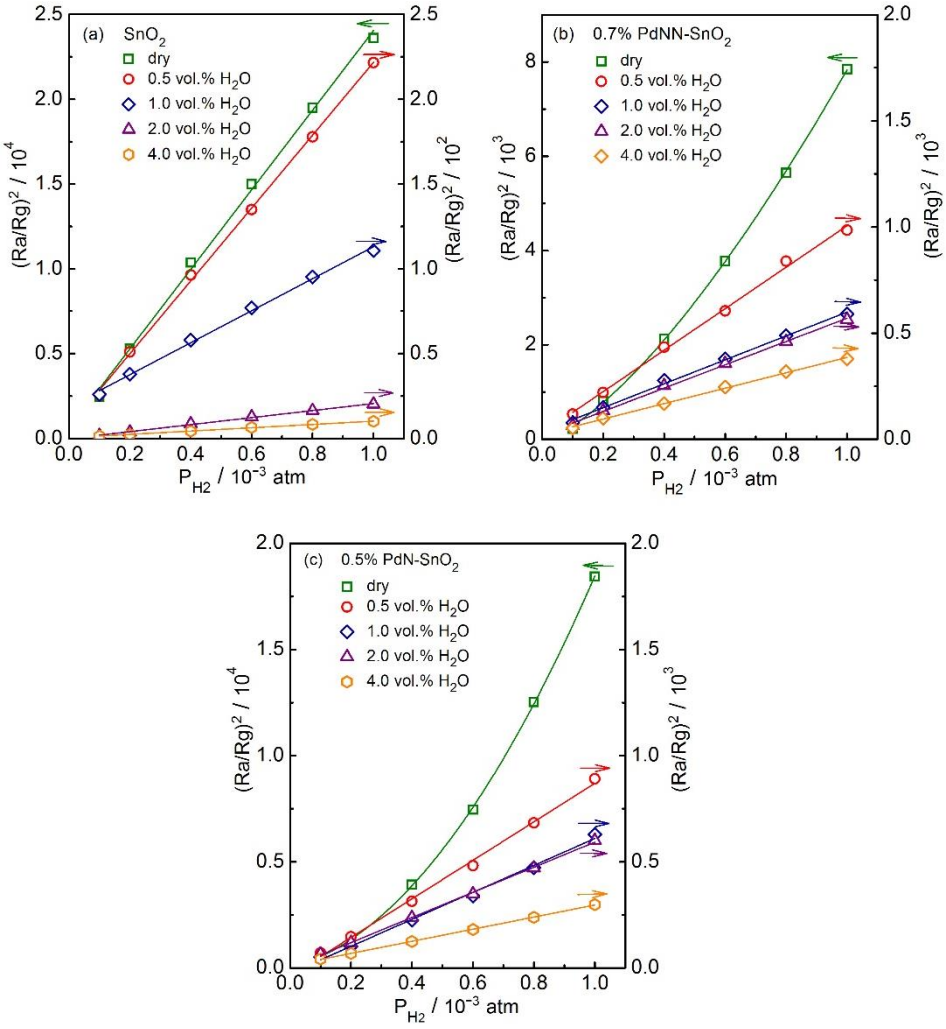

Figure 3-6 The dependence of $(Ra/Rg)^2$ on P_{H2} in different humidity at 350 ℃: (a) SnO_2, (b) 0.7% PdNN-SnO_2, (c) 0.5% PdN-SnO_2.

Figure 3-6 shows the square of sensor response as a function of hydrogen partial pressure in different humidity at 350 ℃. The neat SnO_2 shows that the $(Ra/Rg)^2$ was linearly proportional to the P_{H2} in both dry and humid atmospheres, as shown in Fig. 3-6a. Such a linear relationship was in good agreement with the previously proposed theoretical equation in the volume depletion state of SnO_2.[11]

$$(\frac{Ra}{Rg})^2 = \left(\frac{3c}{aN_D}\right) \cdot P_{H2} + 1 \qquad [3\text{-}3]$$

Here *Ra* and *Rg* are the electrical resistances, respectively, in air and hydrogen gas, *c* a constant, *a* grain radius, N_D donor density and P_{H2} hydrogen partial pressure. In addition, the $(Ra/Rg)^2$ of neat SnO_2 was dramatically reduced about 100 times

by introducing 0.5 vol.% H_2O into dry atmosphere. A nonlinear relationship of $(Ra/Rg)^2$ with P_{H2} was observed for two kinds of Pd-loaded SnO_2 in dry atmosphere (Fig. 3-6b, c). The $(Ra/Rg)^2$ was quickly increased in high hydrogen partial pressure, which seems to be due to the strong catalytic effect of PdO on H_2 oxidation on the SnO_2 surface. A similar phenomenon was also observed in the relationship of $(Ra/Rg)^2$ with P_{CO} for 0.7% PdNN-SnO_2 (Fig. 3-7b). However, 0.5% PdN-SnO_2 showed a convex curve of $(Ra/Rg)^2$ with P_{CO} in dry atmosphere (Fig. 3-7c). This may be due to the different catalytic ability of PdO to CO oxidation. It seems the 0.7% PdNN-SnO_2 with smaller Pd particle size has the stronger catalytic activity.

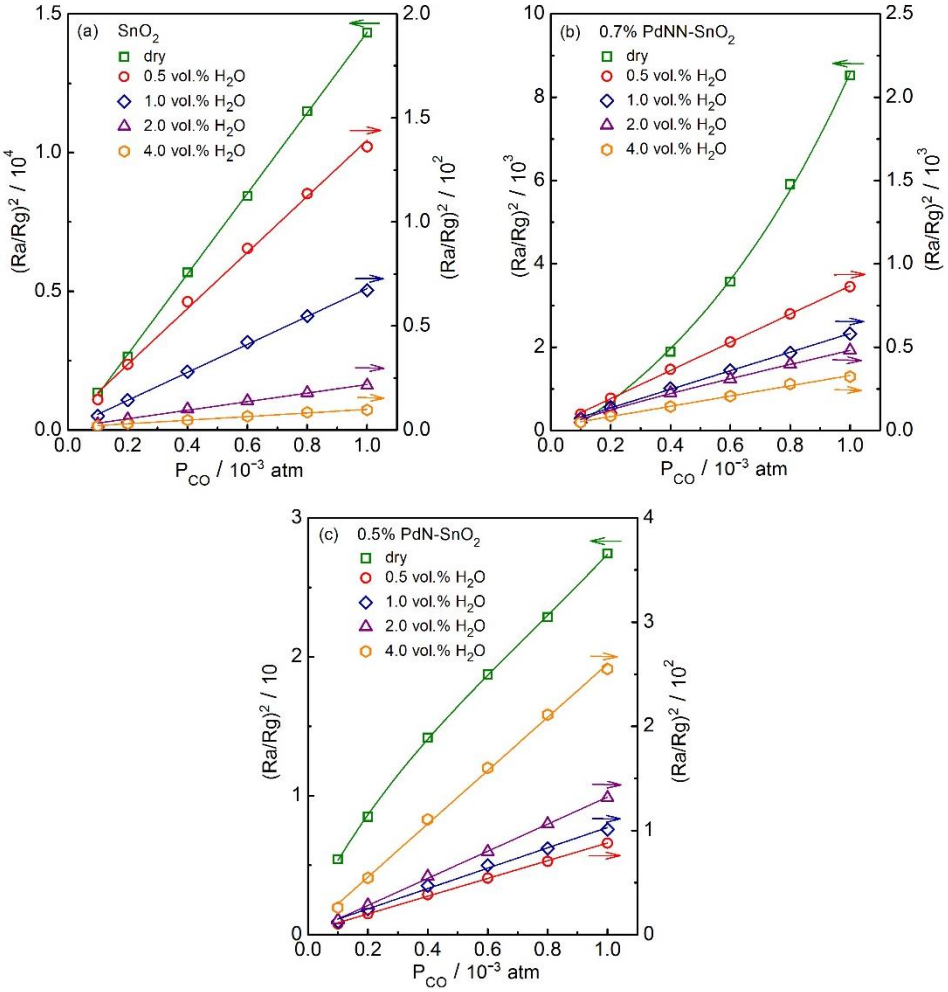

Figure 3-7 The dependence of $(Ra/Rg)^2$ on P_{CO} in different humidity at 350 ℃: (a) SnO_2, (b) 0.7% PdNN-SnO_2, (c) 0.5% PdN-SnO_2.

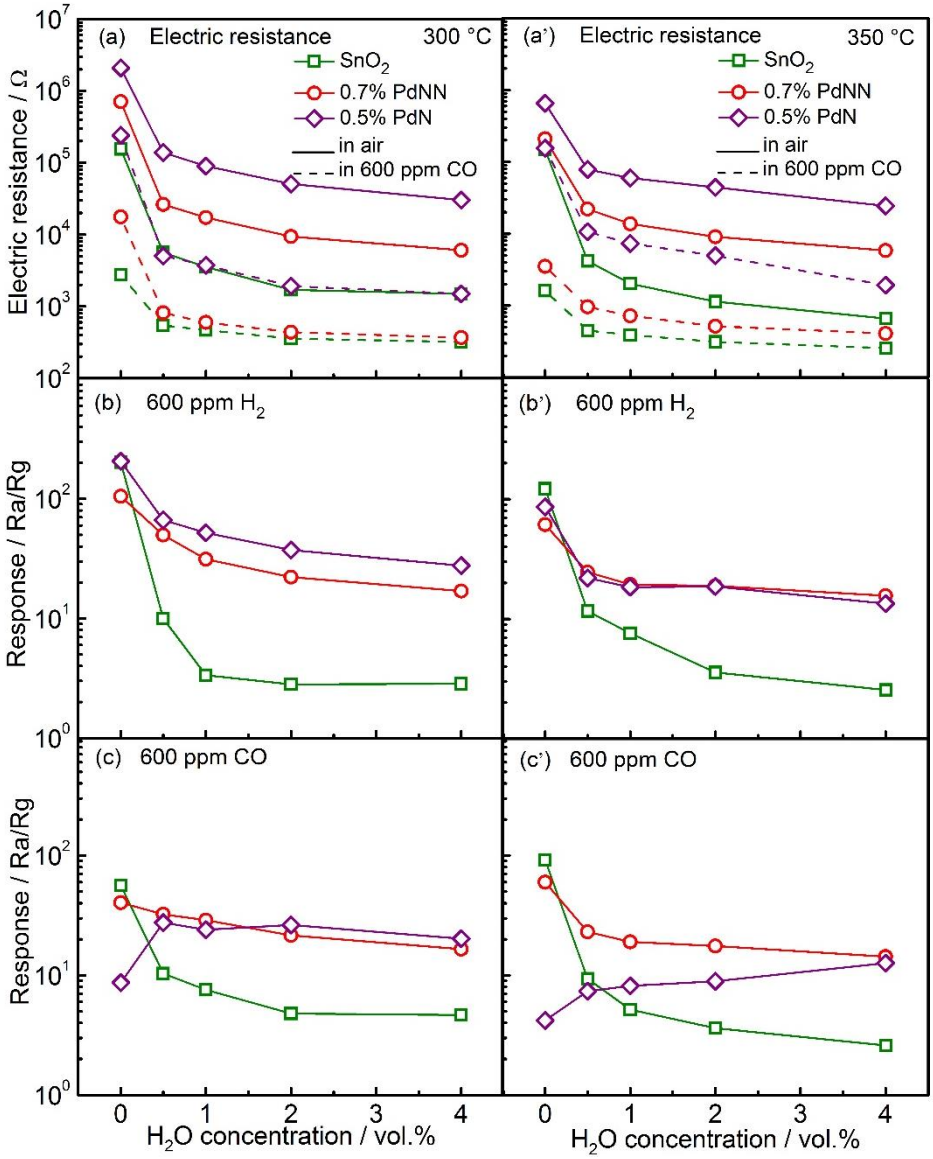

Figure 3-8 Gas sensing properties to H_2 and CO in different humidity at 300 (a-c) and 350 ℃ (a'-c'): (a, a') electric resistance in air and 600 ppm CO; (b, b') response to 600 ppm H_2; (c, c') response to 600 ppm CO.

Figure 3-8 shows the electric resistance and sensor response to H_2 and CO as a function of H_2O concentration for neat SnO_2, 0.7% PdNN-SnO_2, and 0.5% PdN-SnO_2 at 300 and 350 ℃. The electric resistance in air for all devices was reduced by introducing water vapor, which is especially remarkable for neat SnO_2. This means that the oxygen adsorption behavior was changed by loading Pd, as already mentioned. When comparing the enhancement of electric resistance by Pd

loading between 0.7% PdNN-SnO_2 and 0.5% PdN-SnO_2, that of 0.5% PdN-SnO_2 is larger. This result indicated that 0.5% PdN-SnO_2 forms stronger P-N junction. As a result, the sensor response to H_2 at 300 ℃ for 0.5% PdN-SnO_2 seems to be higher than that for 0.7% PdNN-SnO_2. At 350 ℃, it is thought that H_2 gas is easily oxidized, so the sensor response of both elements became almost the same. However, the sensor response to CO at 300 ℃ for 0.5% PdN-SnO_2 was different from that for 0.7% PdNN-SnO_2. In dry atmosphere, the sensor response of 0.5% PdN-SnO_2 was much lower than that for 0.7% PdNN-SnO_2, and the difference became wider by raising the operating temperature. The reason is that electrical resistance reduced less in CO, that is, PdO on the SnO_2 surface for 0.5% PdN-SnO_2 seems not to be reduced so easily in dry atmosphere. Once introducing water vapor, the electric resistance quickly went down and the sensor response went up. The reason why 0.5% PdN-SnO_2 showed such properties is not experimentally clear yet. However, if possible, the water-CO shift reaction may be one of the possible candidates to explain it. CO and H_2O react on the PdO surface and form CO_2 and H_2, resulting that 0.5% PdN-SnO_2 sensor respond to H_2. Usually such a reaction occurs in the absence of oxygen, but it seems to be possible that the formed H_2 immediately reacts with PdO. To clarify such a reaction on 0.5% PdN-SnO_2, further investigation is necessary.

3.3.4 Analysis of Pd size effect

As mentioned above, the Pd size effect on the gas sensing properties of Pd-loaded SnO_2 was confirmed. To further investigate it, CO response at 350 ℃ for PdNN-SnO_2 and PdN-SnO_2 with different Pd amount is shown in Fig. 3-9. As for the CO response of PdNN-SnO_2 in different humidity, all elements showed the same behavior. However, the response behavior of the PdN-SnO_2 sensor greatly changed by Pd loading amount. The response behavior of 0.1% PdN-SnO_2 (Pd size: 3.5 nm in Table 3-1) was same as that of PdNN-SnO_2, but it changed with

increasing Pd loading amount (Pd size). From these results, obviously smaller Pd particle has the stronger catalytic activity. Such difference in catalytic activity between 0.7% PdNN-SnO_2 and 0.5% PdN-SnO_2 was compared by TPR measurement. Figure 3-10 shows H_2O and CO_2 emission spectra of H_2-TPR and CO-TPR, respectively, for neat SnO_2, 0.7% PdNN-SnO_2 and 0.5% PdN-SnO_2. H_2O emission spectra for 0.7% PdNN-SnO_2 and 0.5% PdN-SnO_2 were different from those for neat SnO_2. In the case of neat SnO_2, large peak was observed in the range of 300−400 ℃. This peak seems to be due to O^{2-} and O^- adsorbed on SnO_2 surface as reported previously.[14] However there is no difference between 0.7% PdNN-SnO_2 and 0.5% PdN-SnO_2 except the emission amount of H_2O. Both Pd-SnO_2 showed two large peaks at 180 and 250 ℃. In the CO_2 emission spectra of CO-TPR, the different point from H_2-TPR was to show a peak at 300 ℃. However, the most interesting point is that peaks of 0.7% PdNN-SnO_2 shifted a little towards lower temperature as compared with that of 0.5% PdN-SnO_2. This means that 0.7% PdNN-SnO_2 is more catalytically active. Therefore, PdNN-SnO_2 showed high sensor response and stability under humid condition. The peak at high temperature may be considered by partially reduction of SnO_2 surface because SnO_2 surface is reduced catalytically by Pd under CO existence.[15]

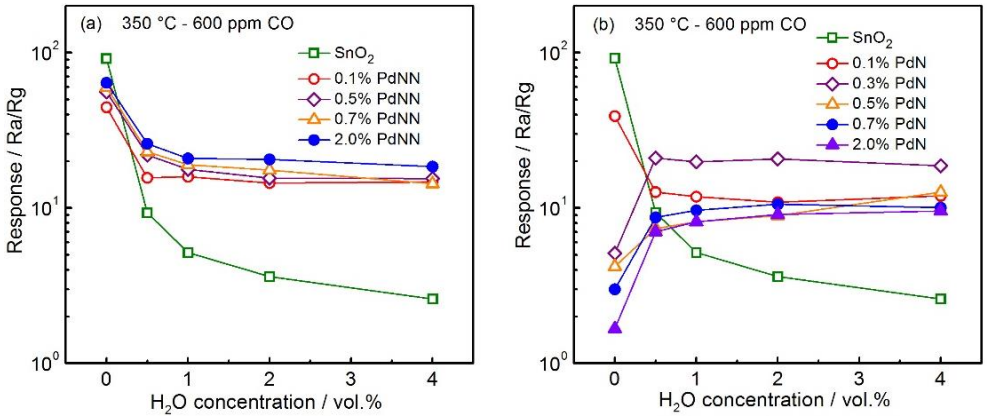

Figure 3-9 Sensor response to 600 ppm CO for PdNN-SnO_2 (a) and PdN-SnO_2 (b) with different Pd amount in different humidity at 350 ℃.

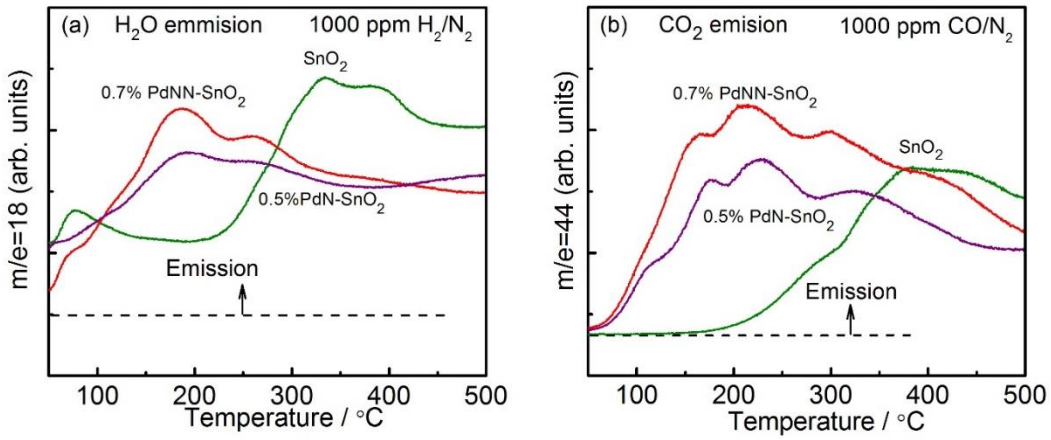

Figure 3-10 H_2O and CO_2 emission spectra of H_2-TPR (a) and CO-TPR (b) for neat SnO_2 and Pd-loaded SnO_2.

The sensor response is closely related to the catalytic properties of the sensing layer. However, the Pd size and the dispersion are some of the most important factors affecting the activity. Many papers reported the particle size effect of the noble metal catalyst involved in reducing gas (H_2, CO and CH_4) oxidation.[16-18] In such a case, the response of the gas sensor greatly depends on the Pd dispersion, since the catalytic activity relates to the dispersion.[7,17,19] The influence of water vapor on the gas sensing properties is complicated and controversial. For the response to H_2, all the sensors showed a similar change in humid atmosphere, reducing sensor response with increasing humidity. This is similar to previous reports [20] and can be explained by the competing reaction with adsorbed oxygen species between H_2 and water vapor. In the case of CO, neat SnO_2 and 0.7% PdNN-SnO_2 showed a decreasing tendency in sensor response with increasing humidity, which was the same as the case of H_2 sensing. 0.5% PdN-SnO_2 sensor even increased CO response in humid atmosphere. We considered that the different Pd/PdO distribution states lead to the different sensitization effect on CO oxidation in humid atmosphere. However, the enhancing effect of water vapor on the CO response in case of 0.5% PdN-SnO_2 is still under consideration, and the detailed reaction mechanism needs to be further

clarified. Regardless of sensing to H_2 or CO, it is doubtless that smaller Pd particles on the SnO_2 surface suppress the water vapor poisoning effect on sensor response.

3.4 Conclusions

The Pd size effect on the gas sensor performance in different humidity was analyzed based on Pd-loaded SnO_2 with smaller and larger Pd particle sizes. The following conclusions are drawn from this chapter.

1. The Pd size has no influence on the oxygen adsorption behavior, that the mainly adsorbed oxygen species was O^{2-} in both dry and humid atmospheres for Pd-loaded SnO_2, no matter Pd in smaller particle sizes or larger particle sizes.
2. Although an interfering effect of water vapor on the sensor response to H_2 was observed for both Pd-loaded SnO_2 sensor, the water vapor poisoning effect was greatly suppressed by loading Pd.
3. In case of CO response, Pd-loaded SnO_2 with smaller Pd particles was reduced in response by introducing water vapor but kept high stability with varying humidity. While Pd-SnO_2 with large Pd particles showed increased CO response in the presence of water vapor and even increased with the rising humidity. This different behavior toward CO sensing was explained by the different catalytic activities of Pd when they were in different distribution states.

The Pd size and amount, which one is the key factor to reduce the water vapor effect on the gas sensing performance? or how to load high amounts of Pd particles with smaller size (< 3.5 nm) on the SnO_2 surface, are meaningful research areas to pursue in the future works.

References

[1] Barsan N, Weimar U. Understanding the fundamental principles of metal oxide based gas sensors; the example of CO sensing with SnO_2 sensors in the presence of humidity. Journal of Physics: Condensed Matter. 2003;15:813–839.

[2] Matsushima S, Maekawa T, Tamaki J, Miura N, Yamazoe N. New methods for supporting palladium on a tin oxide gas sensor. Sensors and Actuators B: Chemical. 1992;9:71–78.

[3] Lim CB, Oh S. Microstructure evolution and gas sensitivities of Pd-doped SnO_2-based sensor prepared by three different catalyst-addition processes. Sensors and Actuators B: Chemical. 1996;30:223–231.

[4] Cabot A, Arbiol J, Morante JR, Weimar U, Barsan N, Göpel W. Analysis of the noble metal catalytic additives introduced by impregnation of as obtained SnO_2 sol–gel nanocrystals for gas sensors. Sensors and Actuators B: Chemical. 2000;70:87–100.

[5] Dieguez A, Vila A, Cabot A, Romano-Rodrıguez A, Morante J, Kappler J, et al. Influence on the gas sensor performances of the metal chemical states introduced by impregnation of calcinated SnO_2 sol–gel nanocrystals. Sensors and Actuators B: Chemical. 2000;68:94–99.

[6] Cabot A, Dieguez A, Romano-Rodrıguez A, Morante J, Barsan N. Influence of the catalytic introduction procedure on the nano-SnO_2 gas sensor performances: Where and how stay the catalytic atoms? Sensors and Actuators B: Chemical. 2001;79:98–106.

[7] Cabot A, Vila A, Morante J. Analysis of the catalytic activity and electrical characteristics of different modified SnO_2 layers for gas sensors. Sensors and Actuators B: Chemical. 2002;84:12–20.

[8] Koziej D, Barsan N, Shimanoe K, Yamazoe N, Szuber J, Weimar U. Spectroscopic insights into CO sensing of undoped and palladium doped tin dioxide sensors derived from hydrothermally treated tin oxide sol. Sensors and Actuators B: Chemical. 2006;118:98–104.

[9] Schmid W, Barsan N, Weimar U. Sensing of hydrocarbons and CO in low oxygen conditions with tin dioxide sensors: possible conversion paths. Sensors and Actuators B: Chemical. 2004;103:362–368.

[10] Großmann K, Wicker S, Weimar U, Barsan N. Impact of Pt additives on the surface reactions between SnO_2, water vapour, CO and H_2; an operando investigation. Physical Chemistry Chemical Physics. 2013;15:19151–19158.

[11] Yamazoe N, Suematsu K, Shimanoe K. Extension of receptor function theory to include two types of adsorbed oxygen for oxide semiconductor gas sensors. Sensors and Actuators B: Chemical. 2012;163:128–135.

[12] Yamazoe N, Suematsu K, Shimanoe K. Gas reception and signal transduction of neat tin oxide semiconductor sensor for response to oxygen. Thin Solid Films. 2013;548:695–702.

[13] Suematsu K, Yuasa M, Kida T, Yamazoe N, Shimanoe K. Determination of oxygen adsorption species on SnO_2: exact analysis of gas sensing properties using a sample gas pretreatment system. Journal of the Electrochemical Society. 2014;161:123–128.

[14] Ma N, Suematsu K, Yuasa M, Kida T, Shimanoe K. Effect of water vapor on Pd-loaded SnO_2 nanoparticles gas sensor. ACS Applied Materials & Interfaces. 2015;7:5863–5869.

[15] Shimnoe K, Arisuda S, Oto K, Yamazoe N. Influence of reduction treatment on CO sensing properties of SnO_2-based gas sensor. Electrochemistry. 2006;74:183–185.

[16] Haruta M, Yamada N, Kobayashi T, Iijima S. Gold catalysts prepared by coprecipitation for low-temperature oxidation of hydrogen and of carbon monoxide. Journal of Catalysis. 1989;115:301–309.

[17] Kocemba I, Rynkowski J. The influence of catalytic activity on the response of Pt/SnO_2 gas sensors to carbon monoxide and hydrogen. Sensors and Actuators B: Chemical. 2011;155:659–666.

[18] Chen X, Cheng Y, Seo CY, Schwank JW, McCabe RW. Aging, re-dispersion, and catalytic oxidation characteristics of model Pd/Al_2O_3 automotive three-way catalysts. Applied Catalysis B: Environmental. 2015;163:499–509.

[19] Li G-J, Zhang X-H, Kawi S. Relationships between sensitivity, catalytic activity, and surface areas of SnO_2 gas sensors. Sensors and Actuators B: Chemical. 1999;60:64–70.

[20] Pavelko RG, Daly H, Hardacre C, Vasiliev AA, Llobet E. Interaction of water, hydrogen and their mixtures with SnO_2 based materials: the role of surface hydroxyl groups in detection mechanisms. Physical Chemistry Chemical Physics. 2010;12:2639–2647.

Chapter 4

Gas Sensing Properties of MEMS Type Sensor Using Pd-Loaded SnO_2 Nanoparticles

In this chapter, to reduce the power consumption, a kind of portable MEMS type gas sensors were fabricated using SnO_2 and Pd-loaded SnO_2 nanoparticles. Their gas sensing properties to H_2 and CO were investigated by constant and pulse heating modes in dry and humid atmospheres. The promoting effect of Pd in humid atmophere for MEMS type gas sensor was further clarified. The influence of heating mode to the gas sensing properties was studied. In addition, the gas sensing properties were compared between the MEMS gas sensors and the conventionally thick-film sensors.

4.1 Introduction

Conventional thick-film gas sensors are usually operated at 200−500 ℃ for achieving good performance. Since high temperature requires high power consumption, such sensors are unfavorable for power saving and device integration.[1] In recent years, the application of MEMS techniques in the field of gas sensors have been attracted great attention, especially for the purpose of reducing power consumption and improving its feasibility as a portable gas sensor.[1-4] The power consumption of MEMS gas sensor can be reduced to tens of mW. Moreover, by heating the MEMS sensor in pulse mode, the power consumption can be further reduced and different sensing properties are expected. Because by pulse heating the sensors are keeped in high temperature for extremely short time and then suddenly reduce to room temperatire. Such high temperature difference loop may cause continuous change of the quantity and the state of adsorbed and physisorbed molecules on the SnO_2 surface.[5] This is very

different from constant heating, which provides sensors a very stable heating state. Therefore, the effect of heating methods on the gas sensing properties should be well studied. In addition, Pd was loaded on the SnO_2 surface to achieve highly sensitive and stable MEMS gas sensor with low power consumption. Based on above consideration, the gas sensing properties to reducing gas (H_2 and CO) were investigated by operating SnO_2 and Pd-loaded SnO_2 MEMS sensors in constant and pulse heating modes in dry and humid atmospheres. Finally, the the gas sensing properties were compared between the MEMS gas sensors and the conventionally thick-film sensors based on the constant heating mode.

4.2 Experimental

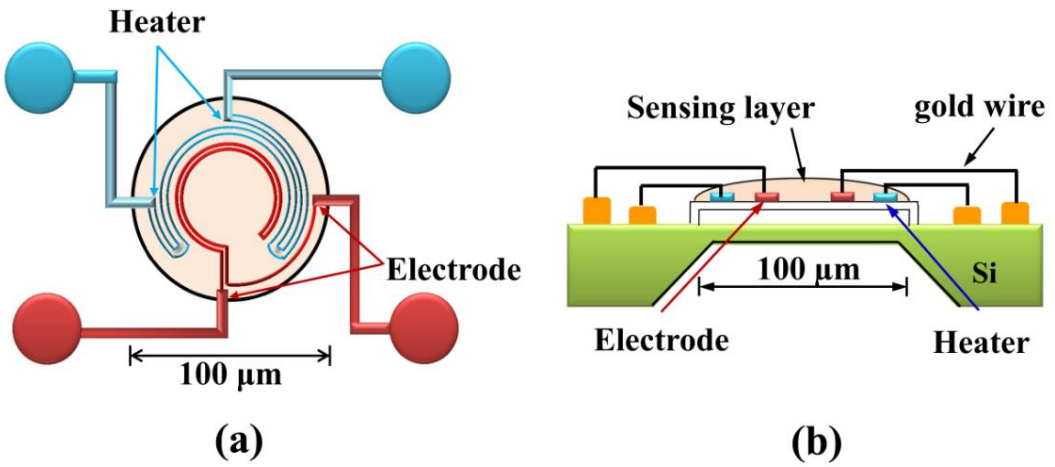

Figure 4-1 Schematic drawing of the MEMS device: (a) patterns of the micro heaters and electrodes; (b) cross-sectional view of MEMS device.

Pd-loaded SnO_2 nano-particles were synthesized by impregnating 0.7 mol.% $Pd(NH_3)_2(NO_2)_2$ solution on the SnO_2 surface as described in Chapter 2. A schematic drawing of MEMS device is depicted in Fig. 4-1. The circular arc Pt electrodes and heaters were embedded on a silicon-based support membrane (diameter: 100 μm). The MEMS device was 9 mm in diameter. To make MEMS-type gas sensors, a uniform paste was firstly prepared by dispersing powders into glycerin by a ratio of 2:3, and then injected on the membrane by a micro injector with a capillary injection tube. The sensing layer was dried at

150 ℃ in an oven and then calcined at 550 ℃ using the micro heater before the sensing measurement.

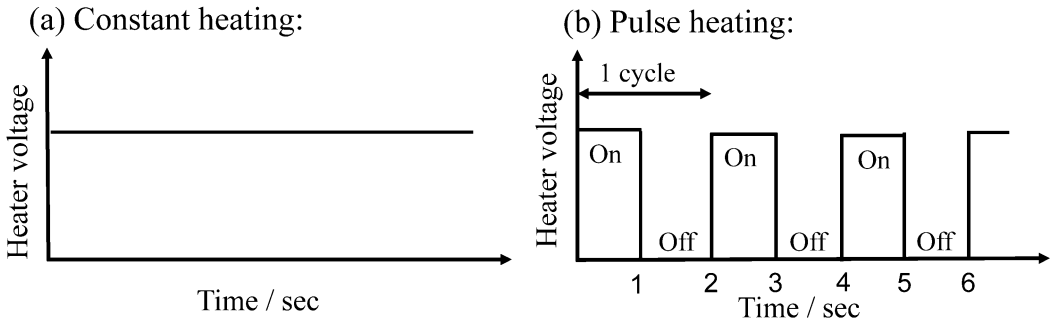

Figure 4-2 MEMS gas sensors were operated by two kinds of heating modes: (a) constant heating; (b) pulse heating.

The gas sensing properties to 200 ppm H_2 and CO were measured in a conventional gas flow apparatus at 300−500 ℃ by applying heater voltage of 0.86−1.371 V. The operating temperature was controlled by the micro heaters using constant heating and pulse heating modes, as shown in Fig. 4-2. For pulse heating, the heater voltage of sensor device was switched to ON and OFF state per one second, and continuously tested 200 cycles. The power consumption of pulse heating is just half of that of constant heating. Typically, the power consumption of pulse heating was just 26 mW at 450 ℃, as shown in Fig. 4-3. The gas flow rate was controlled at a rate of 100 cm^3/min using mass flow controllers. The sensor response ($S = Ra/Rg$) was defined as the ratio of electric resistance in synthetic air (Ra) and target gas (Rg).

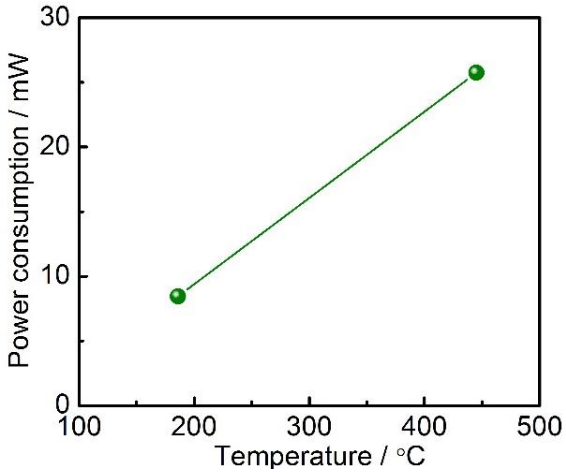

Figure 4-3 Dependence of power consumption on temperature for pulse heating mode.

4.3 Gas Sensing Properties

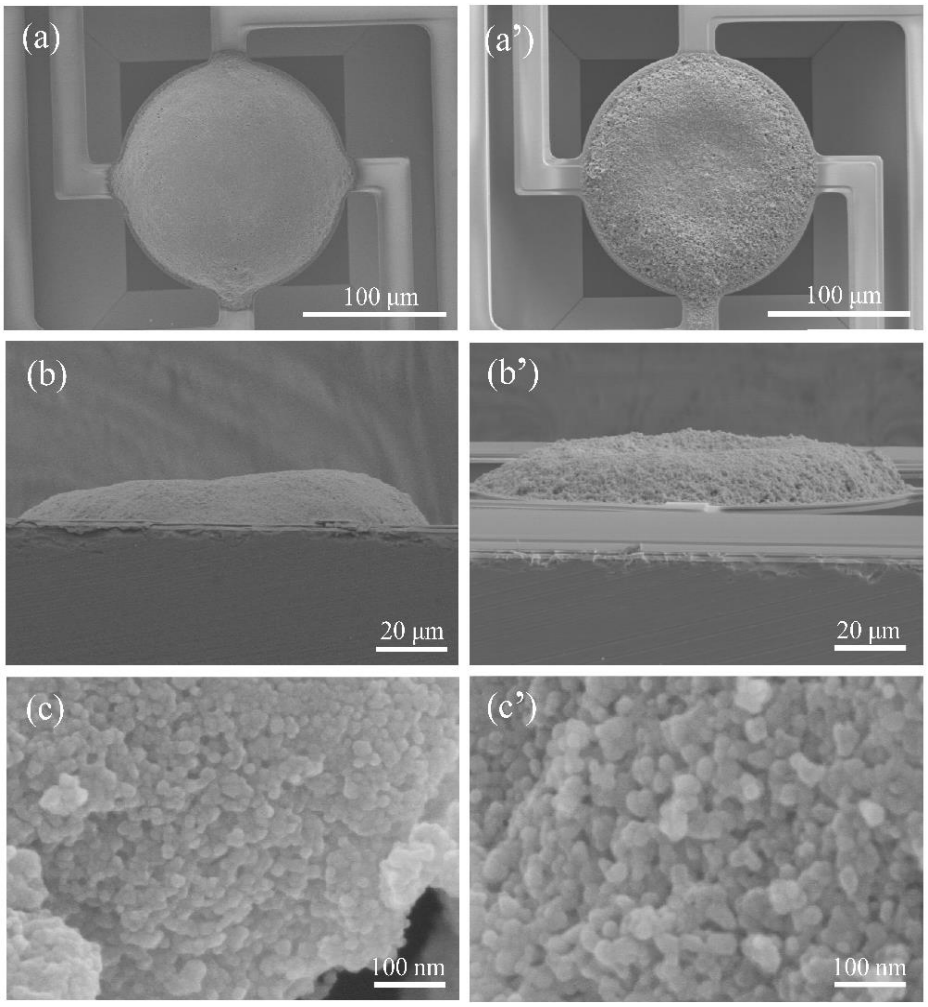

Figure 4-4 SEM images for MEMS sensing layer based on SnO_2 (a-c) and 0.7% Pd-SnO_2 (a'-c'): top view of sensing layer (a, a'); cross-sectional view of sensing layer (b, b'); microstructure of sensing layer (c, c').

Figure 4-4 shows the SEM images of the MEMS sensing layer for SnO_2 and 0.7% Pd-SnO_2. The heaters and electrodes were fully covered by the sensing film, and no clear cracks were observed on the surface of sensing layer. The thickness of film was about 20 μm. The SEM images in Figure 4-4 (c, c') clearly shows that the sensing film had a porous morphology with SnO_2 particle size about 20 nm.

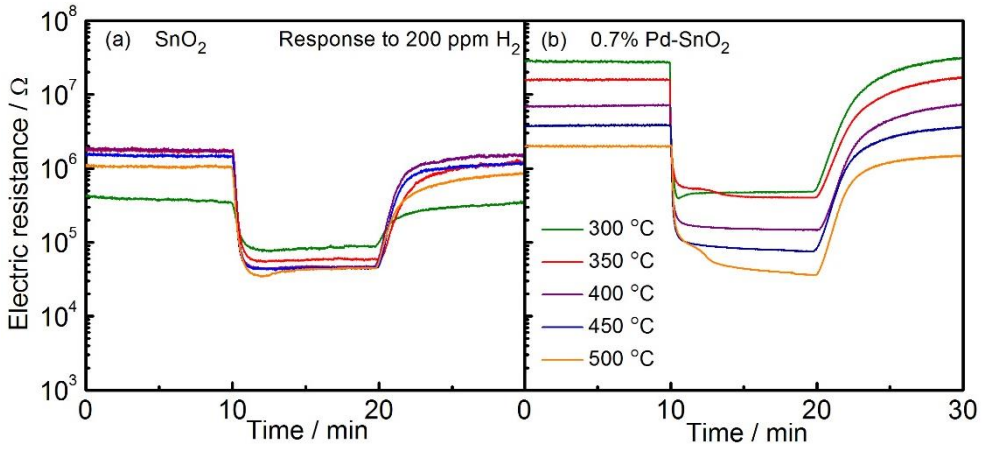

Figure 4-5 H_2 sensing transient to 200 ppm H_2 for SnO_2 and 0.7% Pd-SnO_2 by constant heating at 300−500 ℃ in dry atmosphere.

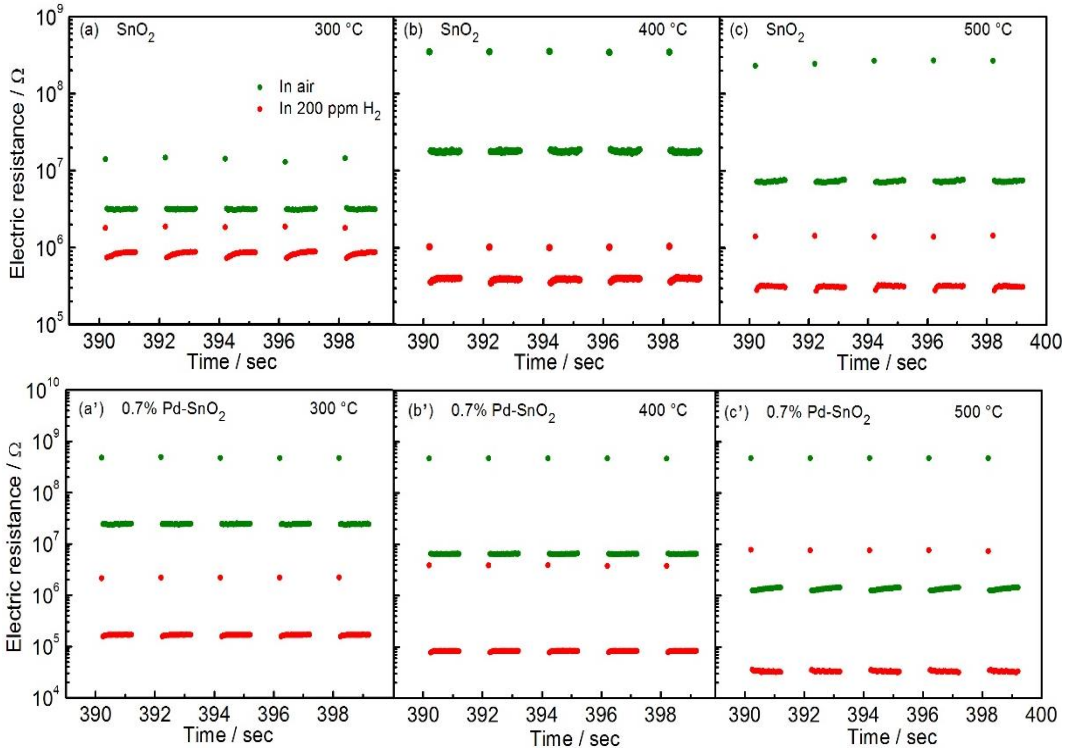

Figure 4-6 Electric resistance in last 5 cycles for SnO_2 (a-c) and 0.7%Pd-SnO_2 (a'-c') using pulse heating mode in dry air and 200 ppm H_2 at 300−500 ℃.

The gas sensing properties of SnO_2 and 0.7% Pd-SnO_2 toward H_2 and CO were measured at 300−500 ℃ by constant and pulse heating modes in dry and humid atmospheres. Figure 4-5 shows the typically transient response to 200 ppm H_2 for SnO_2 and 0.7% Pd-SnO_2 by constant heating in dry atmosphere. For both

two kinds of sensors, the electric resistance quickly reduced after introducing H_2, and it was fully recovered to the original value upon switching to pure air. The results indicated the MEMS gas sensors have good ability for responding and recovering at 300−500 ℃. In order to reduce the power consumption, the sensors were operated by pulse heating mode and continuously measured 200 cycles. Figure 4-6 shows the electric resistance variation with time in the last 5 pulse cycles in dry air and 200 ppm H_2 for SnO_2 and 0.7% Pd-SnO_2 at 300−500 ℃. The electric resistance showed a well repeatability in pulse heating loop for both SnO_2 and Pd-loaded SnO_2. It was extremely high at the beginning of pulse heating, and then it was quickly reached a stable state, no matter in air or in H_2 atmosphere. The high electric resistance may be caused by the insufficient heat conduction at the beginning of heating. The electric resistance values in the last pulse heating cycle were used to calculate the sensor response.

Figure 4-7 summarized the electric resistance in air and sensor response to H_2 and CO by constant and pulse heating at 300−500 ℃ in dry atmosphere. As shown in Fig. 4-7a, a', obviously the electric resistance was greatly enhanced by loading Pd due to the electronic sensitization effect. The constant heating and pulse heating gave similar electric resistance in case of SnO_2 and 0.7% Pd-SnO_2. With increasing temperature, the electric resistance of SnO_2 was first increased and then decreased, while the Pd-loaded SnO_2 showed a monotonic decrease in electric resistance. The electric resistance change with temperature for SnO_2 and Pd-loaded SnO_2 sensors are consistent with previous report.[6-8] The electric resistance of SnO_2 is seriously influenced by the adsorption and desorption of water vapor on the surface. It is thought that the water vapor, which usually present in commercial gas cylinder in low ppm ranges, complicate the temperature dependence in low temperature, especially for neat SnO_2.[6, 7] This phenomenon was more remarkable for SnO_2 by pulse heating mode, which showed highest electric resistance at 400 ℃. The decrease of electric resistance in high

temperature is caused by a thermal excitation of electrons from trapped levels to the conduction band.[7, 8]

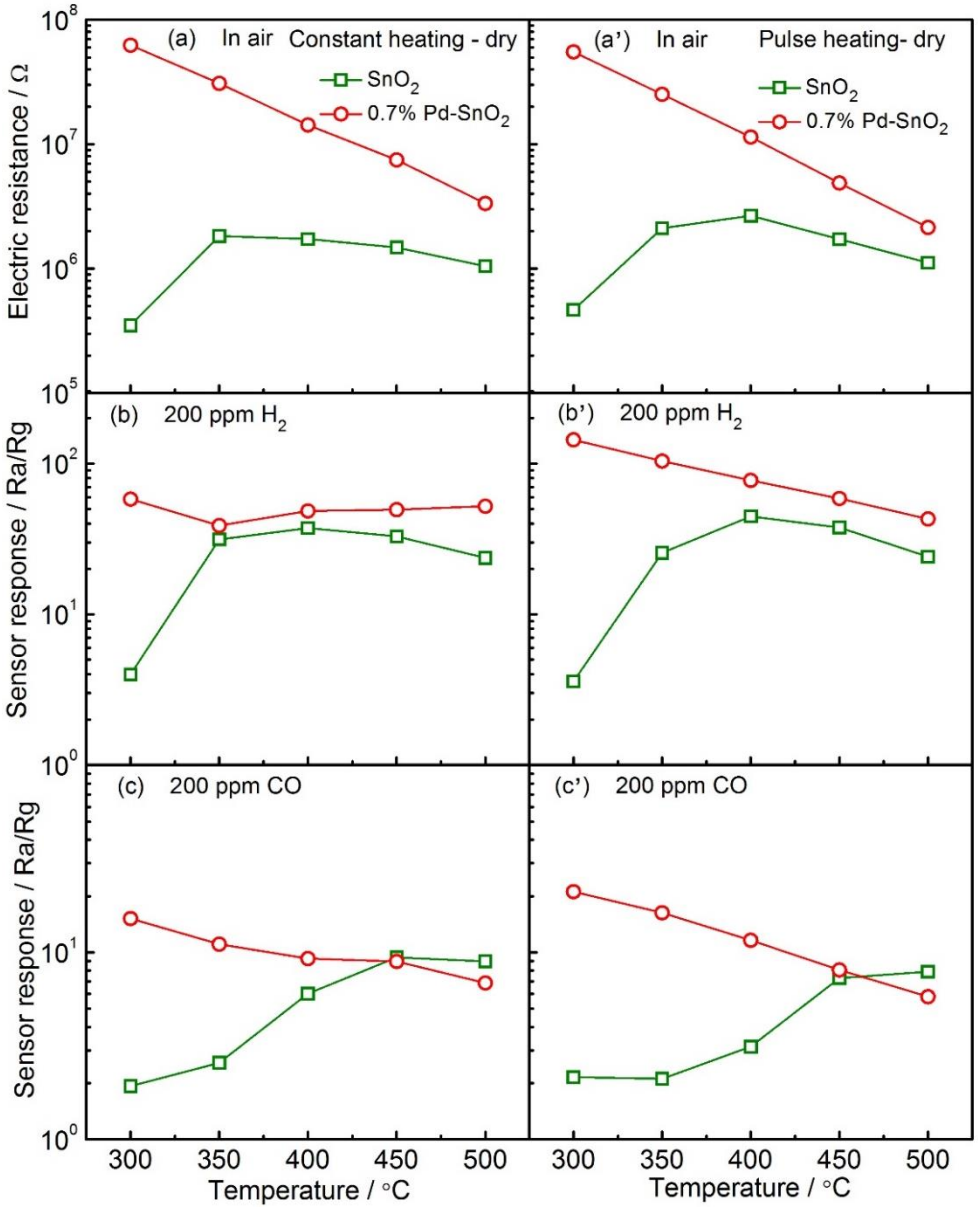

Figure 4-7 Electric resistance in air and sensor response to 200 ppm H_2 and CO as a function of temperature for SnO_2 and 0.7 % Pd-SnO_2 sensors operated by constant heating and pulse heating in dry atmosphere.

Figure 4-7b, b' shows the sensor response to 200 ppm H_2 as the function of temperature for SnO_2 and 0.7% Pd-SnO_2. The sensor response of SnO_2 exhibited

the same behavior by constant and pulse heating. It reached maximum at 400 ℃, then decreased as further increasing temperature. Such volcano-shaped correlations between gas response and temperature is familiar with SnO_2.[9] However, 0.7% Pd-SnO_2 showed not only higher H_2 response but different H_2 sensing behavior compared with SnO_2. Its H_2 response exhibited a maximum value at 300 ℃ by both constant and pulse heating. In low temperature, the sensor response was greatly improved by loading Pd because of the electronic sensitization effect of Pd. While in high temperature, it was just slightly higher for 0.7% Pd-SnO_2 compared with neat SnO_2. The sensor response to reducing gas involves gas diffusion into the sensor layer and subsequently oxidation by adsorbed oxygen species. Such inflammable gas was easily combusted on the surface of sensing film by the catalytic effect of Pd at high temperature, without diffusing into the deep of sensor layer and no sensor signal producing. Thus the promoting effect of Pd to H_2 response was not remarkably at high temperature. This is also the reason why pulse heating gave higher H_2 response for 0.7% Pd-SnO_2. The constant heating mode may greatly contribute the H_2 burning on the surface. While pulse heating mode by repeating heating and cooling, may reduce the Pd catalytic activity for promoting H_2 burning on the surface. Therefore, pulse heating showed higher H_2 response for 0.7% Pd-SnO_2.

The sensor response to 200 ppm CO showed similarly tendency with increasing temperature as that to 200 ppm H_2 for 0.7% Pd-SnO_2, as shown in Fig.4-7c, c'. The sensor response of 0.7% Pd-SnO_2 was 10 times higher than that of neat SnO_2 in low temperature at 300 ℃, and they were almost same in high temperature at 500 ℃. While the CO response of neat SnO_2 increased with raising temperature. At low temperature, CO may cannot fully oxidized and remain on the surface as carbon residue. Thus a lower response to CO was observed in low temperature for neat SnO_2. Compared with H_2, the sensor response to CO was much lower for both SnO_2 and 0.7% Pd-SnO_2. According to the Knudsen

mechanism in the gas diffusion process, the Knudsen diffusion coefficient D_k of H_2 is about 3.7 times higher than that of CO, which is determined by molecular weight in a fixed pore radius and temperature.[10] Therefore, CO is more difficult to diffuse into the film due to the large molecular weight, resulting to the lower response.

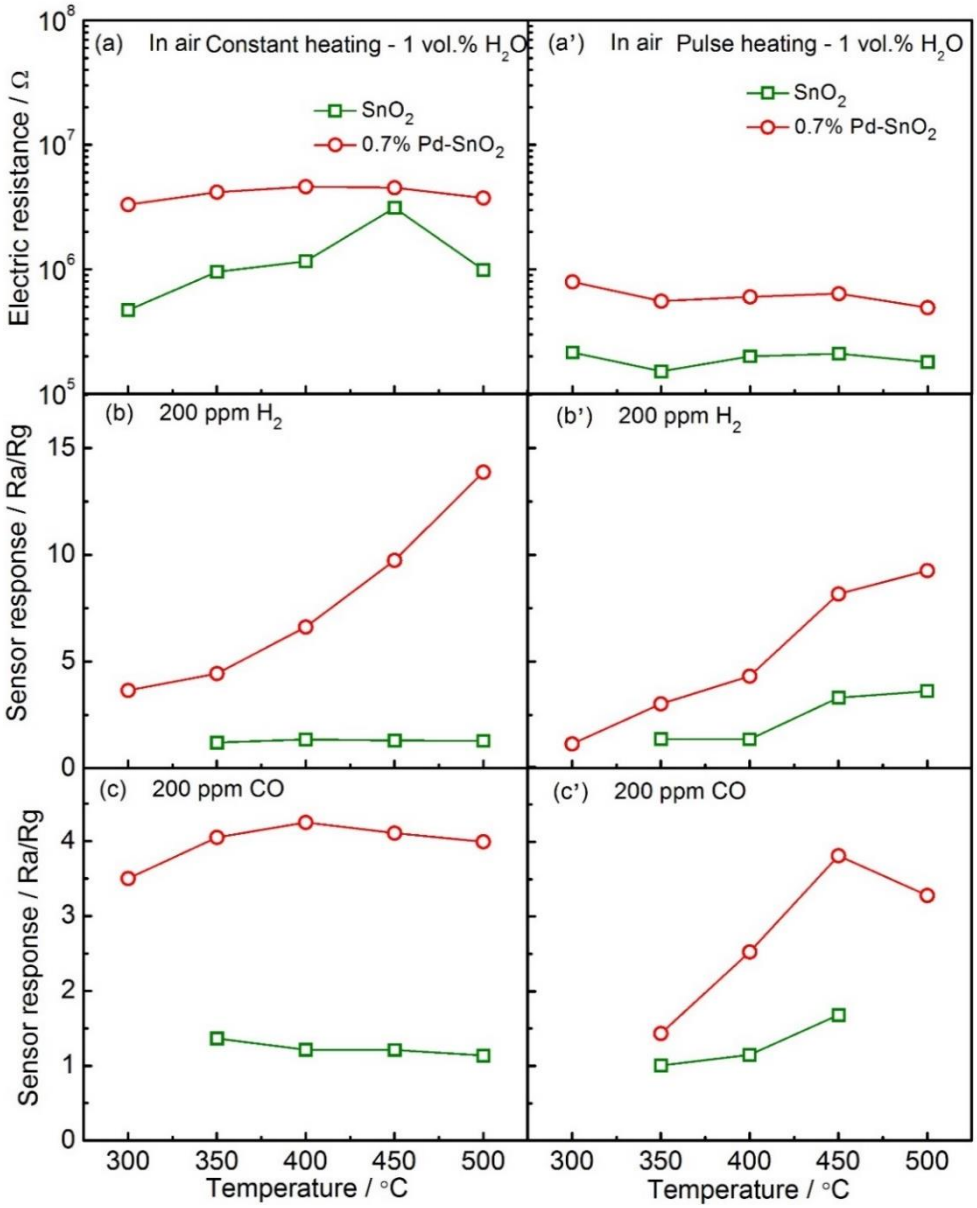

Figure 4-8 Electric resistance in air and sensor response to 200 ppm H_2 and CO as a function of temperature for SnO_2 and 0.7 % Pd-SnO_2 sensors operated by constant heating and pulse heating in humid atmosphere (1 vol.% H_2O).

Figure 4-8 compared the gas sensing performance by constant heating and pulse heating at 300-500 ℃ in humid atmosphere (1 vol.% H_2O). The electric resistance was reduced by introducing water vapor, especially notable for pulse heating mode. The pulse heating mode gave much smaller electric resistance in air for both neat SnO_2 and Pd-loaded SnO_2, as shown in Fig. 4-8a'. The high electric resistance involves more oxygen species adsorption on the surface. It seems the amount of oxygen species on the sensing layer was seriously disturbed by water vapor for pulse heating because of the short heating time, leading to the lower electric resistance. In addition, the electric resistance in air changed less with increasing temperature by pulse heating for SnO_2 and 0.7 %Pd-SnO_2 in humid atmosphere. It seems the water vapor poisoning effect was so strong that cannot reduce by increasing temperature. The sensor response to H_2 and CO was seriously deteriorated by water vapor, especially for neat SnO_2 that the sensor signal was extremely low and even cannot be detected in some temperatures. Moreover, for 0.7% Pd-SnO_2, the gas sensing behavior to H_2 and CO in humid atmosphere was opposite to that in dry atmosphere. It showed a lower sensor response at low temperature for both constant heating and pulse heating in humid atmosphere. Water vapor gives more complicated reactions on the surface of sensor layer. At low temperature the chemisorbed water vapor was in a large amount. Thus a lower response was observed in low temperature for 0.7% Pd-SnO_2.

The sensor response to 200 ppm H_2 were compared between MEMS gas sensor and conventionally thick-film sensor using SnO_2 and 0.7% Pd-SnO_2, as shown in Fig. 4-9. The thick-film gas sensors showed higher H_2 response at 300 ℃, no matter in dry or humid atmosphere. However, their response dramatically reduced with increasing temperature in dry atmosphere due to the stronger burning of H_2 on the surface. Therefore, thick-film sensors showed lower H_2 response at temperature above 450 ℃ in dry atmosphere compared with

MEMS gas sensors. In humid atmosphere, the sensor response of MEMS gas sensor was seriously influenced by water vapor, especially for neat SnO_2. However, MEMS gas sensor based on 0.7% Pd-SnO_2 had an impressive high response at 500 ℃. How to enhance the sensor response of MEMS gas sensor in humid atmosphere is a problem that needs to be solved in future research. Although the sensor response of MEMS sensors was low at low temperature, by considering the extremely lower power consumption, the gas sensing performance is impressive and more research works are needed for further improve the gas sensing properties.

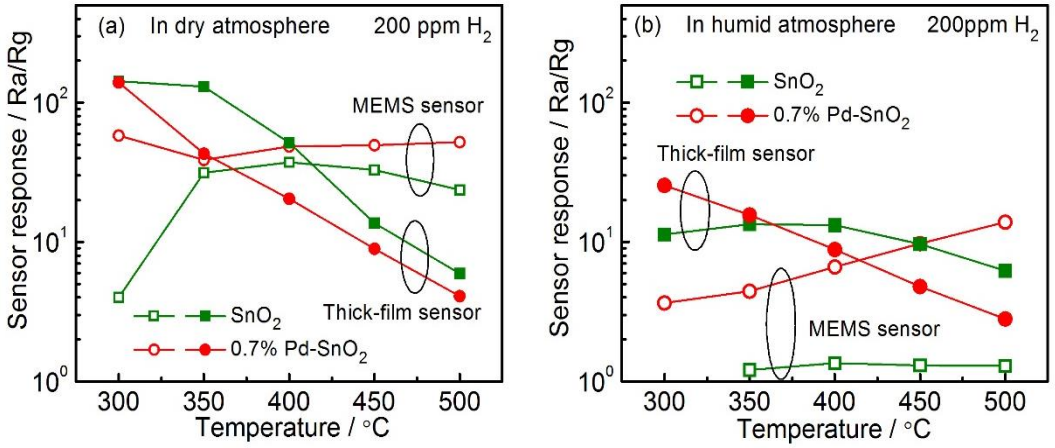

Figure 4-9 Sensor response to 200 ppm H_2 for MEMS sensor and thick-film sensor using SnO_2 and 0.7% Pd-SnO_2 in dry and humid (1 vol.% H_2O) atmospheres.

4.4 Conclusions

In this chapter, we presented a type of Pd-SnO_2 MEMS gas sensor with low power consumption, based on injecting Pd-loaded SnO_2 paste on a Si substrate with micro heater and electrodes. The gas sensing properties to H_2 and CO were investigated by constant and pulse heating modes in dry and humid atmospheres. The following conclusions are drawn from this study.

1. Pd loading greatly enhanced the MEMS sensor response to H_2 and CO especially in low temperature, no matter in dry or humid atmosphere, constant heating or pulse heating.

2. Pulse heating gave higher sensor response to H_2 and CO at low temperature in dry atmosphere for 0.7% Pd-SnO_2 MEMS sensor, whereas, constant heating showed higher response in humid atmosphere.
3. Compare with conventionally thick-film gas sensor, MEMS gas sensor based on 0.7% Pd-SnO_2 showed better gas sensing properties at high temperature. However, the sensing properties of MEMS sensors in humid atmosphere need to be further enhanced.

References

[1] Dai Z, Xu L, Duan G, Li T, Zhang H, Li Y, et al. Fast-response, sensitivitive and low-powered chemosensors by fusing nanostructured porous thin film and IDEs-microheater chip. Scientific reports. 2013;3.

[2] Gong J, Chen Q, Fei W, Seal S. Micromachined nanocrystalline SnO_2 chemical gas sensors for electronic nose. Sensors and Actuators B: Chemical. 2004;102:117–125.

[3] Han CH, Han SD, Singh I, Toupance T. Micro-bead of nano-crystalline F-doped SnO_2 as a sensitive hydrogen gas sensor. Sensors and Actuators B: Chemical. 2005;109:264–269.

[4] Moon S, Lee H, Choi N, Lee J, Choi C, Yang W, et al. Low power consumption micro C_2H_5OH gas sensor based on micro-heater and screen printing technique. Sensors and Actuators B: Chemical. 2013;187:598–603.

[5] Jaegle M, Wöllenstein J, Meisinger T, Böttner H, Müller G, Becker T, et al. Micromachined thin film SnO_2 gas sensors in temperature-pulsed operation mode. Sensors and Actuators B: Chemical. 1999;57:130–134.

[6] Matsushima S, Maekawa T, Tamaki J, Miura N, Yamazoe N. New methods for supporting palladium on a tin oxide gas sensor. Sensors and Actuators B: Chemical. 1992;9:71–78.

[7] Baik N, Sakai G, Miura N, Yamazoe N. Hydrothermally treated sol solution of tin oxide for thin-film gas sensor. Sensors and Actuators B: Chemical. 2000;63:74–79.

[8] Suematsu K, Yuasa M, Kida T, Yamazoe N, Shimanoe K. Determination of oxygen adsorption species on SnO_2: exact analysis of gas sensing properties using a sample gas pretreatment system. Journal of The Electrochemical Society. 2014;161:123–128.

[9] Yamazoe N, Sakai G, Shimanoe K. Oxide semiconductor gas sensors. Catalysis Surveys from Asia. 2003;7:63–75.

[10] Sakai G, Baik NS, Miura N, Yamazoe N. Gas sensing properties of tin oxide thin films fabricated from hydrothermally treated nanoparticles: Dependence of CO and H_2 response on film thickness. Sensors and Actuators B: Chemical. 2001;77:116–121.

Chapter 5

Effect of Pd Loading on the Gas Sensing Properties of Sb-Doped SnO_2 Gas Sensor in Humid Atmosphere

In this chapter, Pd-loaded/Sb-doped SnO_2 gas sensors were prepared for reducing the electric resistance and improving the gas sensitivity and stability in humid atmosphere for their real life application. The Sb doping effect as well as the Pd sensitization effect were further elucidate by investigating the gas sensing properties of Pd-loaded/Sb-doped SnO_2 sensor in dry and humid atmospheres. In addition, the effect of Pd particle size on the gas sensing properties of Sb-doped SnO_2 was examined in different humidity.

5.1 Introduction

To enhance the gas sensing properties in humid atmosphere, Pd was loaded on the SnO_2 surface because of its electronic sensitization effect. For Pd-loaded SnO_2 sensors, high gas sensitivity is always obtained below 200 ℃.[1, 2] Unfortunately, such low temperature also leads to a disadvantage namely very high electric resistance, which complicates the measurement by conventional instruments.[3] One of the effective solutions for this problem is to replace the Sn^{4+} by high valence metal ions, such as Sb^{5+}, increases the carrier concentration.[4-7] It was reported that the electric resistance of SnO_2 can be decreased by several orders of magnitude by doping with Sb.[6, 8] A low electric resistance of sensing layer is very favorable for reducing the noise in the measurement of the resistance and consequently a high signal/noise ratio.[6] Therefore, it is possible to control the electric resistance and sensitivity of SnO_2 by simultaneously doping Sb and loading Pd, making sensors more promising for practical application. In addition, due to the substitution of Sn^{4+} by Sb^{5+}, Sb-doped SnO_2 sensors exhibit some

excellent properties such as quick response and recovery time as well as high stability in humid atmosphere.[6, 9] Moreover, the Pd sensitization effect on the gas sensing properties of SnO_2 sensor was greatly influenced by Pd size, as discussed in Chapter 3. Thus, the Pd size effect was also examined base on the Sb-doped SnO_2. On the basis of above considerations, Pd-loaded/Sb-doped SnO_2 sensors with different Pd particle sizes were prepared, and their gas sensing properties to H_2 and CO were investigated in dry and humid atmospheres. The Pd size effect as well as the role of Pd and Sb in modifying the gas sensitivity and stability of SnO_2 sensors in humid atmosphere was clarified in this chapter.

5.2 Experimental

The Pd-loaded/Sb-doped SnO_2 nanoparticles were prepared by the following route. Firstly, Sb-doped SnO_2 nanoparticles were synthesized by the hydrothermal method. $SbCl_5$ was dispersed in HCl (35 wt.%) solution, and then mixed with $SnCl_4$ (1 mol/L) solution. The obtained mixture was slowly dropped into NH_4HCO_3 solution (1 mol/L) with stirring. After centrifuging and washing by NH_4NO_3 solution (1 mol/L) several times, it was hydrothermally treated in an ammonia solution (pH = 10.5) under the pressure of 10 MPa at 200 ℃ for 3 h. Then the obtained sol was dried at 120 ℃ and heat-treated at 600 ℃ in air to get Sb-doped SnO_2 nanoparticles. The Pd loading method was same as described in Chapter 3. 0.7 mol.% Pd was loaded on Sb-doped SnO_2 surface by impregnation method using $Pd(NH_3)_2(NO_2)_2$ and $Pd(NO_3)_2$ aqueous solution, respectively (abbreviated them to 0.7PdNN/Sb-SnO_2 and 0.7PdN/Sb-SnO_2). The former one followed by ammonia solution treatment (pH = 9.5) and filtration process. Finally, the obtained powders were dried at 120 ℃ and heat-treated at 500 ℃ for 3 h in air. The material preparation process was shown in Fig. 5-1. Thick-film gas sensors were fabricated by screen-printing method using Pd-loaded/Sb-doped SnO_2 powders.

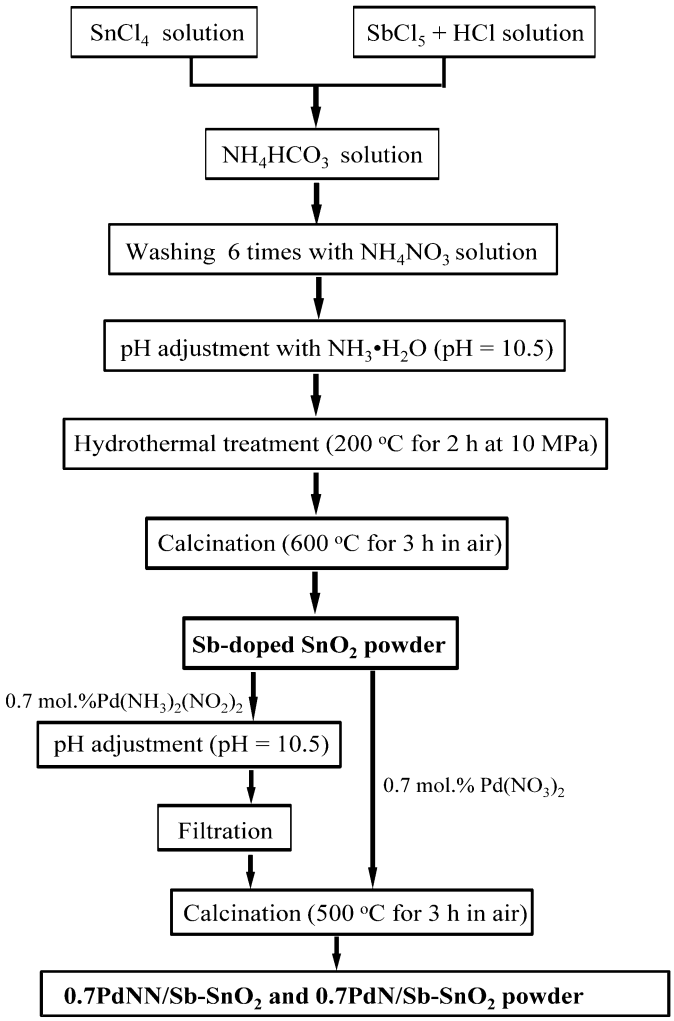

Figure 5-1 Preparation process of Pd-loaded/Sb-doped SnO_2 nanoparticles.

5.3 Results and Discussion

5.3.1 Materials characterization

The pure SnO_2 powders showed a light-yellow color and Sb-doped SnO_2 powders showed a grey-white color, while the addition of 0.7 mol% PdN on SnO_2 and 0.1 mol.% Sb-SnO_2 caused a drab color on powder appearance, as shown in Fig. 5-2. Nevertheless, in Figure 5-3 for Sb-doped SnO_2, Pd-loaded SnO_2 as well as Pd-loaded/Sb-doped SnO_2, no clearly change was found in the XRD patterns due to the extremely low Sb or Pd amount. All the samples exhibited the same tetragonal phase (JCPDS: 41−1445). It was found that crystallite characteristics of

SnO_2 were not affected by Sb and Pd addition. The crystallite sizes calculated from the (110) peak by Scherrer equation were almost the same for all the powders, 16~17 nm. Sb-doping or Pd-loading did not cause significant change in the crystallinity of pure SnO_2 particles, which was in agreement with the reported results.[8]

Figure 5-2 Photo images for SnO_2, 0.1Sb-SnO_2, 0.7PdN-SnO_2 and 0.7PdN/0.1Sb-SnO_2 powders.

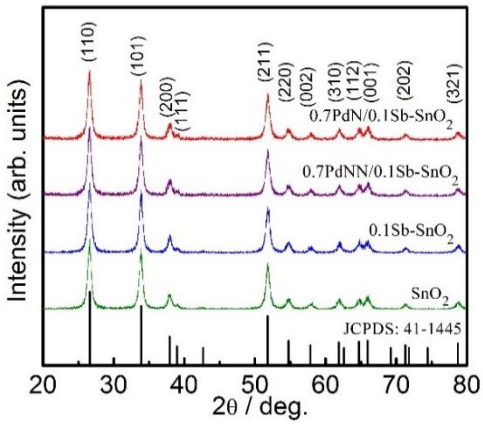

Figure 5-3 X-ray diffraction patterns of SnO_2, Sb-doped SnO_2 and Pd-loaded/Sb-doped SnO_2.

5.3.2 Gas sensing properties

Figure 5-4a shows the dependence of the electric resistance on humidity in air for SnO_2 and Sb-doped SnO_2. On doping with a small amount of Sb, SnO_2 showed a dramatically decrease in electric resistance, due to the substitution of Sn^{4+} by Sb^{5+} leading to the increase of carrier concentration.[6] The carriers

introduced by Sb doping occupy a free-electron-like conduction band, such as Sn 5s atomic character, which is empty for neat SnO_2.[8] Hence, the electric resistance of 0.1Sb-SnO_2 was reduced about 5-10 times in wet air compared with neat SnO_2. By further increasing Sb amount to 0.5 mol.%, the electric resistance was reduced more than 200 times. It was reported when the Sb doping amount was above 2 wt.%, the Sb^{5+} reduced to Sb^{3+} producing acceptor site, leading to the decrease of carriers.[10] Therefore, by doping a small amount of Sb, the electric resistance of SnO_2 was successfully reduced.

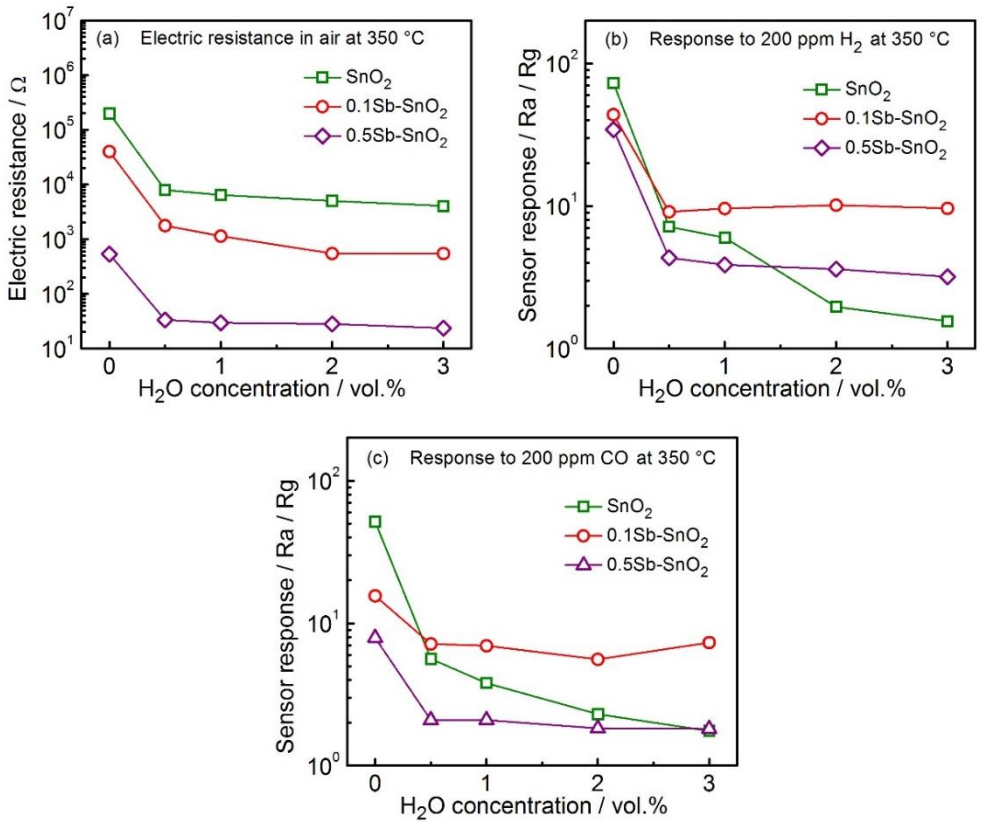

Figure 5-4 Electric resistance in air (a) and sensor response to 200 ppm H_2 (b) and CO (c) for SnO_2 and Sb-doped SnO_2 in different humidity at 350 ℃.

The sensor response of Sb-doped SnO_2 towards 200 ppm H_2 and CO in different humidity was shown in Fig. 5-4b and c. Although neat SnO_2 had higher sensor response toward H_2 and CO in dry atmosphere compared with Sb-doped SnO_2, but its response showed a poor stability in humid atmosphere due to the disturbance of water vapor to the oxygen adsorption. Interestingly, despite Sb-doping worsened the sensor response toward H_2 and CO in dry atmosphere, it

reduced the interference effect of humidity on the sensor responses leading to a high stability in humid atmosphere. This result indicated that Sb-doped SnO_2 with modified surface may inhibit OH^- adsorption on the surface. Especially for 0.1Sb-SnO_2 sensor, not only high stability but also comparable sensor response was obtained in humid atmosphere. Sb-doping increases the carrier concentration of SnO_2, leading to excess carriers involved in the oxygen adsorption/desorption process during gas sensing.[3] Hence, Sb at 0.1 mol.% doping level improved the gas sensitivity of SnO_2 in high humidity. Further increasing Sb amount to 0.5 mol.%, the sensor response was extremely low because the depletion layer became thinner with increasing carriers. Such sensors had very low electric resistance in humid air, and cannot lower their resistance too much in the presence of reducing gas. Therefore, on the basis of the gas sensing properties, 0.1 mol.% Sb was considered to be an optimal doping concentration, and the Pd sensitization effect on the gas sensing properties was studied based on 0.1mol.% Sb-doped SnO_2.

To further enhance the gas sensitivity of 0.1Sb-SnO_2, 0.7 mol.% Pd with different sizes were loaded on the surface. As discussed in Chapter 3, the Pd particle sizes of 0.7 mol.% PdN and 0.7 mol.% PdNN were about 10.3 and 2.6 nm, respectively. The combination effect of Pd-loading and Sb-doping on the gas sensing properties of SnO_2 was checked by investigating the sensor response in dry and humid atmospheres. Figure 5-5 shows the gas sensing performance of SnO_2, 0.1Sb-SnO_2, 0.7PdNN-SnO_2 and 0.7PdNN/0.1Sb-SnO_2 in different humidity at 350 ℃. By doping 0.1 mol.% Sb, SnO_2 gas sensor exhibited low electric resistance and high stability in humid atmosphere, but its sensor response needs to be further enhanced. It is well-known that Pd loading not only enhanced the sensor response but also increased the electric resistance of SnO_2 because of the electronic sensitization effect. Such high electric resistance by loading-Pd greatly complicates the measurement, resulting to high cost. However, by Sb-doping and Pd-loading, the electric resistance of 0.7PdNN/0.1Sb-SnO_2 just slightly increased as compared with 0.1Sb-SnO_2, but still lower than that of neat

SnO_2. The same phenomenon was also observed on the 0.7PdN/0.1Sb-SnO_2, as shown in the Fig. 5-6a. It seems Pd loading had less influence on the electric resistance of 0.1Sb-SnO_2. In Fig. 5-5b and c, 0.7%PdNN/0.1Sb-SnO_2 showed the similar H_2 response as 0.1Sb-SnO_2, but the former one had higher CO response than that of the latter one. 0.7PdNN-SnO_2 and 0.7%PdNN/0.1Sb-SnO_2 showed the similar response toward H_2 and CO in humid atmosphere. Sb doping on 0.7PdNN-SnO_2 sensor lead low electric resistance, but it did not decrease the sensor response. 0.7%PdN/0.1Sb-SnO_2 exhibited higher response to H_2 and CO as compare with 0.1Sb-SnO_2 in humid atmosphere (Fig. 5-6b and c). Obviously, by Pd-loading and Sb-doping, SnO_2 sensors showed low electric resistance and improved sensor response and stability in humid atmosphere. Pd-loaded/Sb-doped SnO_2 sensors show a great potential for practical application.

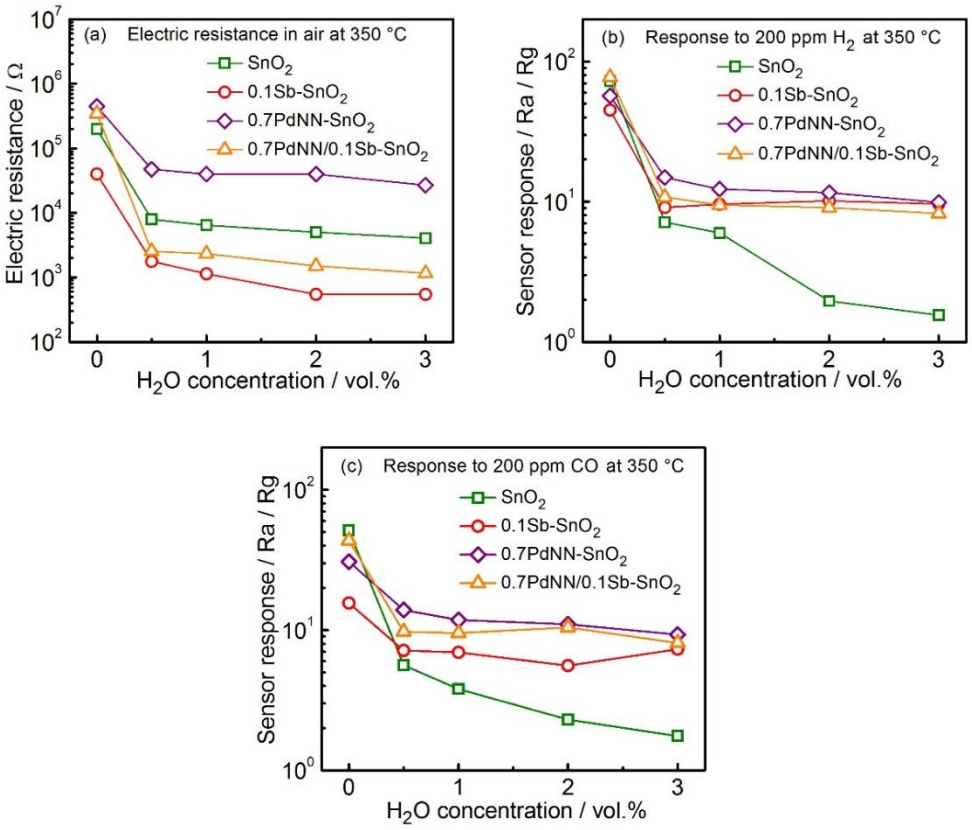

Figure 5-5 Electric resistance in air (a) and sensor response to 200 ppm H_2 (b) and CO (c) for SnO_2, 0.1Sb-SnO_2, 0.7PdNN-SnO_2 and 0.7%PdNN/0.1Sb-SnO_2 in different humidity at 350 ℃.

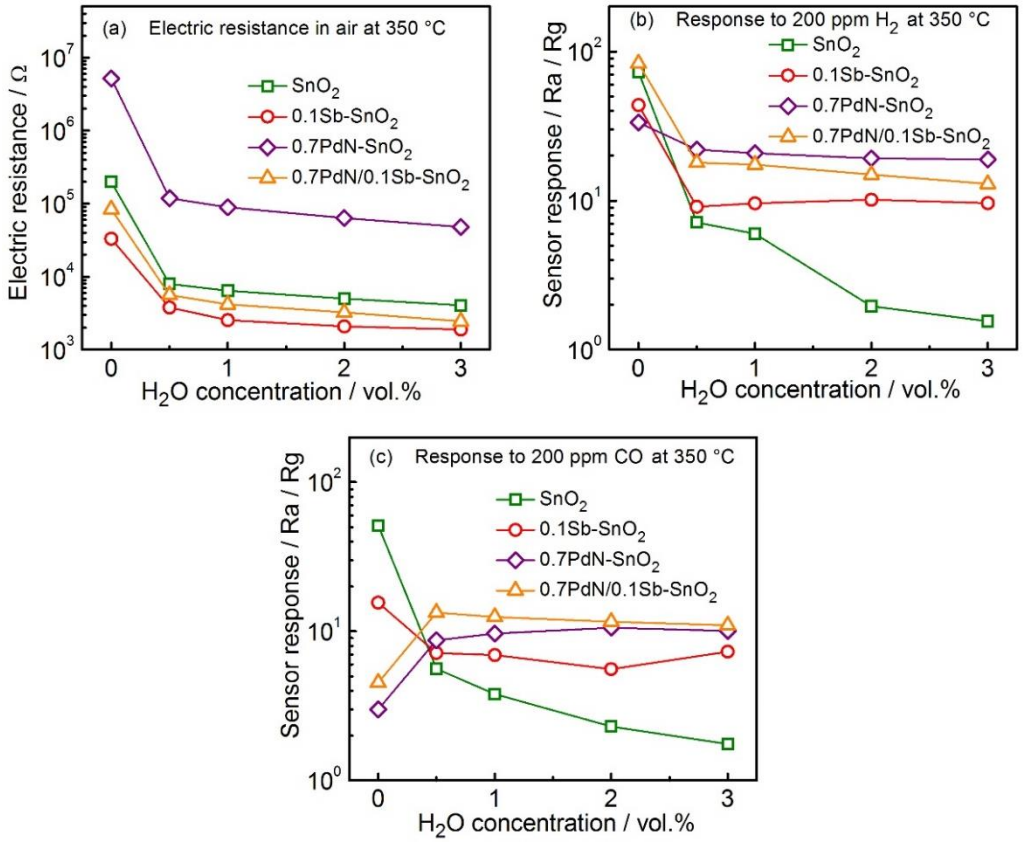

Figure 5-6 Electric resistance in air (a) and sensor response to 200 ppm H_2 (b) and CO (c) for SnO_2, 0.1Sb-SnO_2, 0.7PdN-SnO_2 and 0.7%PdN/0.1Sb-SnO_2 in different humidity at 350 ℃.

Figure 5-7 compared the gas sensing performance of 0.7PdNN/0.1Sb-SnO_2 and 0.7PdN/0.1Sb-SnO_2. 0.7PdN/0.1Sb-SnO_2, which had larger Pd size, showed higher sensor response and stability toward H_2 and CO sensing in humid atmosphere. This may be due to the stronger P-N junction effect of larger Pd particles, reflecting by the higher electric resistance of 0.7PdN/0.1Sb-SnO_2 in air under humid condition. The Pd size effect on the CO sensing behavior in humidity was also observed in the 0.1Sb-SnO_2, which was same as the phenomenon observed in SnO_2. 0.7PdNN/0.1Sb-SnO_2 with smaller Pd size showed a decreasing trend in the CO response in the presence of water vapor, whereas, 0.7PdN/0.1Sb-SnO_2 with larger Pd size exhibited increased CO response in humidity. This different behavior toward CO sensing was attributed to the different catalytic activities of different nano-sized Pd particles. Although

0.7PdN/0.1Sb-SnO_2 showed a little higher response in humid atmosphere, its CO sensing behavior from dry to humid atmosphere complicated the detection of CO. Therefore, to further enhance the gas sensing properties of 0.1Sb-SnO_2, it is necessary to increase the loading amount of small Pd particles on the 0.1Sb-SnO_2 surface.

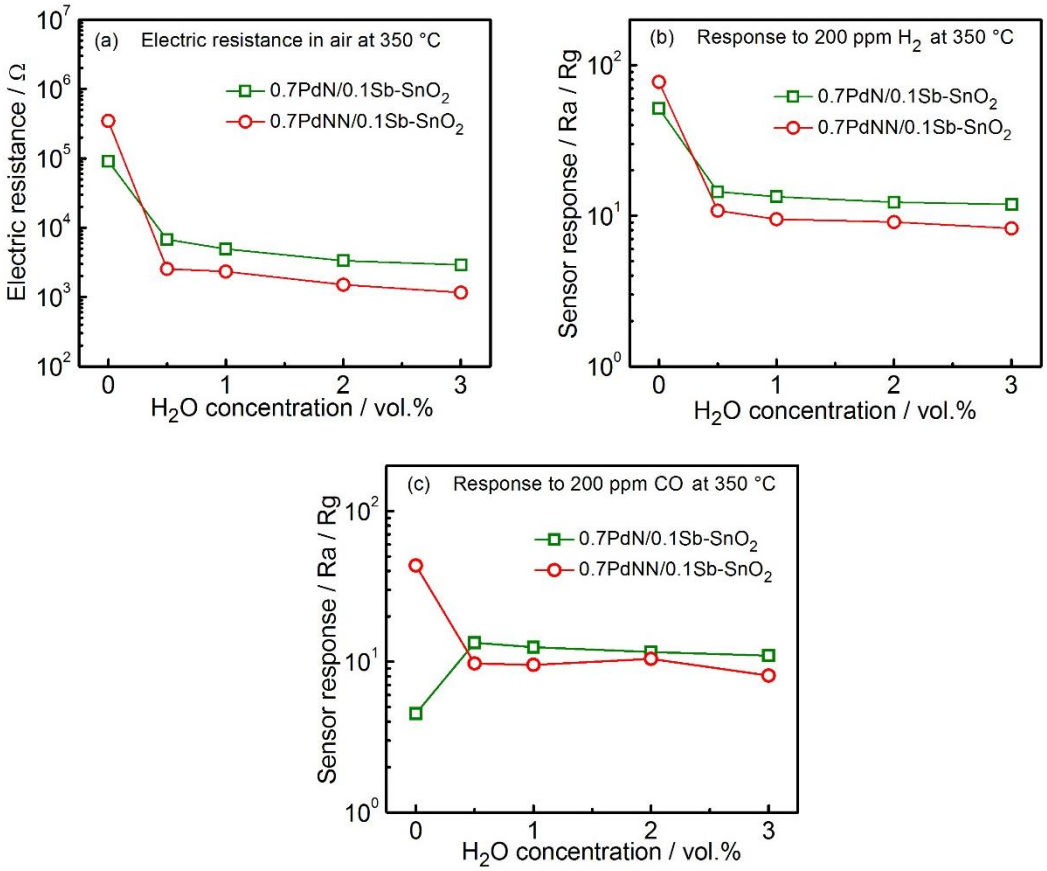

Figure 5-7 Electric resistance in air (a) and sensor response to 200 ppm H_2 (b) and CO (c) for 0.7PdNN/0.1Sb-SnO_2 and 0.7%PdN/0.1Sb-SnO_2 in different humidity at 350 ℃.

5.4 Conclusions

The effect of Pd loading and Sb doping on the gas sensing properties as well as the Pd size effect were analyzed by investigating the gas sensing performance of 0.7PdN/0.1Sb-SnO_2 and 0.7PdNN/0.1Sb-SnO_2 in different humidity. The following conclusions were drawn from this chapter:

1. The electric resistance of SnO_2 was effectively reduced by doping Sb. Sb-doped SnO_2 exhibited high stability in humid atmosphere.
2. Pd-loading combined with Sb-doping on SnO_2 greatly reduced the electric resistance and improved the sensor response and stability in humid atmosphere. Pd-loaded/Sb-doped SnO_2 sensors showed a great potential for practical application.
3. The Pd size effect on the CO response was also observed on the 0.1Sb-SnO_2 gas sensor, reflecting by the decreased response for 0.1Sb-SnO_2 with smaller Pd particles and increased response for 0.1Sb-SnO_2 with larger Pd particles in the presence of water vapor. The further confirmation of Pd size effect on the gas sensing performance is favorable for better understanding the role of Pd in the gas sensing process.

References

[1] Matsushima S, Maekawa T, Tamaki J, Miura N, Yamazoe N. New methods for supporting palladium on a tin oxide gas sensor. Sensors and Actuators B: Chemical. 1992;9:71–78.

[2] Schweizer-Berberich M, Zheng J, Weimar U, Göpel W, Barsan N, Pentia E, et al. The effect of Pt and Pd surface doping on the response of nanocrystalline tin dioxide gas sensors to CO. Sensors and Actuators B: Chemical. 1996;31:71–75.

[3] Chatterjee K, Chatterjee S, Banerjee A, Raut M, Pal N, Sen A, et al. The effect of palladium incorporation on methane sensitivity of antimony doped tin dioxide. Materials Chemistry and Physics. 2003;81:33–38.

[4] Lee SY, Park BO. Structural, electrical and optical characteristics of SnO_2: Sb thin films by ultrasonic spray pyrolysis. Thin Solid Films. 2006;510:154–158.

[5] Zhang D, Deng Z, Zhang J, Chen L. Microstructure and electrical properties of antimony-doped tin oxide thin film deposited by sol–gel process. Materials Chemistry and Physics. 2006;98:353–357.

[6] Krishnakumar T, Jayaprakash R, Pinna N, Donato A, et al. Sb-SnO_2-nanosized-based resistive sensors for NO_2 detection. Journal of Sensors. 2009;2009.

[7] Krishnakumar T, Jayaprakash R, Pinna N, Phani A, Passacantando M, Santucci S. Structural, optical and electrical characterization of antimony-substituted tin oxide nanoparticles. Journal of Physics and Chemistry of Solids. 2009;70:993–999.

[8] Großmann K, Kovács KE, Pham DK, Mädler L, Barsan N, Weimar U. Enhancing performance of FSP SnO_2-based gas sensors through Sb-doping and Pd-functionalization. Sensors and Actuators B: Chemical. 2011;158:388–392.

[9] Wan Q, Wang T. Single-crystalline Sb-doped SnO_2 nanowires: synthesis and gas sensor application. Chemical Communications. 2005:3841–3843.

[10] Zhang B, Tian Y, Zhang J, Cai W. The FTIR studies of SnO_2: Sb (ATO) films deposited by spray pyrolysis. Materials Letters. 2011;65:1204–1206.

Chapter 6

Conclusions and Outlook

In this thesis, the effect of Pd on the gas sensing process in humid atmosphere was studied by focusing on four parts, namely, (1) the gas sensing mechanism of Pd-SnO_2 in humidity; (2) the Pd size effect on the gas sensing properties of Pd-SnO_2 in humidity; (3) the gas sensing performance of Pd-SnO_2 MEMS type gas sensor; (4) the application of Pd sensitizer on Sb-doped SnO_2 gas sensor. The followings are the conclusions derived from the present study and some suggestions for the future research.

6.1 Conclusions

Firstly the microstructure of Pd-loaded SnO_2 nanoparticles were investigated in terms of crystallite, particle size, specific surface area and peak pore radius for Pd-SnO_2 as well as Pd amount, particle size, distribution and surface area for Pd particles. Pd did not cause significant change in the microstructure of SnO_2 particles by loading Pd on the calcined SnO_2 surface. The Pd particle sizes were controlled in the range of 2.6−10.3 nm by different Pd loading methods and loading amounts. The role of Pd as well as its particle size effect on the gas sensing properties was well investigated based on the Pd-loading method adopted in this study. Additionally, the sensitization effect of Pd was examined based on SnO_2 MEMS sensors and Sb-doped SnO_2 thick-film sensors.

The oxygen adsorption behavior and sensor response toward H_2 and CO were studied in dry and humid atmospheres based on SnO_2 and Pd-loaded SnO_2. The mainly adsorbed oxygen species on the SnO_2 surface in humid atmosphere was changed by loading Pd, more specifically, for neat SnO_2 was O^- but for Pd-SnO_2 was O^{2-}. The sensor response for H_2 and CO for neat SnO_2 was

dramatically deteriorated in the presence of water vapor. However, the water vapor poisoning effect on the sensor response was significantly reduced by loading Pd. The TPR results indicated that Pd was existed in PdO form and O^{2-} adsorbed on the surface. Therefore, we propose that O^{2-} adsorption on PdO enlarged the depletion layer of the interface and prevented OH^- adsorption on the SnO_2 surface, leading to high sensor response in humid atmosphere for Pd-loaded SnO_2.

The Pd size effect on the gas sensing performance in different humidity was analyzed based on Pd-loaded SnO_2 with smaller and larger Pd particle sizes. The Pd size has no influence on the oxygen adsorption behavior, that the mainly adsorbed oxygen species was O^{2-} in both dry and humid atmospheres for Pd-SnO_2, no matter Pd in smaller or larger sizes. The sensor response to H_2 was reduced in the presence of humidity for both two kinds of Pd-loaded SnO_2 sensors. However, different CO sensing behavior was observed for Pd-SnO_2 with different Pd sizes. Pd-SnO_2 with smaller Pd particles was reduced in response by introducing water vapor, but kept high stability with the varying humidity. While Pd-SnO_2 with large Pd particles showed increased CO response in the presence of water vapor and it increased with the rising humidity. By combining with the H_2-TPR and CO-TPR results, it was though that different Pd/PdO distribution states lead to the different sensitization effect to CO oxidation in humid atmosphere.

The Pd sensitization effect on the gas sensing performance in dry and humid atmospheres was also checked on the MEMS-type SnO_2 gas sensor. To achieve highly sensitive and stable MEMS gas sensors with low power consumption, Pd was loaded on the SnO_2 surface, and the gas sensing properties to reducing gas (H_2 and CO) were investigated by operating MEMS sensor in constant and pulse heating modes in dry and humid atmospheres. It was demonstrated that Pd-loading greatly enhanced the sensor response to H_2 and CO in low temperature. Pulse heating gave higher sensor response at low temperature in dry atmosphere,

while constant heating gave higher sensor response in humid atmosphere. Although the sensor response of 0.7% Pd-SnO_2 MEMS sensor was a little lower in humid atmosphere compared with conventionally thick-film sensor, by considering the low power consumption, the gas sensing performance was still impressive.

The role of Pd and its size effect were also analyzed by using Sb-doped SnO_2. Pd-loading combined with Sb-doping on SnO_2 greatly reduced the electric resistance and improved the sensor response and stability in humid atmosphere, due to the electronic sensitization effect of Pd and the modified SnO_2 surface by Sb doping. The Pd size effect on the CO response was also observed in the Sb-doped SnO_2 gas sensor, reflecting by the decreased response for Sb-SnO_2 with smaller Pd particles and increased response for 0.1Sb-SnO_2 with larger Pd particles in the presence of water vapor. To further confirm the Pd size effect on the gas sensing performance of SnO_2-based gas sensor is favorable for designing high performance gas sensor.

6.2 Outlook

The present study demonstrated that Pd is one of effective sensitizers to reduce water vapor poisoning effect. O^{2-} adsorption on Pd/PdO enlarged the depletion layer of the interface and prevented OH^- adsorption on the SnO_2 surface. The Pd size greatly affects the CO sensing behavior in dry and humid atmospheres due to different catalytic activities to CO oxidation for different nano-sized Pd particles. The Pd-loading greatly enhanced the gas sensing properties of SnO_2 MEMS sensors and Sb-doped SnO_2 thick-film sensors.

On the basis of above research, we can understand the role of Pd in gas sensing process in humidity, the Pd size effect on the gas sensing properties as well as the Pd sensitization effect on the sensor performance, which are beneficial for designing high performance MOS gas sensors. To further clarify the role of Pd

in humidity and reduce the water vapor poisoning effect, the following aspects for future research are proposed based on the present study.

1. For conventional thick-film sensors, although Pd-loading enhances the sensor response and stability in humid atmosphere, Pd-SnO_2 sensors still show deteriorated gas sensing properties by introducing a small amount of water vapor into dry atmosphere. How to avoid the reduction of sensor response from dry to humid atmosphere is a problem that needs to be further solved.
2. For MEMS gas sensors, they have obviously advantage of low power consumption, and they are promising for practical application. However, their bad gas sensing performance in humid atmosphere greatly hinders the practical use. Therefore, to enhance the gas sensing properties of Pd-SnO_2 MEMS sensor in humid atmosphere is necessary in future research.
3. Pd is just one of common sensitizers for gas sensors. To fully clarify the role of Pd in the gas sensing process is helpful to understand the role of other similarly noble metal additives such as Au and Pt. The role of Au and Pt in the gas sensing process in humidity can be studied by investigating the oxygen adsorption behavior and gas sensing properties towards reducing gas. The mechanism of noble metal additives in the gas sensing process in humidity can be systemically studied based on SnO_2 gas sensor and other MOS sensors. This is good for designing high performance gas sensor.

ACKNOWLEDGEMENT

The work presented here was carried out at Interdisciplinary Graduate School of Engineering Sciences, Kyushu University from October 2012 to July 2015 with the financial support of China Scholarship Council (CSC).

Foremost, I wish to express my sincere gratitude to my advisor Prof. Kengo Shimanoe who directly instructed me for three years, for his patience, enthusiasm, motivation, and immense knowledge. His guidance and advice helped me all the time not only in research and writing of papers, but also in my oversea life in Japan.

Besides my advisor, I would like to thank the rest of my thesis committee: Prof. Michitaka Ohtaki and Prof. Hisahiro Einaga for their encouragement and insightful comments.

My sincere thanks also go to all the former and present members in laboratory: Assistant Prof. Yuasa, Dr. Suematsu, Dr. Hua, Miss Sasaki, Mr. Yamaga, Mr. Kato, Mr. Ishado, Mr. Oyama and all other staff in our laboratory for the research discussions and for their helps during my stay in Japan. I am grateful to Mr. Uchiyama for the experimental technical supports.

I would like to express my appreciation to Prof. Bo-Ping Zhang for her advice and recommendation to study in Japan. I will benefit from the experience of live and study in Japan in whole life. Last but not the least; I would like to thank my parents, my sister, my boyfriend and many friends for giving encouragement to me and supporting me spiritually throughout my life.